REACTIVATION OF A HYDRAULIC FRACTURE IN PERMEABLE ROCK

by

Erfan Sarvaramini

Submitted in partial fulfillment of the requirements
for the degree of Doctor of Philosophy

at

Dalhousie University
Halifax, Nova Scotia
August 2015

TABLE OF CONTENTS

LIST OF TABLES

LIST OF FIGURES

ABSTRACT

The problem of massive fluid injection into a pre-existing fracture has many applications in petroleum industry including underground liquid waste disposal (e.g., hydraulic fracturing wastewater, supercritical CO2) and waterflooding to increase the hydrocarbon recovery from a reservoir. Understanding the conditions leading to the reactivation of pre-existing fractures and ensuing propagation is critical for a successful injection project design, and it may also help to mitigate potential environmental hazards, such as contamination of underground aquifers and induced seismicity.

Extensive analytical and numerical studies are carried out to quantify the transient pressurization and breakdown of a pre-existing fracture due to a fluid injection in the context of unconventional hydraulic fracturing when the fluid diffusion can vary over wide range of scales from 1-D to 2-D or 3-D. We establish the range of the problem parameters and injection time when the fluid pressure is approximately uniform along the crack. The pressure uniformity assumption allows for a simpler and more accurate solution method (based on the Green's function approach).

As the fracture is pressurized, the condition for the onset of propagation (the breakdown condition) is eventually reached. We quantify how the breakdown depends upon the problem parameters, such as fluid and rock properties, the in-situ stress, and the fluid injection rate. The poroelastic effects on the transient pressurization and initiation of the fracture in a critically over-pressured reservoir (i.e., when the initial reservoir pore pressure p_0 is approximately equal to the minimum confining stress σ_0) are also investigated. We show that the poroelastic effects will substantially delay the breakdown time compared to the non-poroelastic case when the fracture breakdown occurs at later stages of injection characterized by large-scale (2D) pore pressure perturbation in the reservoir. Finally, we extend the analysis to the transient pressurization of multiple fractures.

The results of this study are transportable to the production well test analysis of a fractured well. The history of the transient pressurization prior to breakdown can also be used to provide the initial conditions for the fracture propagation problem.

LIST OF ABBREVIATIONS AND SYMBOLS USED

DEP	United States Department of Environmental Protection
EIA	United States Energy Information Administration
KGD	Khristianovic and Geertsma and de Klerk
PKN	Perkins and Kern and Nordgren
b	Biot coefficient
c_t	formation bulk compressibility
d	spacing between fractures
$d\Sigma$	crack surface increment
E	Young's modulus
E'	plane-strain modulus
F	influence function
$\hat{F}$	Laplace image of influence function
$F_{1\mathrm{D}}$	1-D influence function
$\hat{F}_{1\mathrm{D}}$	Laplace image of 1-D influence function
$\langle F \rangle$	crack-averaged influence function
$\left\langle \hat{F} \right\rangle$	Laplace image of crack-averaged influence function
$\bar{g}$	height-averaged fluid leak-off rate
$\bar{g}_*$	characteristic leak-off scale
$\bar{g}^{(2)}$	fluid leak-off rate in mode 2 loading
G	spatial influence function
h	fracture height
k	formation permeability
k_f	propped fracture permeability
k_{ni}	initial normal fracture stiffness
K_{Ic}	rock toughness

ℓ	crack half-length
p	internal fluid pressure
p_{uni}	uniformity pressure
p_0	initial pore pressure
p_1	1-D pressure scale
p_{1c}	closed-crack 1-D pressure scale
p_2	2-D pressure scale
p_{2c}	closed-crack 2-D pressure scale
$\overline{p}$	net fluid pressure
$\overline{p}_{uni}$	uniformity net pressure
$\bar{p}_B$	net breakdown pressure
p_*	characteristic pressure
$p^{(2)}$	pressure in mode 2 loading
$\bar{q}$	average volumetric flow rate
Q_0	total volumetric flow rate
Q_0^1	volumetric flow rate per fracture in multi-fractured wells
s	Laplace transform parameter
S	storage coefficient
t	time
t_o	fracture re-opening time
t_{uni}	uniformity time
t_B	breakdown time
t_*	characteristic time scale
$t_*^{\text{1-D}}$	1-D diffusion time scale
$t_*^{\text{2-D}}$	2-D diffusion time scale
t_1	1-D time scale

t_{1c}	closed-crack 1-D diffusion time scale
t_1^{KGD}	KGD 1-D time scale
t_2	2-D time scale
t_{2c}	closed-crack 2-D diffusion time scale
T	temperature
U	total internal energy
U_{ps}	internal energy stored in a thin slice
V	cumulative injected volume
V_{aux}	cumulative injected volume in the auxiliary problem
V_{crack}	fracture volume
V_{leak}	cumulative leak-off volume
V_1	1-D volume scale
V_2	2-D volume scale
V_*	characteristic cumulative volume
$V_{\text{crack}}^{\text{np}}$	non-poroelastic crack volume
$V_{\text{leak}}^{\text{aux}}$	total leak-off volume in the auxiliary problem
$V_{\text{leak}}^{(2)}$	leak-off volume in the mode 2 loading
w	crack opening
w_{ini}	initial hydraulic opening
w_0	neutral hydraulic opening
$\bar{w}$	height-averaged crack opening
$\bar{w}^{(1)}$	average opening in mode 1 loading
$\bar{w}^{(2)}$	average opening in mode 2 loading
$\bar{w}^{\text{aux}}$	total crack opening in the auxiliary problem
x	spatial coordinate in 3D
y	spatial coordinate in 3D
z	spatial coordinate in 3D

α	diffusivity coefficient
γ	Euler's constant
Δw	induced crack width
ΔV_{crack}	fracture dilation
η	poroelasticity stress coefficient
$\eta^{'}$	effective poroelasticity stress coefficient
$\epsilon^{(1)}$	elastic volumetric deformation in mode 1 loading
μ	fluid viscosity
ν	poisson ratio
Π	non-dimensional pressure
$\hat{\Pi}$	Laplace image of non-dimensional pressure
Π_B	non-dimensional breakdown pressure
Π_{uni}	non-dimensional uniformity pressure
Π_0	non-dimensional initial net-pressure
$\bar{\rho}$	average fluid density
σ_b	generated backstress
σ_0	minimum principal stress
σ_b^{aux}	generated backstress in the auxiliary problem
$\langle\sigma_b^{\text{aux}}\rangle$	spatial average of backstress in the auxiliary problem
τ	non-dimensional time
τ_{uni}	non-dimensional uniformity time
ϕ	porosity
χ	non-dimensional y coordinate
Φ	non-dimensional cumulative leak-off volume
$\hat{\Phi}_{\text{aux}}$	Laplace image of non-dimensional cumulative leak-off volume
Φ_{aux}	non-dimensional cumulative volume in the auxiliary problem
$\Phi^{(2)}$	non-dimensional cumulative volume in the mode 2 loading

ψ	non-dimensional leak-off rate
$\hat{\psi}$	Laplace image of non-dimensional leak-off rate
$\psi^{(2)}$	non-dimensional leak-off rate in mode 2 loading
$\hat{\psi}^{(2)}$	Laplace image of non-dimensional leak-off rate in mode 2 loading
$\mathcal{A}$	crack height-to-length ratio
$\mathcal{A}_c$	closed-crack aspect ratio
$\mathcal{A}^{\mathrm{KGD}}$	crack height-to-length ratio in KGD crack
$\mathcal{F}$	fracture response
$\mathcal{F}^{aux}$	fracture response in the auxiliary problem
$\mathbb{K}$	permeability number
$\mathcal{W}_0$	non-dimensional neutral opening

ACKNOWLEDGMENTS

First and foremost, I would like to express my deepest gratitude to my advisor Dr. Dmitry Garagash for his guidance, patience, and support during my PhD studies at Dalhousie University.

I would also like to thank my PhD advisory committee, Dr. Mysore Satish and Dr. Theodore Kolokolnikov for their time and support.

I take this opportunity to express my gratitude to Dr. Andrew Bunger, Mr James Kear, and Dr. Robert Jeffery at the Commonwealth Scientific and Industrial Research Organization (CSIRO), Melbourne, Australia for giving me the opportunity to visit their hydraulic fracturing laboratory. This opportunity has broadened my vision in this field.

I wish to express my sincere thanks to my parents for their unlimited love and support. In particular, I am grateful to my brother Dr. Amin Sarvaramini for being my mentor during these challenging years.

The financial support of the Natural Science and Engineering Research Council of Canada is gratefully acknowledged.

CHAPTER 1: INTRODUCTION

1.1 INJECTION OF A LOW VISCOSITY FLUID

The massive injection of a low viscosity fluid into a pre-existing fracture in permeable rock has been practiced in the oil and gas industry for several decades. The injection of water into a pre-existing fracture to displace the hydrocarbon toward the production well [e.g., 1] or injection of petroleum related wastes (e.g., hydraulic fracturing wastewater or CO_2) into the deep geological underground formation for the purpose of fluid storage [e.g., 2, 3] are among the most typical examples of injection of a low viscosity fluid into fractured reservoirs. The injection of fluid into the underground formation may cause the reactivation of pre-existing fractures and ensuing fracture propagation.

One of the main challenges in mathematical modeling of hydraulic fracture reactivation is to develop an appropriate model accounting for the massive fluid leak-off into the formation. The problem of injection of a low viscosity fluid into a permeable formation can be distinguished from conventional hydraulic fracturing (with gel-like fluids) by the mechanism of fluid leak-off into the surrounding permeable rock. In the latter, high viscosity and cake building properties of injected fluid limit leak-off to a 1-D boundary layer incasing the crack [4, 5]. In the case of injection of low viscosity fluid into a fracture, leak-off and related pore fluid diffusion will take place over wider range of scales, from 1-D to 2 or 3-D necessitating a different approach [6, 7, 8, 9]. Moreover, the high fluid leak-off and associated large-scale pore pressure perturbation may significantly alter the mechanical properties of the formation through the poroelastic effect [10].

Several studies have been performed to simulate the fracture propagation during the injection of a low viscosity fluid in permeable rock. The complex nature of

mechanisms of interaction between fracture, fluid and rock during the fracture growth had limited the simulation to numerical models [6, 11, 12]. Recent attempts have been carried out to develop more universal analytical models [7, 8, 13]. In most approaches, the mathematical modeling of fracture propagation was carried out assuming that the fracture is initiated from a borehole [13, 9].

There are only a handful of papers investigating the transient pressurization of a stationary and pre-existing fracture in permeable rock due to low viscosity fluid injection. The history of the transient pressurization prior to breakdown can be used to provide the initial conditions for the fracture propagation problem initiated from a stationary and pre-existing fracture [e.g., 14].

An important class of pre-existing fractures is tensile joints that can occur in underground formations due to various geological reasons [15, 16], one of which is an excessive pore pressure in undercompacted rocks [17]. The pervasive existence of subparallel arrays of tensile joints has been identified in a number of locations [18, 19]. In elastic rock, joints are normally contained to specific bedding layers and reach lateral dimensions many times their height [20]. On the other hand, the previously induced, man-made hydraulic fractures constitute another class of pre-existing fractures encountered during injection projects in depleted reservoir rock formations.

1.2 OBJECTIVES AND ORGANIZATION OF THE RESEARCH

A comprehensive study is conducted to investigate the physical interaction between the fluid, fracture and surrounding rocks during injection of a low viscosity fluid into a pre-existing stationary fracture in a permeable rock. We mainly focus on modeling of the reactivation of a pre-existing fracture when the viscous dissipation in the fluid flow along the fracture is neglected. In other words, pressure is assumed to be uniform along the fracture for the majority of the developed results. To substantiate the

pressure uniformity assumption in a non-propagating crack, we establish a parametric range when the fluid pressure can be considered equilibrated along the fracture length. The pressure uniformity assumption allows for a simpler and more accurate solution method (based on the Green's function approach).

The crack geometry in our study is assumed to be of the Perkins-Kern-Nordgren (PKN) type [21]. Since the length of such a fracture is much larger than its height, elastic response in any vertical section can be approximated by that of uniformly pressurized plane-strain (Griffith's) crack. Fracture height is assumed to span a permeable (reservoir) layer sandwiched between impermeable (cap) rock layers.

In this study, two general reservoir conditions are considered. 1) A critically over-pressured reservoir condition when the initial reservoir pore pressure p_0 is approximately equal to the minimum confining stress σ_0 (i.e., $p_0 \simeq \sigma_0$). The pre-existing crack in a critically over-pressured reservoir is initially mechanically-open. 2) A normal reservoir condition when the initial reservoir pore pressure p_0 is smaller than the minimum confining stress σ_0 (i.e., $p_0 < \sigma_0$). In this case, the pre-existing fracture is initially mechanically-closed.

The layout of the thesis is as following.

In Chapter 2, the mathematical formulation of the transient pressurization of a non-poroelastic PKN crack due to fluid injection is presented. The basic assumptions of the crack model are discussed.

In Chapter 3, the transient pressurization and initiation of a non-poroelastic initially mechanically-open (or in a critically over-pressured reservoir) PKN crack are quantified. We establish a criterion when the assumption of uniformly pressurized crack is justified.

In Chapter 4, the mathematical formulation for a non-poroelastic fracture (Chapter 3) is modified to account for the poroelastic effects. We investigate the poroelastic effects on the transient pressurization and the onset of fracture propagation for an

initially mechanically-open fracture.

In Chapter 5, we relax the assumption of an initially mechanically-open crack. We consider the transient pressurization and breakdown of single non-poroelastic initially-closed fracture, which can be either propped or not. The applicability of uniformly pressurized assumption is again investigated. We also extend the analysis to the pressurization of multi-fractured wells.

This study can improve the understanding of the physical processes involved during the pressurization, breakdown and propagation of fractures in a permeable and poroelastic medium.

1.3 BACKGROUND AND LITERATURE REVIEW

1.3.1 Background

The significant growth in global demand for natural gas and continuous decline of conventional gas resources around the world encourage the investment into production from unconventional gas reservoirs, such as tight sandstone, coal seams and shale gas reservoirs. According to United States Energy Information Administration (EIA) [22], in 2011 the shale gas resources represented 32 percent of natural gas resources in the USA. These resources are also expected to significantly increase as better geological information become available.

Due to the poor shale matrix permeability, gas production from these formations usually requires special stimulation techniques. The primary technology extensively used in petroleum industry to extract gas from shale formations is hydraulic fracturing. In this technique, a fluid is pumped from a borehole under high pressure to create and propagate fractures in rock formation. These newly created conductive channels may significantly improve the permeability of the formation [23].

The combination of horizontal drilling with hydraulic fracturing has revolutionized the shale gas industry. These technologies have increased shale gas production

several fold and provided a greater access to difficult hydrocarbon resources. The rapid development of shale gas formations has also brought controversy related to potential environmental threats, which include the contamination of underground water [24] and induced seismicity [25].

Hydraulic fracturing technique has been used in oil and gas industry for various purposes. The first generation of hydraulic fracturing treatments aimed to bypass the near-wellbore damage [23]. The latter is caused by the infiltration of the drilling-mud in the vicinity of the wellbore leading to obstruction of the hydrocarbon flow [26, 27]. The hydraulic fracturing is used to bypass this zone by creating highly conductive channels connecting the reservoir to the well. The application of hydraulic fracturing technique was later extended to the tight gas formations (e.g., shales or tight sandstone reservoirs)[23]. The purpose of hydraulic fracturing is not only bypassing the damage zone. The massive fluid injection is used for creation of permeable surfaces to increase the production from the tight gas reservoirs [23]. There are two main types of fracturing fluids commonly used in the oil and gas industry. These are the gel-like fluids and low viscosity fluids (e.g., slickwater). In the last two decades, hydraulic fracturing using a low viscosity fluid has become mainstream in the shale oil/gas developments.

The creation of hydraulic fractures during the injection of a low viscosity fluid is not always desirable. The low viscosity fluid has been injected in subsurface formations for various applications, such as disposals of industrial wastes (e.g., CO_2, hydraulic fracturing wastewater) to store the liquid wastes in proper underground geological formations, or waterflooding processes to increase productivity from hydrocarbon reservoirs. In the latter, injection of the fluid at/above the fracturing pressure is commonly considered to be a bad practice due to the potential environmental risk associated with large injection volume for extended periods of time (e.g., contamination of underground water).

The problem of the injection of a low viscosity fluid is significantly different from a gel-like fluid injection in the mechanism of the fluid leak-off to the surrounding formation. The latter is usually controlled by the nature of the injected fluid. For example, during conventional hydraulic fracturing with a gel-like fluid, the mud cake build-up properties of the gel will minimize the fluid loss to surrounding rock and limit the related pore pressure diffusion to the vicinity of the fracture (i.e. the 1-D diffusion). However, in the case of a low viscosity fluid injection, the leak-off and related pore fluid pressure diffusion can take place over wider range of scales, from the 1-D to 2 or 3-D.

1.3.2 Conventional hydraulic fracturing

1.3.2.1 Background

Hydraulic fracturing is performed by pumping a fluid through the annulus (wellbore) under high pressure to create and propagate the fracture in rock formation. The exposure of the fracturing fluid to the formation will cause the partial loss of the fluid. With continuing the fluid injection, more permeable surfaces will be created until the pumps are shut down. After the well shut-in, the "flowback" is typically performed by lowering the pressure at the well in order to flow the fracturing fluid back to the surface and "clean" the fracture. During the cleaning process, the net pressure along the fracture is gradually reduced until the fracture becomes mechanically-closed. The closure may significantly reduce the permeability of fracture. In order to prevent the closure of fracture, propping agents mixed with the hydraulic fracturing fluid are often used to hold the fracture open [23].

1.3.2.2 Hydraulic fracturing modeling

Since the early days when the concept of hydraulic fracturing was first introduced, the mechanics of hydraulic fracturing has been progressively studied by many in-

vestigators. The key issue is to accurately understand the interaction of the fluid, fracture and the rock during the fracture propagation.

Early modeling

Following the pioneering work by Khristianovic & Zheltov [28] and Spence and Sharp [29], many investigations were performed to construct rigorous analytical and numerical solutions for simple fracture geometries. The most widely used fracture geometry types are (Figure 1.1):

(1) KGD (Khristianovic, Zheltov, Geertsma, de Klerk) [28, 30] crack characterized by infinite height such that any horizontal cross section is in the state of plane-strain crack.

(2) Penny-shaped or radial crack.

(3) PKN (Perkins, Kern, Nordgren) crack, which assumes that the length of the crack is much larger than its height [21]. These assumptions allow to approximate any vertical section of the crack away from the fracture tips by that of a uniformly pressurized plane-strain crack.

One of the seminal studies in the area of hydraulic fracture modeling was carried out by Perkins and Kern [21] who studied the propagation of vertical fracture confined between two impermeable layers. A solution that relates the fracture width to the net pressure in fracture was constructed. They showed that the width of fracture at any point along the fracture length is proportional to the net pressure at that point. In their work, the exchange of the fluid with the surrounding rock (i.e., fluid leak-off) was neglected. Nordgren [5] modified the work by Perkins and Kern by including the fluid leak-off in the solution of the governing equations.

After Perkins and Kern [21] and Nordgren [5], the mathematical modeling of conventional hydraulic fracturing has been extensively studied. The main objectives of these investigations have been to evaluate the crack growth rate, fluid pressure

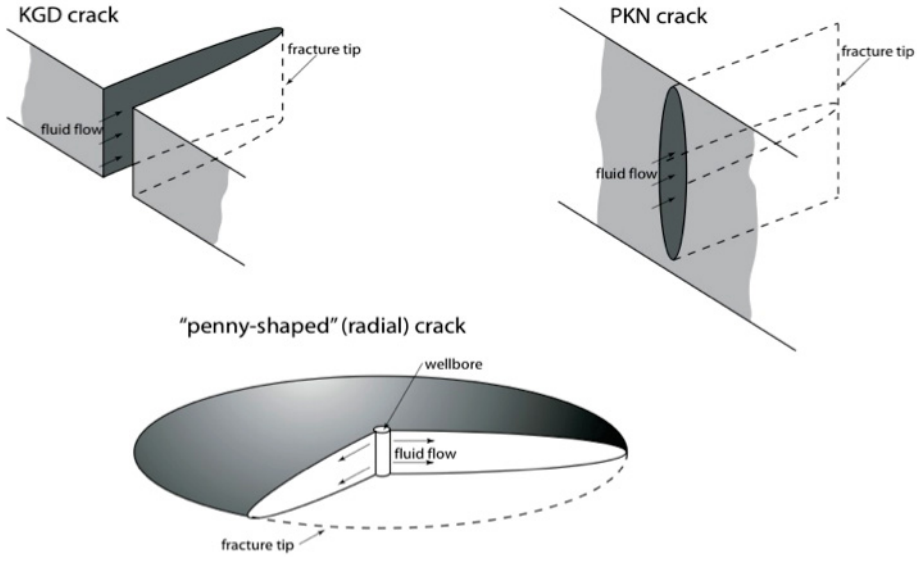

Figure 1.1: Simple fracture geometry shapes [31, 9].

evolution, and crack opening for various energy partition regimes. These limiting regimes correspond to (i) viscosity-dominated regime when the energy required to break the rock is negligible compared to viscous dissipation in the fluid, and (ii) toughness-dominated regime when the fluid viscous loss along the fracture can be considered to be negligible compared to the energy required to break the rock [32].

Advances in hydraulic fracturing modeling

A simplified mathematical model of crack propagation includes: 1) lubrication equation describing the flow of fluid in the fracture channel; 2) elasticity equation which relates the deformation of the fracture to the net fluid pressure in the crack; 3) criterion for fracture propagation. In case of fracture propagation in permeable rock, the exchange of fluid with surrounding rock is also important.

The main mathematical challenges of the simultaneous solution of these equations are: (i) the non-local behavior of elasticity, (ii) strong coupling between the lubrication equation and elasticity equation, and (iii) moving unknown problem boundaries;

i.e., fracture and fluid fronts [33]. The solution of these equations can be used to investigate the behavior at fracture tips, the far field region away from tips, and construction of a boundary layer to match the near tip and far field regions for various limiting propagation regimes [for the summary see, 32].

The difficulties involved in modeling of complex fracture geometries have limited most of the studies to the simple fracture geometries where the fracture height is specified or crack is assumed to be radial. However, the analysis of field data logs shows that the fixed-height limitation may not always be representative of the actual crack geometry. In other words, during hydraulic fracturing the fracture height may grow before it is restrained [23]. The existing 3D models (e.g., 3D, Planar 3D and Pseudo 3D model) accounting for fracture height growth attempt to address the possible limitations due to complex fracture geometry [12]. However, the mathematical modeling of 3D fracture models still remains computationally intensive.

1.3.3 Unconventional hydraulic fracturing

By definition, hydraulic fracturing treatment using a low viscosity fluid (e.g., CO_2 or "slickwater") to drive the fracture in permeable formation is usually referred to as unconventional hydraulic fracturing. This term is used to differentiate between unconventional and conventional hydraulic fracturing. During conventional hydraulic fracturing, a high viscosity fluid with the cake build-up property is used to propagate the fracture, which helps to limit fluid losses to the surrounding rock; whereas in case of unconventional hydraulic fracturing, no cake buildup is expected to form, and fluid leak-off is not constrained.

Unconventional hydraulic fracturing is widely used in stimulation of the tight formations in the last two decades. A typical fracturing fluid used to initiate and propagate a hydraulic fracture in tight formations is "slickwater" which is primarily composed of water. Additional chemicals can also be added to the water to provide

other benefits to the fracturing process, one of which is reducing the friction of the water in the pipe.

Unconventional hydraulic fracturing may also accidentally happen in many applications in the oil and gas industry where the fracturing is usually considered to be undesirable. For example, injection of fluid above the fracturing pressure during the underground disposal of industrial wastes is considered to be a bad practice.

One of the most typical wastes associated with petroleum industry is the wastewater generated from hydraulic fracturing and produced (formation) water. With the boom in shale gas production, the proper disposal of wastewater from hydraulic fracturing has become one of the greatest challenges of the shale gas industry. The amount of water required to drill a horizontal well in shale formations is estimated to be 3 to 5 million gallons of water. The latter is estimated based on the 1500 horizontal wells drilled in Marcellus shale, Pennsylvania [34]. Depending on geological environment, 10 to 30 percent of the wastewater will be recovered. For example, according to US Department of Environmental Protection (DEP), the shale gas industry produced 235 million gallons of wastewater from Marcellus shale in the second half of 2010 [34].

Although the wastewater can be treated on the surface, the poor quality of the wastes from hydraulic fracturing has limited the recycling options. Ultimately, the underground disposal of wastewater has become one of the most common ways to dispose of the wastewater. The wastewater can be injected either in new suitable geological formations or in depleted and previously fractured reservoirs. Other typical industrial wastes are liquid CO_2 [35, 36] and drilling cuttings [37, 3, 2].

The possible environmental impacts associated with the deep well injection of a fluid, such as contamination of underground aquifers [24] and induced seismicity [38, 39, 40] necessitate comprehensive studies of the processes involved during the injection of a low viscosity fluid. The above environmental risks may be directly

related to fluid injections which result in pressurization of the formation above the critical pressure required to break the rock (i.e., breakdown pressure) or reactivation of pre-existing fractures. Pressure in excess of the breakdown pressure may lead to the following scenarios 1) In the presence of pre-existing fractures, the formation pressurization may lead to fracture reactivation and ensuing fracture propagation. 2) Alternatively, in the previously unfractured reservoir, may lead to the generation of a new hydraulic fracture.

The focus of this research work is on the pressurization of the formation leading to reactivation of the fracture and ensuing fracture propagation.

1.3.3.1 Injection of a low viscosity fluid into a pre-existing fracture

"Un-propped" fracture

The first category of pre-existing fractures is natural fractures. Originating from various geological processes [18], the natural fractures are associated with (1) shearing displacement mode (e.g., faults) and (2) opening displacement mode ("joints") [41]. The latter are created by the formation pore pressure in excess of the minimum principal stress. This may lead to creation of systematic sets of joints extending to many meters in length [18].

Hydraulic fractures used to stimulate production from a now depleted reservoir are another category of pre-existing fractures. The underground depleted oil and gas reservoirs can be well suited for waste disposal purposes due to existence of the reservoir and geological data and infrastructure (e.g., pipes, wells).

The injection of the fluid either into naturally or man-made fractures may lead to reactivation of these fractures and ensuing fracture propagation. The detailed knowledge of interaction between the fracture, fluid and surrounding rock from the beginning of the injection time is critical for a successful injection project design.

The mechanical and hydraulical behavior of the fracture during injection may

strongly depend upon the initial state of the net fluid pressure ($p_0 - \sigma_0$) defined as the difference between the reservoir ambient pore pressure (p_0) and minimum principal stress (σ_0). The crack can be initially subjected to a negative net pressure (i.e. the normal stress is exceeding the pore pressure). In this case, the interaction of the fracture rough surfaces may significantly affect the fluid transport through the channel due to smaller cross sectional area and the longer tortuous path [42].

Ideally for the purpose of fluid flow modeling, a fracture can be represented by two parallel plates separated by a gap. This assumption allows to significantly reduce the complexity of mathematical models in fluid transport problems. For example, the parallel plate approximation has been extensively used in studies of mechanically-open fluid-driven fractures where the fluid pressure along the fracture is exceeding the minimum principal stress. The parallel plate theory results in the so-called "cubic law", where the volumetric flow rate through a fracture is proportional to the cube of the aperture [e.g., 43, 44]. For mechanically-closed fractures, the validity of parallel plate approximation for fracture with surfaces in partial contact has been the subject of various investigations [45, 46, 47]. These studies have shown that the fluid transport in mechanically-closed fractures subjected to low to moderate effective stress can be well approximated by the cubic law [48, 47], while the significant departures from the cubic law were observed for larger effective stress acting on the fracture.

"Propped" fracture

The knowledge of fracture deformation with pressure during the fluid injection is only relevant for an un-propped fracture. The use of proppant to keep the fracture open is a common practice in the petroleum industry. The study of interaction of a propped fracture with surrounding rock has been extensively carried out in analysis of post-fracture production data in fractured wells. The transient pressure analysis can provide valuable information on hydraulic fracture properties, such as fracture length,

height, and propped opening [49, 50]. This information can be used to improve the hydraulic fracturing design.

Some of the seminal contributions to the analysis of transient production data from fractured wells were by Gringarten et al. [49] and Cinco-Ley et al. [50]. Gringarten et al. considered a propped fracture from which a fluid was produced via the crack inlet. The pressure distribution was considered to be uniform along the fracture. In other words, the fracture is assumed to be highly conductive such that the viscous pressure loss along the crack could be neglected. The validity of the uniform pressure distribution assumption was studied in details by Cinco-Ley et al. [50]. They considered the general problem of transient data analysis for a finite-conductivity fracture, and identified conditions when the assumption of infinite-conductivity fracture could be justified. Although the injection and production problems can be mathematically similar, the knowledge of fracture reactivation, including re-opening, fracture breakdown, and ensuing fracture propagation become irrelevant in production problems. In injection problems, it is crucial to investigate the condition leading to reactivation of pre-existing fractures.

1.3.4 Low viscosity fluid injection versus gel-like fluid injection

The problem of the injection of a low viscosity fluid is different from gel-like fluid injection mainly by the mechanism of the fluid leak-off to the surrounding formation. The latter is usually controlled by the nature of the injected fluid. For example, during conventional hydraulic fracturing (i.e., fracturing using a gel-like fluid), the mud cake build-up properties of the fracturing fluid will minimize the fluid loss to surrounding rock by limiting the leak-off diffusion to the vicinity of the fracture (i.e. 1-D diffusion). However, in the case of low viscosity fluid injection, the leak-off and related pore fluid diffusion will take place over wider range of scales, from 1-D to 2 or 3-D (Fig. 1.2).

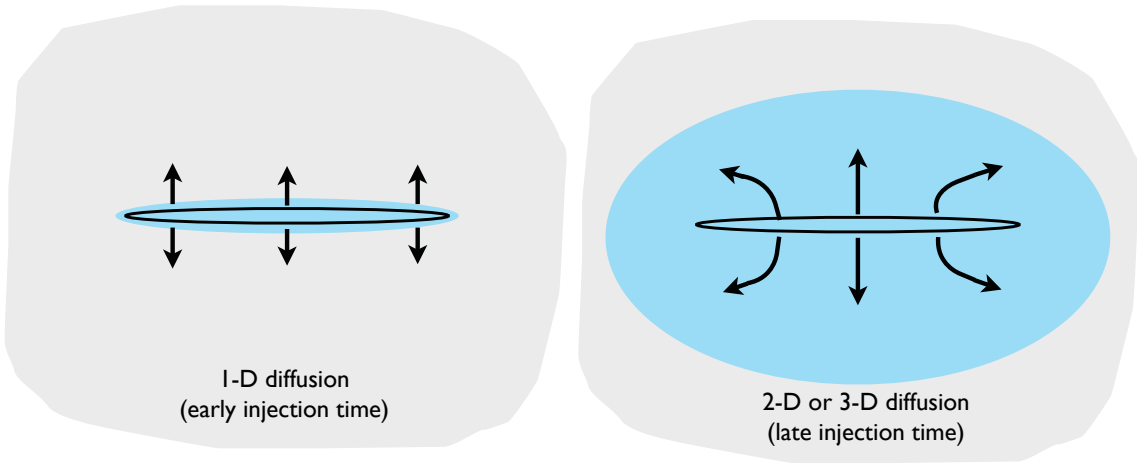

Figure 1.2: Leak-off diffusion pattern during the injection of a low viscosity fluid.

1.3.4.1 Diffusion mechanism

The engineering properties of the fluid used to propagate the fracture during the conventional hydraulic fracturing aim to minimize the amount of fluid loss to the formation. The fracturing fluid is designed to build a filter cake characterized by low permeability to limit the diffusion to the close vicinity of the pressurized fracture. In this context, the rate of leak-off rate can be mathematically represented by a 1-D diffusion model [4]. The 1-D model may significantly reduce the complexity of the problem. In contrast, in applications such as waste disposal or supercritical CO_2 injection into the deep geological underground formation (examples of unconventional hydraulic fracturing), large volume of fluid leak-off is favored [51]. The fluid diffusion follows a 1-D diffusion pattern during the early injection times when the diffusion length scale is small compared to the crack length. As injection continues, the diffusion length scale becomes greater or of the same order of magnitude as the crack scale (2-D diffusion) invalidating the 1-D assumption.

1.3.4.2 Energy dissipation mechanism

In the modeling of fluid-driven fractures, two limiting energy partition regimes can be identified. 1) Toughness-dominated regime where the dissipation of energy to break the rock is greater than the energy dissipated in the viscous fluid flow. 2) Viscosity-dominated regime where the dissipated energy in the rock is negligible compared to the energy dissipation in the fluid flow [32]. The viscosity-dominated regime is favored in the case of fracture propagation driven by a high viscosity fluid. Conversely, for the low viscosity fluid the dissipation of energy associated with fracturing of rock may dominate the energy needed for fluid flow into the crack. As a result, the fracture toughness is important in evaluating the propagation driven by a low-viscosity fluid. Possible exceptions include the cases with high injection rates and/or late stages of fracture growth, when the dissipation in the fluid flow may be substantial [52, 8].

1.3.4.3 Poroelasticity

The massive fluid leak-off during injection of low viscosity fluid over extended period of time can modify the mechanical response of the porous media [10]. Specifically, the increase of pore pressure in the surrounding porous rock leads to rock dilation, which its effect on the closing fracture can be modified by additional confining stress, referred to as "poroelastic" backstress [53]. The existence of the coupling between fluid diffusion and deformation adds another layer of difficulty to the modeling of the problems related to injection of a low viscosity fluid into permeable rock. The poroelastic rock dilation may be considered negligible in conventional hydraulic fracturing where diffusion is limited to a small zone near the crack walls.

1.3.5 Mechanics of low viscosity fluid injection

1.3.5.1 Leak-off model

The now standard equation used to characterize the fluid leak-off rate was given by Carter [4]. In his model, the fluid exchange rate to the formation adjacent to the fracture is anticipated to be proportional to the inverse square-root of time with a constant proportionality referred to as the Carter leak-off coefficient. The Carter leak-off model was originally derived to characterize the fluid loss to the formation when there is a thin layer of cake build-up formed on fracture walls. The cake layer has very low permeability which limits the fluid leak-off to a small zone near the fracture walls. This implies that the diffusion of the fluid can be simply represented by a 1-D model. The high contrast of permeabilities between the filter cake and surrounding rock establishes an approximate constant pressure boundary condition.

The Carter leak-off model is extensively used in design of conventional hydraulic fracturing in permeable formations [54, 55]. However, application of the Carter's model to fracture propagation without significant cake on the fracture walls (e.g., low viscosity fluid injection) may lead to overestimation of fracture propagation rate [6, 13]. As an alternative, the pressure-dependent 1-D diffusion model has been used to forecast the fluid leak-off for early times when the diffusion is still 1-D [56, 13]. For the large injection time, the full 2 or 3-D leak-off diffusion models should be considered.

The injection of a low viscosity fluid in a crack with 2 or 3-D leak-off has been investigated by several authors. Detournay and Cheng [57] considered the fundamental solution of a stationary crack subjected to a step pressure increase when the fluid diffusion pattern varies from the 1-D to 2-D. Their results confirmed that the 1-D fluid diffusion pattern is only valid when the size of diffusion zone is small compared to the crack length. The diffusion pattern changes from the 1-D to the full 2-D at large injection times.

Murdock and Germanovich [14] carried out an experimental and theoretical studies of a stationary fracture intersecting a wellbore. Initially, the crack is mechanically-closed. As injection starts and crack is pressurized, the opposing fracture surfaces are initially in contact and are gradually unloaded until the crack becomes mechanically-open. The mechanically-open crack is analyzed under plane-strain conditions. The numerical results of the model are validated by experiment.

Grodeyev and Zazovsky [52] investigated propagation of a vertical crack with constrained height (PKN fracture) in the viscosity-dominated regime and under the condition of 2-D leak-off diffusion. In their study, the process of initiation and propagation is not addressed. Instead, the authors focus on self-similar solutions for fracture propagation of the form $\ell = \ell_0 (1 + At)^{1/4}$, where A is related to injection rate and material parameters of the problem, while the initial crack length ℓ_0 is undetermined in their solution (presumably related to the crack initiation problem).

Gordeyev and Entov [8] constructed a self-similar solution for plane strain and penny-shaped cracks assuming that the pressure along the fracture remains constant and the crack length evolves according to $\ell \propto t^{1/2}$. The self-similar formulation provides the exact solution for the fluid leak-off rate and the pressure distribution in the surrounding rock for large injection time when the leak-off diffusion is 2-D or 3-D.

Kovalyshen [9] carried out a comprehensive study of penny-shaped crack propagation in various asymptotic regimes. First, he defined an auxiliary problem in which an impulse pressure is applied inside a stationary crack. The asymptotes of the fluid leak-off rate for a crack subjected to a pressure impulse were derived for small and large injection times, respectively. A convolution integral approach was used to find the solution for the fluid leak-off rate in the transient pressurization problem. This solution then was used to predict the crack length growth for different propagating scenarios. A similar approach based on fundamental solution of a crack subjected to

an impulse pressure was used by Berchenko et al. [58] to investigate the problem of natural hydraulic fracture propagation characterized by full 2-D diffusion.

1.3.5.2 Poroelastic model

The theory of poroelasticity accounts for coupling of the elastic deformation of porous medium and pore fluid diffusion. The key mechanisms in coupling between the pore fluid and the rock are: 1) rock dilation due to the pore pressure increase; 2) temporal increase of pore pressure due to mechanical compression of the rock [59, 10].

In the context of hydraulic fracturing, there are only handful of papers investigating the effect of poroelasticity on fracture propagation. Detournay et al. [60] considered the poroelastic effects on a propagating PKN fracture. The classical Carter's leak-off theory was used to account for exchange of fluid with surrounding rock. Their study suggests that the poroelastic backstress can significantly increase the breakdown pressure. The results obtained by Detournay et al. [60] were also confirmed by Boone et al. [61]. Number of studies also considered the 1-D pressure dependent leak-off model instead of Carter's leak-off model to investigate the effect of poroelasticity on the propagation process [e.g., 62].

Study of poroelastic effects on crack propagation is not limited to propagation problems with the 1-D leak-off diffusion. Detournay and Cheng [57] investigated the poroelastic effects for a stationary crack subjected to step pressure increase. They showed that the diffusion is nearly uncoupled from stress changes and the effects of poroelasticity on pore pressure diffusion can be reasonably neglected.

Kovalyshen [9] considered the propagation of a penny-shaped crack in poroelastic medium with 3-D leak-off. The generated back stress was evaluated for various propagating regimes. He showed that the fracture arrest may be expected at long injection times when the leak-off diffusion is 3-D.

CHAPTER 2: MATHEMATICAL FORMULATION

2.1 PROBLEM SETTING

In this Chapter, the mathematical formulation of the transient pressurization for a pre-existing stationary non-poroelastic PKN crack due to the fluid injection is described. The modifications of mathematical formulation to account for the poroelastic effects will be discussed in Chapter 4.

We consider a pre-existing crack of length 2ℓ and height h within a linearly elastic, permeable rock characterized by the Young's modulus E, Poisson's ratio ν and toughness K_{Ic} (Fig. 2.1). The crack is aligned perpendicular to the minimum in-situ stress σ_0 and is loaded internally by fluid pressure p, generated by the fluid injection at the crack center at a constant rate Q_o. The following assumptions are used in this work. 1) The crack height is small compared to the length, such that the deformation field in any vertical cross-section that is not immediately close to the crack edges ($x = \pm\ell$) is approximately plane-strain, and the fluid pressure is equilibrated within a vertical crack cross-section (the PKN assumptions). 2) The minimum in-situ stress σ_0 and the initial reservoir pore pressure p_0 are uniform along the crack. 3) The crack is confined between two impermeable layers, which, together with the assumption of pressure equilibrium within a vertical crack cross-section, suggests a 2-D fluid diffusion within the permeable reservoir rock layer. 4) The injected and reservoir fluids have similar rheological properties.

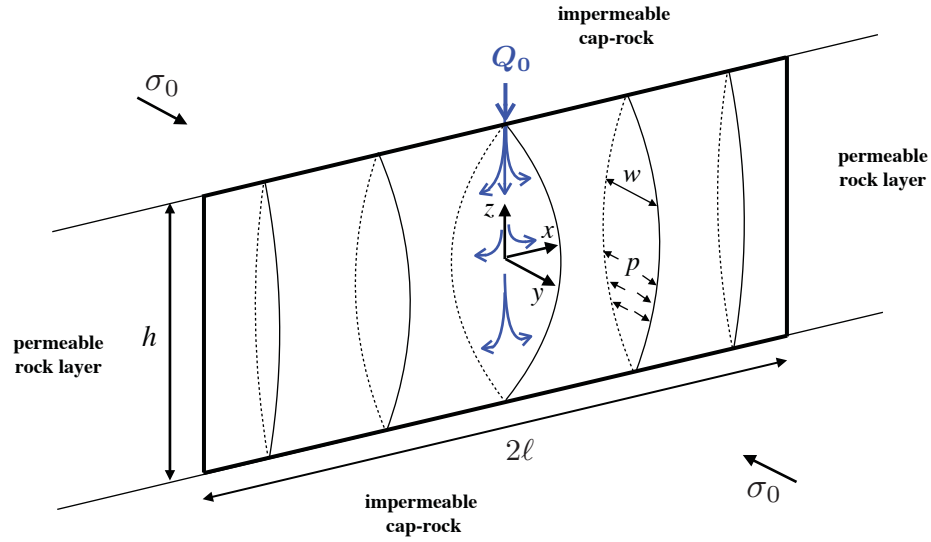

Figure 2.1: Injection into a pre-existing fingerlike crack with length 2ℓ and height h ($\ell \gg h$).

2.2 FRACTURE OPENING

The opening of a PKN crack is related to the net fluid pressure $\bar{p} = p - \sigma_0$ by:

$$w(x,z) = (w_0 + \Delta w(\bar{p}(x))) \sqrt{1 - \frac{4z^2}{h^2}}, \tag{2.1}$$

where Δw is the induced crack width expressed as a function of the net fluid pressure $\bar{p}$. Note that an opening distribution scaled by value w_0 has been added in (2.1) to Δw. The former reflects the "neutral" hydraulic opening available to the flow when the net fluid pressure is zero (i.e. $\bar{p} = 0$).

For the particular case of a mechanically-open PKN crack, the induced crack width Δw is given by the elasticity relation [5]

$$\Delta w = \frac{2h\bar{p}}{E'}, \tag{2.2}$$

where $E' = E/(1-\nu^2)$ is plane-strain modulus.

Expressions for the height-averaged crack opening

$$\bar{w}\,(x) = \frac{1}{h}\int_{-h/2}^{h/2} w\,(x,z)\,dz = \frac{\pi}{4}\left(w_0 + \Delta w(\bar{p}(x))\right), \tag{2.3}$$

and the fracture volume

$$V_{crack} = \frac{\pi h}{4}\left(2w_0\ell + \int_{-\ell}^{\ell}\Delta w(\bar{p}(x))dx\right), \tag{2.4}$$

follow from (2.1)

2.3 BREAKDOWN CONDITION

In view of the plane-strain conditions approximately valid away from the edges ($|\ell - x| \gg h$) of a fingerlike crack of height h (Fig. 2.1), the internal energy stored in a thin slice of thickness dx centered at x can be approximated by $U_{ps}(x)dx$, where

$$U_{ps}(x) = \frac{\pi h^2 \bar{p}^2(x)}{4E'} \tag{2.5}$$

is the internal energy of the solid (per unit extent in the x-direction) in the presence of a uniformly pressurized vertical Griffith crack of height h. Contributions to the total internal energy U stored in the elastic space from the regions near the $x = \pm\ell$ edges (where the plane-strain approximation is not applicable) of a fingerlike crack are small compared to the contributions from the rest of the crack. Thus,

$$U \simeq \int_{-\ell}^{\ell} U_{ps}(x)dx. \tag{2.6}$$

Evaluating energy release rate corresponding to the symmetric extension of the crack length by $2d\ell$ and corresponding crack surface increment of $d\Sigma = 2hd\ell$ (Appendix

A) we get

$$G = \left(\frac{\partial U}{\partial \Sigma}\right)_p \approx \frac{2U_{ps}(\ell)}{2h} = \frac{\pi h\, \bar{p}^2(\ell)}{4E'}, \tag{2.7}$$

A special case of (2.7) corresponding to a uniform net pressure along the crack has been extensively used in the fracture mechanics of composites [e.g., 63].

The breakdown (onset of propagation) and the ensuing fracture propagation in mobile equilibrium requires that the energy release rate G (equation (2.7)) is equal to the fracture energy of the rock $G_c = K_{Ic}^2/E'$ (expressed here in terms of the rock toughness parameter K_{Ic}). Resulting breakdown/propagation condition can be written in terms of the net pressure value at a finger-crack tip as

$$\bar{p}\,(\ell) = \bar{p}_B \equiv \frac{2K_{Ic}}{\sqrt{\pi h}}. \tag{2.8}$$

We note in passing that similar forms of the PKN fracture propagation condition have been proposed previously from *ad hoc* consideration of the tip region of a fingerlike crack. For example, Nolte [64] suggested that the tip pressure is approximately that of a propagating radial fracture with the diameter equal to the finger-crack height, i.e. $\bar{p}\,(\ell) = \sqrt{\pi/2h}K_{Ic}$, a value about 10% larger than given by (2.8). Propagation condition in the form of (2.8) is preferred here as it follows directly from the global energy balance for a fingerlike crack, and does not require any *ad hoc* assumptions about the nature of its near-tip region.

2.4 FLUID CONTINUITY

2.4.1 Local fluid continuity

The flow of fluid inside the PKN crack is governed by the height-averaged form of the local mass conservation equation

$$\frac{\partial \bar{w}}{\partial t} + \bar{g} = -\frac{\partial \bar{q}}{\partial x}, \quad (t > 0, |x| < \ell)\,, \tag{2.9}$$

where $\bar{w}$, $\bar{q}$, and $\bar{g}$ are the height-averaged crack opening (equation (2.3)), volumetric flow rate in the crack channel, and fluid leak-off rate, respectively. In view of the Poiseuille's law, $v(x,z) = -(w^2(x,z)/12\mu)(\partial p/\partial x)$, and crack opening equation (2.1), the height-averaged flow rate can be expressed as [e.g., 65]

$$\bar{q}(x) = \frac{1}{h}\int_{-h/2}^{h/2} w(x,z)\, v(x,z)\, dz = -\frac{\bar{w}^3}{\pi^2\mu}\frac{\partial p}{\partial x}. \tag{2.10}$$

Substituting (2.10) in (2.9) yields

$$\frac{\partial \bar{w}}{\partial t} + \bar{g} = \frac{1}{\pi^2\mu}\frac{\partial}{\partial x}\left(\bar{w}^3\frac{\partial p}{\partial x}\right). \tag{2.11}$$

Initial and boundary conditions for the constant-rate of injection (Q_0) problem are, accounting for the symmetry,

$$\bar{p}|_{t=0} = 0, \quad \bar{q}|_{x=0^+} = -\frac{\bar{w}^3}{\pi^2\mu}\left.\frac{\partial \bar{p}}{\partial x}\right|_{x=0} = \frac{Q_0}{2}, \quad \bar{q}|_{x=\ell} = -\frac{\bar{w}^3}{\pi^2\mu}\left.\frac{\partial \bar{p}}{\partial x}\right|_{x=\ell} = 0, \tag{2.12}$$

where the last equation prescribes a no-fluid-flow condition at the crack tip.

2.4.2 Global fluid continuity

The global fluid volume balance in the fracture is given by:

$$V(t) = \Delta V_{crack}(t) + V_{leak}(t), \tag{2.13}$$

where $V(t) = Q_0 t$ is the cumulative injected volume, $\Delta V_{crack}(t) = V_{crack}(t) - V_{crack}(t=0)$ is the dilation of crack volume from the start of injection ($t = 0$), and V_{leak} is the cumulative leak-off volume, which can be expressed as:

$$V_{leak}(t) = h\int_0^t \int_{-\ell}^{\ell} \bar{g}\left(x', t'\right) dx' dt'. \tag{2.14}$$

2.5 DIFFUSIVITY EQUATION AND BOUNDARY INTEGRAL REPRESENTATION

Pore pressure evolution in permeable rock surrounding the "leaky" fracture is described by the diffusion equation [66], and the leak-off boundary condition:

$$\frac{\partial p}{\partial t} = -\alpha \nabla^2 p, \quad -\frac{k}{\mu} \left. \frac{\partial p}{\partial y} \right|_{y=0^+} = \frac{1}{2} \bar{g}\left(x,t\right), \tag{2.15}$$

where $\alpha = k/\left(\mu \phi c_t\right)$ and $S = \phi c_t$ are diffusivity and fluid storage coefficients, respectively, expressed in terms of the formation permeability k, bulk compressibility c_t, and porosity ϕ. Due to the presence of the impermeable cap rock boundaries at $z = \pm h/2$ and pressure equilibrium in a vertical cross-section ($\partial p/\partial z = 0$), the diffusion problem is two dimensional (2-D). The general 2-D boundary integral for the pressure perturbation due to a distribution of instantaneous sources $\bar{g}(x,t)$ along a crack, $y = 0$ and $|x| \leq \ell$, is given (in the plane of the crack) by [67]

$$p(x,t) - p_0 = \int_0^t \int_{-\ell}^{\ell} \frac{\bar{g}\left(x',t'\right)}{4\pi S \alpha \left(t-t'\right)} \exp\left(-\frac{\left|x-x'\right|^2}{4\alpha\left(t-t'\right)}\right) dx' dt'. \tag{2.16}$$

CHAPTER 3: TRANSIENT PRESSURIZATION OF A NON-POROELASTIC AND MECHANICALLY-OPEN FRACTURE

3.1 OBJECTIVES

In this Chapter, we study transient pressurization due to the injection of a fluid at a constant volumetric flow rate into a pre-existing, stationary crack (Fig. 2.1) in a critically over-pressured reservoir, $p_0 \simeq \sigma_0$.

We start with investigating the conditions when the pressure drop in the crack is negligible, and, therefore, the pressure along the crack can be considered approximately uniform.

3.2 CONDITIONS FOR A UNIFORM PRESSURE DISTRIBUTION ALONG THE CRACK

3.2.1 Case of impermeable rock

Considering the case of impermeable rock first, the fluid flow along the fracture is described by lubrication equation (2.11) with $\bar{g} = 0$. We can define the non-dimensional time ($\tau = t/t_*$), coordinate ($\xi = x/\ell$), and pressure ($\Pi = p/p_*$) using the characteristic time $t_* = \left(\mu \ell^5 h^4 / E' Q_0^3\right)^{1/4}$, length ℓ, and pressure $p_* = \left(\mu Q_0 E'^3 \ell / h^4\right)^{1/4}$ scales, respectively, and non-dimensionalize the lubrication equation (2.11) and initial-boundary conditions (2.12) accordingly. Note that the induced crack width for a mechanically-open fracture (2.2) is used to obtain the height average crack opening (equation $(2.3)_a$). The resulting normalized equations, parametrized by a single non-dimensional neutral opening parameter

$$\mathcal{W}_0 = w_0 \left(\frac{E'}{\mu Q_0 \ell}\right)^{1/4}, \tag{3.1}$$

and numerical method of their solution are discussed in Appendix B.

Figure 3.1a shows the evolution of the normalized pressure with time at selected positions ξ along the crack in an impermeable rock in the case when the neutral crack opening is null ($\mathcal{W}_0 = 0$). The solution assuming a uniform pressure distribution along the crack (as later obtained in Section 3.4) is shown by a dashed line for comparison. As expected, for large enough time, the pressure equilibrates along the crack. We can define "uniformity" pressure (Π_{uni}) and time (τ_{uni}) thresholds corresponding to the 5% difference between the inlet and the tip values of pressure. Based on the numerical solution (Fig. 3.1a), the dimensional uniformity pressure and time are

$$\bar{p}_{uni} = 1.94 \left(\frac{\mu Q_0 \ell E'^3}{h^4} \right)^{1/4}, \qquad t_{uni} = 5.89 \left(\frac{\mu \ell^5 h^4}{E' Q_0^3} \right)^{1/4}, \tag{3.2}$$

respectively.

Allowing for a non-zero neutral opening (Appendix B) shows that the uniformity pressure and time are decreasing functions of $\mathcal{W}_0$ (Fig. B.1). In other words, the uniformity values for $\mathcal{W}_0 = 0$ reported in (3.2) provide the upper bound of the uniformity conditions for the case of impermeable rock.

3.2.2 Case of permeable rock

Relaxing the assumption of impermeable rock and solving the corresponding set of equations numerically (Appendix B), we can show that the uniformity pressure $\bar{p}_{uni}$ remains practically unchanged from its value for the impermeable case (equation (3.2)), if

$$\mathbb{K} = k \left(\frac{\ell^{1/3} E'}{Q_0 \mu} \right)^{3/4} \lesssim 1. \tag{3.3}$$

Here, $\mathbb{K}$ is a non-dimensional permeability parameter, and, as we exemplify further, condition (3.3) is typically satisfied for reservoir applications. We also note that the uniformity time t_{uni} does depend on $\mathbb{K}$ in the range (3.3) (see Appendix B for details). An example of pressure evolution with time in the case of a permeable rock

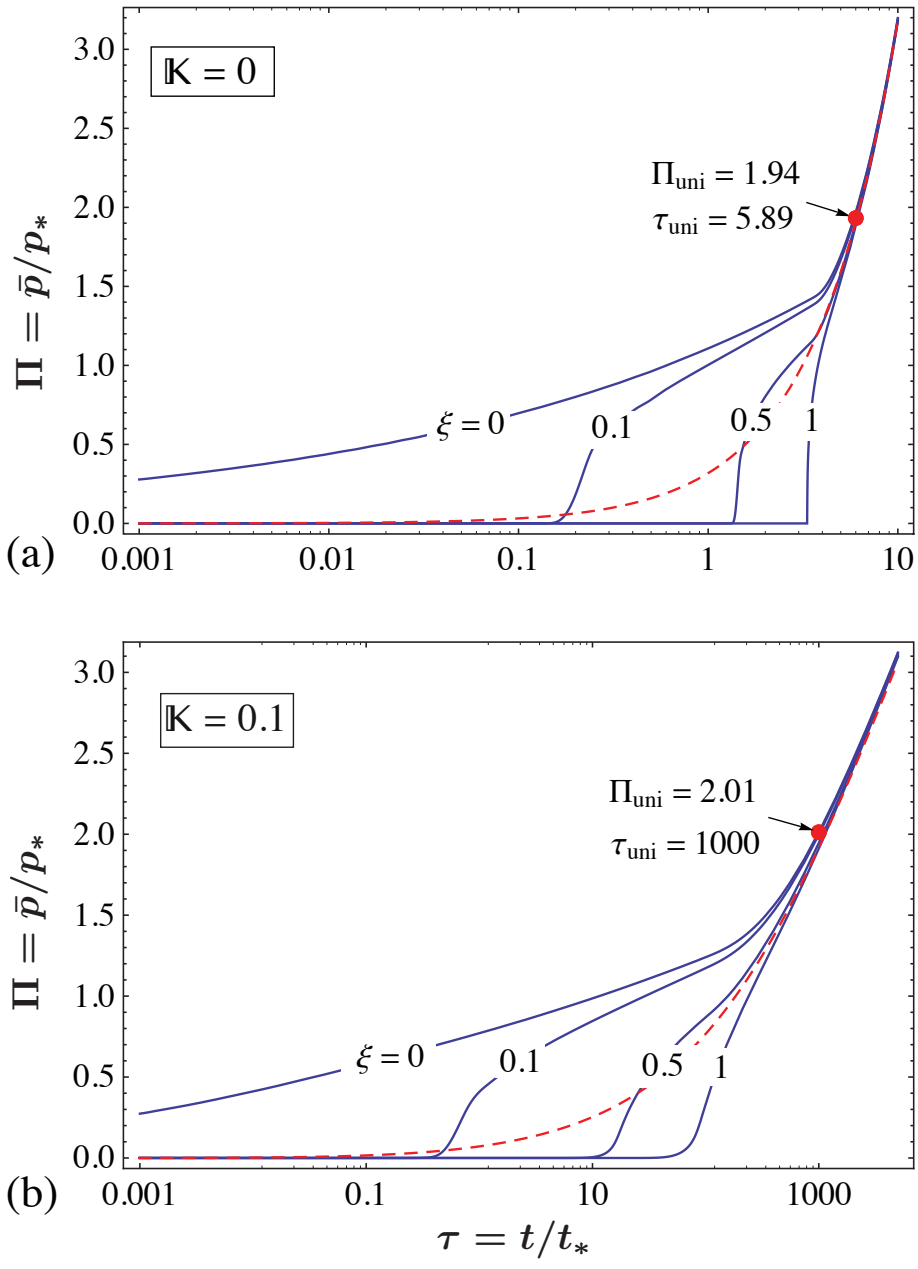

Figure 3.1: Injection at a constant rate into a crack in (a) impermeable rock ($\mathbb{K} = 0$), and (b) permeable rock ($\mathbb{K} = 0.1$): evolution of the normalized net pressure $\Pi = \bar{p}/p_*$ with normalized time $\tau = t/t_*$ at selected positions along the crack $\xi = x/\ell = 0$ (inlet), $0.1, 0.5, 1$ (tip) in the case of zero neutral crack opening ($\mathcal{W}_0 = 0$). The characteristic pressure and time scales are $p_* = \left(\mu Q_0 E'^3 \ell/h^4\right)^{1/4}$ and $t_* = \left(\mu \ell^5 h^4/E' Q_0^3\right)^{1/4}$, respectively. Marked points correspond to the onset of approximate pressure uniformity in the crack.

with $\mathbb{K} = 0.1$ is shown in Fig. 3.1b.

In summary, we showed that the solution based on the uniformity pressure assumption is approximately valid when $\bar{p} \gtrsim \bar{p}_{uni}$, with $\bar{p}_{uni}$ given by $(3.2)_a$, and, in particular, it can be used to predict the breakdown when $\bar{p}_B \gtrsim \bar{p}_{uni}$.

3.3 AUXILIARY PROBLEM: STEP PRESSURE INCREASE IN CRACK

In order to facilitate the solution of the transient pressurization problem, we first revisit the fundamental solution to an auxiliary problem of a step pressure increase in crack, due to Detournay and Cheng [57], and introduce a new result for the large time asymptote of this problem. This fundamental solution is then used to formulate and solve a convolution integral equation governing the solution for the transient pressurization.

Consider a fracture subjected to a step pressure increase,

$$p = 1, \quad (|x| < \ell,\, y = 0,\, t > 0). \tag{3.4}$$

To facilitate solution of (2.16) with (3.4), we rewrite it in the normalized form

$$1 = \frac{1}{\pi} \int_0^{\tau} \int_{-1}^{1} \psi(\xi', \tau') \exp\left(-\frac{\left|\xi - \xi'\right|^2}{\tau - \tau'} \right) \frac{d\xi' d\tau'}{\tau - \tau'}, \tag{3.5}$$

where the non-dimensional time (τ), coordinate (ξ), leak-off rate (ψ), and cumulative leak-off volume (Φ) are defined as,

$$\tau = \frac{t}{t_*}, \quad \xi = \frac{x}{\ell}, \quad \psi = \frac{\bar{g}}{\bar{g}_*}, \quad \Phi = \frac{V_{leak}}{V_*}, \tag{3.6}$$

in terms of the respective scales,

$$t_* = \frac{\ell^2}{4\alpha}, \quad \ell, \quad \bar{g}_* = \frac{4\alpha S}{\ell}, \quad V_* = Sh\ell^2. \tag{3.7}$$

After applying Laplace transform, (3.5) becomes

$$\frac{1}{s} = \frac{2}{\pi} \int_{-1}^{1} \hat{\psi}(\xi', s) K_0 \left(2\sqrt{s} |\xi - \xi'| \right) d\xi', \tag{3.8}$$

where K_0 is the modified Bessel function of the second kind, s is the transform variable, and $\hat{\psi}(\xi, s)$ is the Laplace image of $\psi(\xi, \tau)$.

Before integral convolution equation (3.8) is treated numerically, it is useful to consider its small and large time asymptotes. When the characteristic length scale for fluid diffusion $\sqrt{\alpha t}$ is small compared to the crack size ℓ, or in terms of the normalize time, $\tau \ll 1$, the fluid diffusion pattern is approximately 1-D, and the solution for the normalized leak-off rate is given by [57, 67]:

$$\psi(\tau) = \frac{1}{\sqrt{\pi \tau}} \quad (\tau \ll 1). \tag{3.9}$$

As time increases, the 1-D fluid diffusion pattern is no longer valid and a 2-D fluid diffusion pattern must be considered. For long enough injection time, we establish in Appendix C the asymptotic expressions for the fluid leak-off rate in the Laplace domain,

$$\hat{\psi}(\xi, s) = -\frac{1}{\sqrt{1 - \xi^2}} \frac{1}{s \left(\ln(s/4) + 2\gamma \right)} \quad (s \ll 1), \tag{3.10}$$

($\gamma \approx 0.5772$ is the Euler's constant), and the time,

$$\psi(\xi, \tau) = \frac{1}{\sqrt{1 - \xi^2}} \left(\frac{1}{\ln 4\tau - \gamma} - \frac{\pi^2}{6} \frac{1}{(\ln 4\tau - \gamma)^3} + ... \right), \quad (\tau \gg 1), \tag{3.11}$$

domains. Equation (3.11) improves on the earlier $O(1/\ln \tau)$ result [57], and allows for much more accurate representation of the large-time leak-off solution.

The solution of (3.8) for the intermediate values of Laplace variable s is obtained numerically by Gauss-Chebyshev quadratures (Appendix D). The result is inverted

to the time domain using Stehfest algorithm [68]. Figure 3.2 shows the numerical solution $\psi(\xi,\tau)$, contrasted to the small (3.9) and large time asymptotes (3.11).

The normalized cumulative leak-off volume,

$$\Phi(\tau) = \int_0^\tau \int_{-1}^1 \psi(\xi,\tau)\, d\xi d\tau, \tag{3.12}$$

is shown on Fig. 3.3. Its small time asymptote follows from (3.9) in the form

$$\Phi(\tau) = \frac{4}{\sqrt{\pi}}\sqrt{\tau}, \quad (\tau \ll 1). \tag{3.13}$$

The large-time asymptote follows from integration of (3.12) with $\psi(\xi,\tau)$ given by (3.11),

$$\Phi(\tau) \approx \left(\frac{\pi}{4} - \frac{\pi^3}{48}\right) e^\gamma \,\mathrm{Ei}\,(\ln 4\tau - \gamma) + \frac{\pi^3\tau}{12}\left[\frac{1}{\ln 4\tau - \gamma} + \frac{1}{(\ln 4\tau - \gamma)^2}\right] + ..., \quad (\tau \gg 1), \tag{3.14}$$

where Ei is the exponential integral function.

3.4 TRANSIENT PRESSURIZATION PROBLEM: CONSTANT RATE OF INJECTION INTO A CRACK

Assuming a uniform pressure along the crack, i.e. $\bar{p} \gtrsim \bar{p}_{uni}$, where $\bar{p}_{uni}$ given by $(3.2)_a$, the cumulative leak-off volume V_{leak} can be obtained by applying the Duhamel's theorem [67]

$$V_{leak}(t) = \int_0^t V_{\mathrm{aux}}(t-t') \frac{d\bar{p}}{dt'} dt', \tag{3.15}$$

where $V_{\mathrm{aux}}(t) = \ell^2 h S\, \Phi_{\mathrm{aux}}(4\alpha t/\ell^2)$ is the cumulative leak-off volume of the fracture subjected to a unit step pressure increase, with $\Phi_{\mathrm{aux}}(\tau)$ given in Fig. 3.3.

The elastic dilation of the finger crack volume due to the uniform net pressure

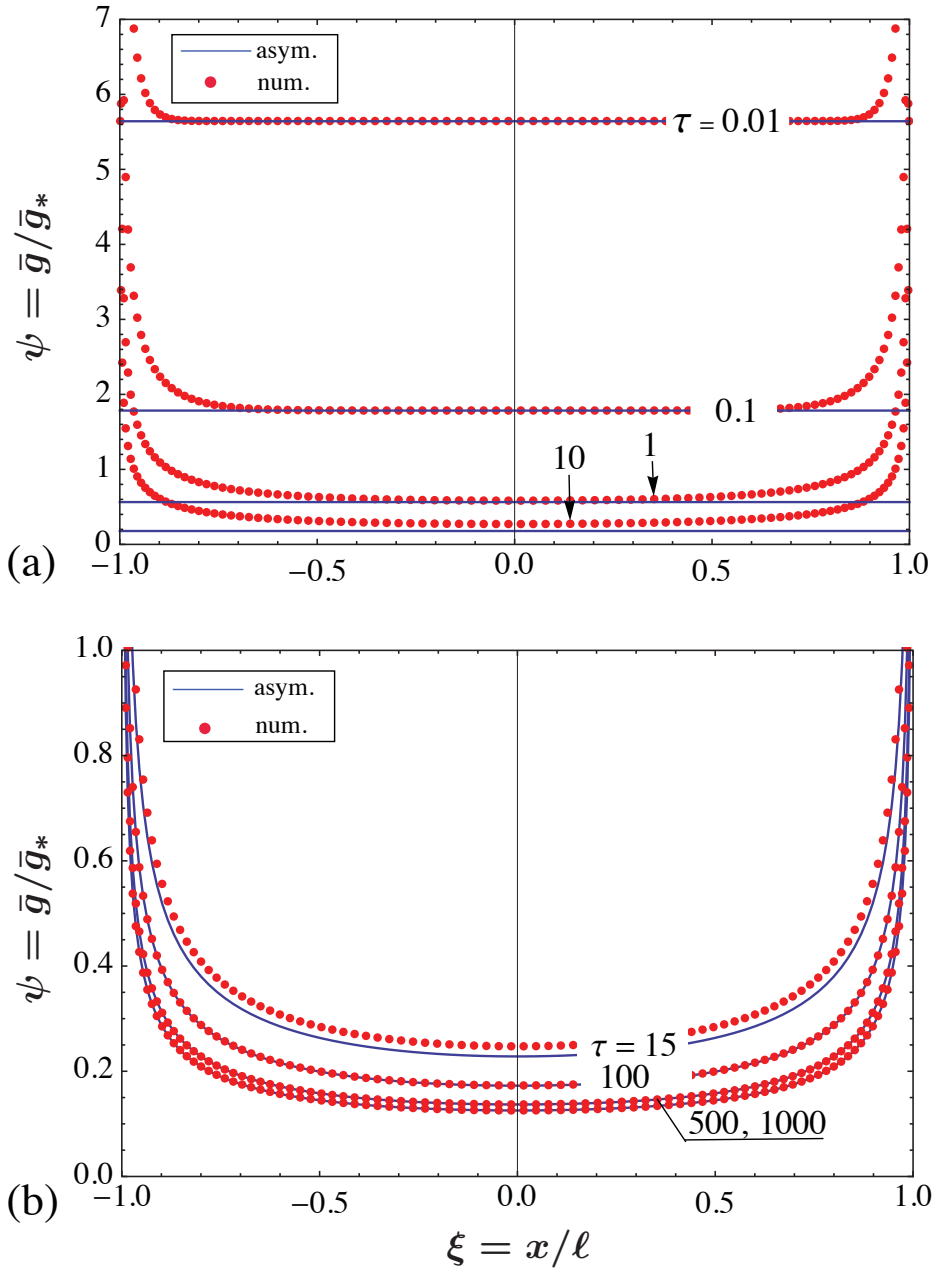

Figure 3.2: Comparison of the numerical solution for the normalized leak-off rate in the auxiliary problem of an instantaneous step pressure increase with (a) the small time (equation (3.9)), and (b) the large-time (equation (3.11)) asymptotes shown as dashed red lines. The time and leak-off rate scales are $t_* = \ell^2/4\alpha$ and $\bar{g}_* = 4S\alpha/\ell$, respectively.

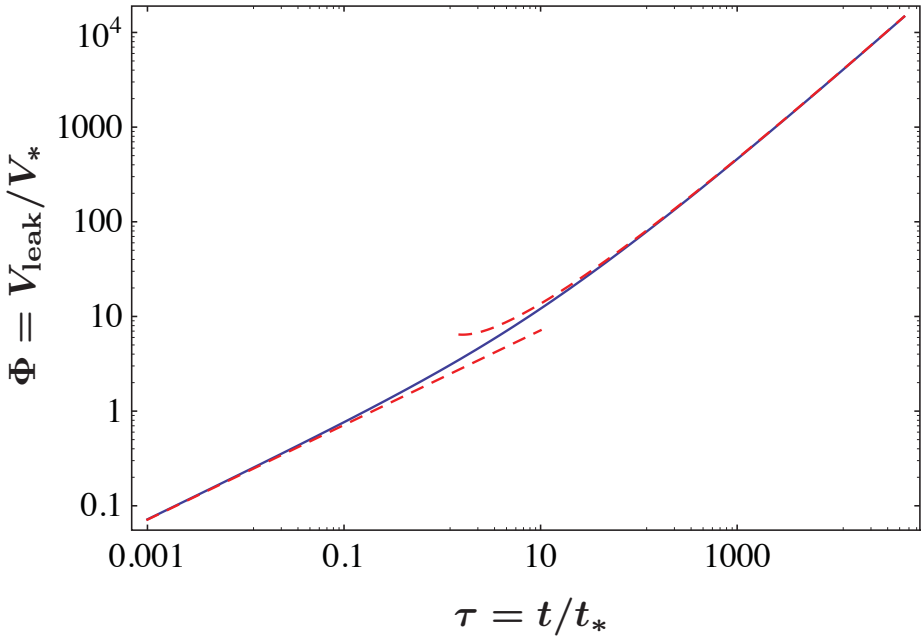

Figure 3.3: Evolution of the cumulative leak-off volume in the auxiliary problem (step pressure increase along the crack). The numerical solution is contrasted to small (3.13) and large-time (3.14) asymptotes. The time and volume scales are $t_* = \ell^2/4\alpha$ and $V_* = hS\ell^2$, respectively.

$\bar{p} > 0$ is obtained from (2.4) as:

$$\Delta V_{crack}\left(t\right) = \frac{\pi h^2 \ell}{E'} \bar{p}\left(t\right). \tag{3.16}$$

In view of (3.15) and (3.16), the global volume balance (2.13) can be expressed as:

$$Q_0 t = \frac{\pi h^2 \ell}{E'} \bar{p}\left(t\right) + \ell^2 h S \int_0^t \Phi_{\text{aux}}\left(\frac{4\alpha(t-t')}{\ell^2}\right) \frac{d\bar{p}}{dt'} dt'. \tag{3.17}$$

Equation (3.17) governs the evolution of the net pressure in the crack, $\bar{p} = \bar{p}\left(t\right)$, and its solution is sought next.

The problem is characterized by three lengthscales: the time-dependent diffusion length $\sim \sqrt{4\alpha t}$, crack height h, and crack half-length ℓ ($\ell \gg h$). We, therefore, anticipate three different end-members, namely, the crack-storage-dominated regime when $\sqrt{4\alpha t} \ll h$, the 1-D leak-off dominated regime when $h \ll \sqrt{4\alpha t} \ll \ell$, and the 2-D leak-off dominated regime when $\sqrt{4\alpha t} \gg \ell$. It is then convenient to define the corresponding "1-D" and "2-D leak-off" time and net-pressure scales as

$$t_1 = \frac{1}{\left(SE'\right)^2} \frac{h^2}{4\alpha}, \qquad p_1 = \frac{Q_0 t_1}{h^2 \ell} E' \tag{3.18}$$

$$t_2 = \frac{\ell^2}{4\alpha}, \qquad p_2 = \frac{Q_0 t_2}{\ell^2 h} \frac{1}{S}, \tag{3.19}$$

such that the three end-member regimes correspond to $t \ll t_1$ (storage), $t_1 \ll t \ll t_2$ (1-D leak-off), and $t \gg t_2$ (2-D leak-off), respectively. The pressure scales in (3.18) and (3.19) follow from balancing the injection volumes over the corresponding characteristic times, i.e. $Q_0 t_1$ and $Q_0 t_2$, with the crack-storage ΔV_{crack} and the leak-off V_{leak} volumes, respectively.

Let us write the governing equation (3.17) in the 2-D scaling, (3.19), using non-

dimensional variables $\Pi = \bar{p}/p_2$ and $\tau = t/t_2$,

$$\tau = \pi \mathcal{A}\, \Pi(\tau) + \int_0^\tau \Phi_{\text{aux}}(\tau - \tau^{'}) \frac{d\Pi(\tau^{'})}{d\tau^{'}} d\tau^{'}. \tag{3.20}$$

Its solution in Laplace domain is given by

$$\hat{\Pi}(s) = \frac{1}{s^2 \left(\pi \mathcal{A} + s\, \hat{\Phi}_{\text{aux}}(s) \right)}, \tag{3.21}$$

where

$$\mathcal{A} = \frac{p_1}{p_2} = \sqrt{\frac{t_1}{t_2}} = \frac{1}{SE'} \frac{h}{\ell} \tag{3.22}$$

is the dimensionless parameter with the meaning of a scaled crack aspect-ratio, which is expected to be small for fingerlike cracks since $h \ll \ell$ and $SE^{'} \gtrsim 1$ for rock. Note that $\hat{\Pi}$ and $\hat{\Phi}_{\text{aux}}$ are the Laplace images of Π and Φ_{aux}, respectively.

For $\tau = t/t_2 \ll 1$, $\Phi_{\text{aux}}(\tau) \simeq 4\sqrt{\tau/\pi}$, and (3.20) can be solved explicitly by the Laplace transform method. This solution is more conveniently written in the 1-D scaling, (3.18),

$$\frac{\bar{p}}{p_1} = \frac{\pi}{4} \left[\text{Erfc} \left(\frac{2}{\pi} \sqrt{\frac{t}{t_1}} \right) \exp \left(\frac{4}{\pi^2} \frac{t}{t_1} \right) - 1 \right] + \sqrt{\frac{t}{\pi t_1}}, \quad (t \ll t_2)\,. \tag{3.23}$$

The solution in the storage ($t \ll t_1$) and the 1-D leak-off ($t_1 \ll t \ll t_2$)[1] dominated regimes are recovered as appropriate end-members of (3.23)

$$\frac{\bar{p}}{p_1} = \frac{t}{\pi t_1}, \quad (t \ll t_1)\,, \qquad \frac{\bar{p}}{p_1} = \sqrt{\frac{t}{\pi t_1}} - \frac{\pi}{4}, \quad (t_1 \ll t \ll t_2)\,. \tag{3.24}$$

For $\tau = t/t_2 \gg 1$, the storage term ($\propto \mathcal{A}$) in equations (3.20) and (3.21) is negligible, and $\hat{\Phi}_{\text{aux}}(s) = \pi/s^2 \left[\ln(4/s) - 2\gamma \right]$, as follows from integrating (3.10) over

[1]Existence of 1-D leak-off regime relies on separation of timescales, $t_1 \ll t_2$, or $\mathcal{A} \ll 1$ (equation (3.23))

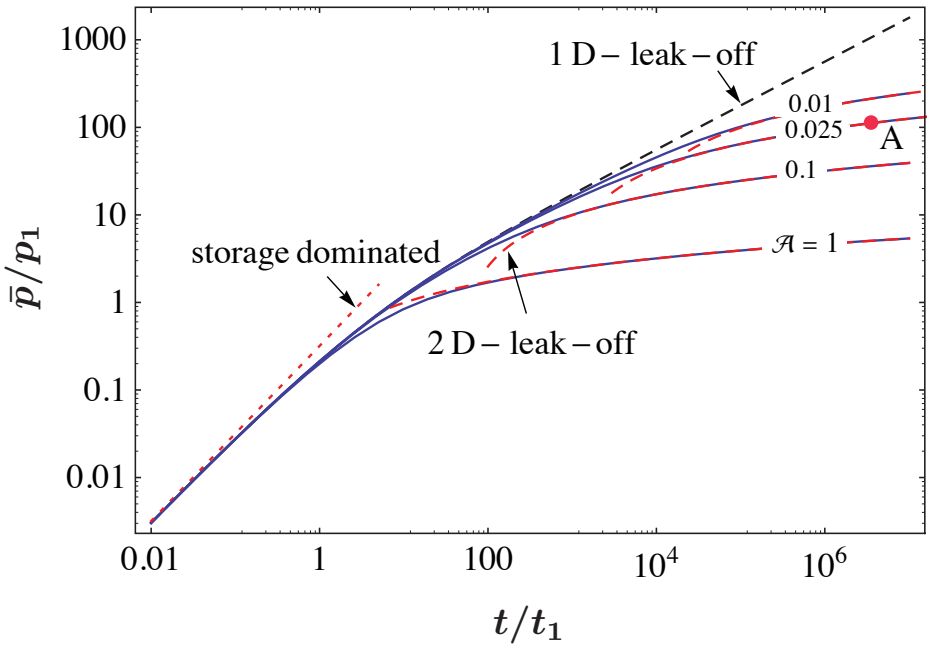

Figure 3.4: Evolution of the normalized net pressure $\bar{p}/p_1$ during the transient pressurization of a crack for various values of the crack aspect ratio parameter $\mathcal{A} = h/(\ell SE')$. The 1-D (equation (3.23)) and 2-D (equation (3.25)) leak-off asymptotic solutions are shown by black and red dashed lines, respectively. The dotted line shows the early time storage-dominated solution, (equation $(3.24)_a$). The 1-D pressure and time scales are $p_1 = Q_0 E' t_1/h^2\ell$ and $t_1 = (1/SE')^2(h^2/4\alpha)$, respectively.

the crack length. Resulting solution for the 2-D leak-off dominated regime is

$$\frac{\bar{p}}{p_2} = \frac{1}{\pi}\left[\ln\frac{4t}{t_2} - \gamma\right], \quad (t \gg t_2)\,. \tag{3.25}$$

In the intermediate time range, $t_1 \lesssim t \lesssim t_2$, solution is obtained by numerically evaluating the inverse Laplace transform of (3.21). Figure 3.4 shows the solution for the transient pressurization for several values of the aspect ratio parameter $\mathcal{A}$, contrasted to the 1-D (equation (3.23)) and the 2-D (equation (3.25)) leak-off asymptotic solutions shown by dashed lines. The dotted line shows the early time storage-dominated solution (equation $(3.24)_a$).

The "uniformity" pressure (equation $(3.2)_a$) expressed in the 1-D scaling,

$$\frac{\bar{p}_{uni}}{p_1} = 7.76\frac{\mathbb{K}}{\mathcal{A}}, \tag{3.26}$$

($\mathbb{K}$ and $\mathcal{A}$ are the previously defined non-dimensional permeability (equation (3.3)) and crack aspect-ratio (equation (3.22)) parameters, respectively), can be used together with the solution in Fig. 3.4 to infer the "uniformity" time t_{uni}/t_1.

Extension of the solution to the plane-strain (KGD) crack

Although the main focus of this paper is on fingerlike ($h \ll \ell$) cracks, we note that our transient pressurization solution can be easily translated to the case of the plane-strain, KGD (Khristianovic, Zheltov, Geertsma, de Klerk [28, 30]) crack ($h \gg \ell$). This is accomplished by replacing the expression (3.16) for the elastic crack volume ΔV_{crack} in global balance for fingerlike crack (3.17) by the volume of the plane-strain crack of height h and half-length ℓ [e.g., 69],

$$\Delta V_{crack}(t) = \frac{2\pi h\ell^2}{E'}\bar{p}(t), \quad (h \gg \ell). \tag{3.27}$$

The plane-strain crack solution is obtained from the fingerlike crack solution presented in the above by replacing the 1-D-leak-off time and pressure scales[2], (3.18), with

$$t_1^{\mathrm{KGD}} = \left(\frac{2}{SE'}\right)^2 \frac{\ell^2}{4\alpha}, \qquad p_1 = \frac{Q_0 t_1^{\mathrm{KGD}}}{2\ell^2 h}E', \tag{3.28}$$

respectively, and parameter $\mathcal{A}$, (3.22), with $\mathcal{A}^{\mathrm{KGD}} = 2/SE'$.

Application in well testing analysis of fractured wells

It is worthwhile to mention that the results of this study can be used in the production pressure transient data analysis (well testing) of a propped hydraulic fracture (i.e. a

[2]Note that the 2-D scales, (3.19), are the same for the two crack geometries.

fracture filled with particulate materials during the fracturing treatment, which purpose is to prevent/minimize the fracture closure during production pressure decline.) The pressure transient formulation in the production context is obtained from the injection problem by reversing the direction of volumetric flow rate Q_0 and reasonably neglecting changes of a propped hydraulic fracture volume (in response to pressure decline in production). Thus, we can use the analysis of this study in production well testing of a fractured well by nullifying the storage term in global volumetric balance equation (3.20), i.e. setting $\mathcal{A} = 0$, and changing the sign of the left hand side (i.e., flow reversal).

3.5 BREAKDOWN CALCULATION EXAMPLE

Consider synthetic example of fracture breakdown calculations for a supercritical CO_2 injection in a sandstone formation characterized by porosity $\phi = 0.17$, permeability $k = 13$ md, minimum in-situ stress $\sigma_0 = 30.8$ MPa, ambient pore pressure $p_0 = 20$ MPa, rock toughness $K_{Ic} = 1$ MPa m$^{1/2}$, Young's modulus $E = 6$ GPa, Poisson's ratio $\nu = 0.2$, and average reservoir temperature $T = 90^0$C [70, 71]. The supercritical CO_2 is assumed to be injected at the total mass flow rate $\dot{m} = 100$ t/day into a single vertical, fingerlike fracture with half-length $\ell = 50$ m, height $h = 20$ m (assumed to span the height of the sandstone layer), and neutral hydraulic opening $w_0 = 0.4$ mm. The latter value corresponds to the measured neutral opening of a highly weathered fracture [72].

Assuming an over-pressurized reservoir, $p_0 \simeq \sigma_0$, the supercritical CO_2 can be considered as an incompressible fluid until the onset of propagation, forecasted to take place when the fluid net-pressure reaches breakdown value $\bar{p}_B \simeq 0.25$ MPa (based on equation (2.8) and the assumed values of reservoir/fracture parameters). The representative values for the supercritical CO_2 properties are calculated at the breakdown pressure $p_B = 31.05$ MPa and average reservoir temperature $T = 90^0$C:

density $\bar{\rho} = 714$ kg/m^3, viscosity $\mu = 0.06$ cp, and bulk compressibility $c_t = 15.9$ GPa.

In view of the above, we have $Q_0 = 0.0016$ m^3/s (volumetric injection rate), $S = 2.7$ GPa^{-1} (storage), $\alpha = 0.08$ m^2/s (diffusivity coefficient), $t_1 = 4.4$ seconds (time scale), $p_1 = 2.2$ KPa (pressure scale), $\mathcal{A} = 0.024$ (non-dimensional aspect ratio parameter), $\mathbb{K} = 0.14$ (non-dimensional permeability parameter), and $\mathcal{W}_0 = 2.4$ (non-dimensional neutral hydraulic crack opening parameter). The corresponding upper bound of the uniformity pressure is $\bar{p}_{uni,\mathcal{W}_0=0} = 0.1$ MPa (equation (3.26)), while the actual value for this particular example ($\mathcal{W}_0 = 2.4$) can be inferred from Fig. B.1, $\bar{p}_{uni} = 0.05$ MPa. Since $\bar{p}_B > \bar{p}_{uni}$, the analysis based on the pressure uniformity assumption is deemed to be valid. Locating the point with $\bar{p}_B/p_1 = 112$ (and on $\mathcal{A} = 0.024$) on Fig. 3.4 (point A), the onset of the fracture propagation is forecasted at $t_B/t_1 = 3.6 \times 10^6$, or in $t_B \simeq 183.3$ days from the beginning of the injection.

We note possible limitations of our solution in application to realistic reservoir injection scenarios are related to the assumptions of (i) a critically pressurized reservoir (ambient pore pressure equal to the minimum in-situ stress, $p_0 \simeq \sigma_0$), (ii) negligible poroelastic (backstress) effects [10], and (iii) a single injected fracture (or non-interacting multiple fractures). In view of the first assumption, the predicted breakdown time t_B from our analysis is a lower bound for a more realistic reservoir case with $p_0 < \sigma_0$, when the value of t_B in our analysis has to be augmented by the time it takes to pressurize the fracture to $p = \sigma_0$.

3.6 SUMMARY OF CHAPTER RESULTS

Important applications of injection of a low viscosity fluid into a pre-existing fracture, such as waterflooding, wastewater and supercritical CO_2 injection for geological storage, necessitate a comprehensive study of mechanical and hydraulically properties of

fractures from the beginning of injection.

To this end, we have studied model describing the transient pressurization of an un-propped fingerlike crack in a critically over-pressured reservoir. We established the range of the problem parameters and injection time when the fluid pressure is approximately uniform along the crack. Assuming uniform pressure distribution, we first revisited the auxiliary problem of a crack subjected to step pressure increase [57], which then allowed us to formulate and solve for the transient crack pressurization (due to constant rate of injection) using the Green's function approach. As the fracture is pressurized, the condition for the onset of propagation (the breakdown condition) is eventually reached. We have quantified how the breakdown of a fingerlike fracture depends upon the rock and fluid properties, the in-situ stress and the fluid injection rate; and how one can translate these results to another (KGD) fracture geometry. An example of the breakdown calculations for a supercritical CO_2 injection into a fingerlike crack was also considered.

CHAPTER 4: POROELASTIC EFFECTS ON THE TRANSIENT PRESSURIZATION OF A MECHANICALLY-OPEN FRACTURE

4.1 OBJECTIVES

The primary focus of this Chapter is to investigate the poroelastic effects on the transient pressurization and onset of fracture propagation for a fingerlike crack in a critically over-pressured reservoir (i.e., $p_0 \simeq \sigma_0$). In Chapter 3, we assumed that a fluid is injected into a pre-existing fracture while the poroelastic effects were neglected. However, during injection of a low viscosity fluid characterized by large fluid leak-off to the surrounding rock, the mechanical properties of the formation can be modified due to the poroelastic effects. The dilation of porous rock as the result of increase in the pore pressure is one of the key mechanism of interaction between the fluid and the porous rock [10]. The dilation of the rock may lead to the generation of an additional confining stress ("backstress").

In this Chapter, the following assumptions are used. 1) The fluid pressure in the fracture is assumed to be spatially uniform (i.e., viscous dissipation in the flow is negligible). The parametric range corresponding to the validity of this assumption was established in Chapter 3. 2) The initial hydraulic opening of the fracture corresponding to zero initial net loading is neglected. The effect of the latter on the transient pressurization was investigated in Chapter 3. 3) The weak coupling of the pore pressure to the stress changes is neglected [57].

The mechanical response of crack to the transient pressurization $p = p(t)$ can be obtained using Green's function approach, where the Green's function corresponds to the solution of an auxiliary problem of a unit step pressure change in a crack [53, 57], which we revisit in the following.

4.2 POROELASTIC AUXILIARY PROBLEM (STEP PRESSURE CHANGE IN THE CRACK)

Following Detournay and Cheng [53, 57], the loading on the crack can be decomposed into two fundamental modes. Mode 1 corresponds to a unit rise of normal traction at the crack surface with no pore pressure change:

$$\text{Mode 1:} \qquad \sigma_{yy}^{(1)} = -1, \quad p^{(1)} = 0, \quad (|x| < \ell,\, y = 0,\, t > 0). \tag{4.1}$$

Mode 2 corresponds to a step pore pressure increase along the crack with no stress change:

$$\text{Mode 2:} \qquad \sigma_{yy}^{(2)} = 0, \quad p^{(2)} = 1, \quad (|x| < \ell,\, y = 0,\, t > 0). \tag{4.2}$$

Simple superposition of solutions under the mode 1 and mode 2 loadings can be used to find the fracture opening, fracture volume, cumulative leak-off volume, and generated poroelastic backstress in the auxiliary problem of step pressure change in the crack.

The mode 1 and 2 poroelastic solutions were obtained for a plane-strain crack in [57] and later extended by the same authors to the case of a fingerlike crack [53]. These latter solutions (particularly for that mode 2 loading) relied on the assumption of 1-D pore pressure diffusion, which limits their applicability. In the following we recount main results of [53] and extend their solution by relaxing the 1-D assumption.

The following discussion of the transient poroelastic response of a crack due to a step loading will make use of two fundamental timescales:

$$t_{1\mathrm{D}} = \frac{h^2}{4\alpha}, \qquad t_{2\mathrm{D}} = \frac{\ell^2}{4\alpha}, \tag{4.3}$$

which pertain to the pore pressure diffusion on the spatial scales corresponding to the fingerlike crack height (h) and half-length ($\ell \gg h$), respectively. These timescales

therefore can be associated with the 1-D (on the scale h or smaller) and 2-D (on the scale ℓ or large) diffusion.

4.2.1 Poroelastic mode 1 crack opening

The response of the crack to the mode 1 unit loading can be approximated as purely elastic on the assumption of small (negligible) solid-to-fluid poroelastic coupling [53, 57]. The corresponding average opening over a given x cross-section of a poroelastic fingerlike crack due to the mode 1 is given by

$$\bar{w}^{(1)}(x,t) = \frac{\pi h}{2E'}. \tag{4.4}$$

The aforementioned assumption neglects the difference between the initial (undrained) response to the mode 1 loading and the final, after a time transient, drained response, as given by (4.4); and can be justified when the values of the Poisson's ratio of poroelastic solid under drained and undrained conditions are similar [53].

4.2.2 Poroelastic mode 2 crack opening

The mode 2 component of the opening can be obtained using the reciprocity [53]

$$\bar{w}^{(2)}(x,t) = \frac{2b}{h} \int_0^{\infty} \int_{-h/2}^{h/2} p^{(2)}(x,y,t) \epsilon^{(1)}(y,z)\, dydz, \tag{4.5}$$

where b is the Biot coefficient, $\epsilon^{(1)}$ is the mode 1 elastic volumetric deformation corresponding to the field around uniformly pressurized plane-strain crack section

$$\epsilon^{(1)}(y,z) = \frac{2(1-2\nu)}{\pi E'(1-\nu)} \int_{-h/2}^{h/2} \frac{2z'(z-z')dz'}{\sqrt{h^2-4z'^2}\,[(z-z')^2+y^2]}, \tag{4.6}$$

and $p^{(2)}(x,y,t)$ is the pore pressure change due to the mode 2 loading.

Due to the presence of the impermeable cap rock boundaries at $z = \pm h/2$ and pressure equilibrium in a vertical cross section ($\partial p/\partial z = 0$), the pore pressure diffusion problem is two dimensional. The mode 2 pore pressure field can be expressed as a convolution integral in space (along the crack) and time of the instantaneous point source solution [67]

$$p^{(2)}(x,y,t) = \int_0^t \int_{-\ell}^{\ell} \frac{\bar{g}^{(2)}(x',t')}{4\pi S\alpha(t-t')} \exp\left(-\frac{(x-x')^2+y^2}{4\alpha(t-t')}\right) dx'\,dt', \tag{4.7}$$

where $\bar{g}^{(2)}$ is the mode 2 local fluid leak-off rate, which solution,

$$\bar{g}^{(2)}(x,t) = \frac{4\alpha S}{\ell}\,\psi^{(2)}\left(\frac{x}{\ell}, \frac{t}{t_{2D}}\right), \tag{4.8}$$

is expressed here in terms of the normalized leak-off rate $\psi^{(2)}(\xi,\tau)$ function of the normalized position along the crack $\xi = x/\ell$ and time $\tau = t/t_{2D}$ (where timescale $t_{2D} = \ell^2/4\alpha$, (4.3)). The latter was obtained in Chapter 3 and shown in Fig. 3.2.

Substituting expression (4.6) for $\epsilon^{(1)}$ in (4.5) and integrating in z allows to find the general expression for the average opening in mode 2 [53], which is expressed below as a multiple of the mode 1 opening value, (4.4),

$$\bar{w}^{(2)}(x,t) = -2\eta F(x,t)\bar{w}^{(1)}, \tag{4.9}$$

where $\eta = b\,(1-2\nu)\,/2\,(1-\nu)$ is the poroelastic stress coefficient, and

$$F(x,t) = \frac{8}{\pi h}\int_0^{\infty} p^{(2)}(x,y,t)G\,(2y/h)\,dy, \qquad G\,(\chi) = 1 - \sqrt{\frac{\chi}{2}}\sqrt{\sqrt{4+\chi^2}-\chi} \tag{4.10}$$

are the temporal and spatial influence functions, respectively. Note that $F(x,t)$ is varying from 0 and 1 as time varies from 0 to ∞.

Evaluation of influence function $F(x,t)$

The problem of finding the crack opening due to the mode 2 loading has been reduced to evaluating the influence function $F(x,t)$ given by an integral (4.10) of the pore pressure field (equations (4.7) with (4.8) and Fig. 3.2).

Detournay and Cheng [53] considered the early-time asymptotics of the pore pressure solution, when the spatial scale of the leak-off diffusion diffusion in the direction normal to the crack plane $\sim \sqrt{\alpha t}$ is small compared to the crack half-length ℓ, given by the well-known 1-D diffusion solution [67]

$$t \ll t_{2D}: \qquad p^{(2)}(x,y,t) \approx \operatorname{Erfc}\left(\frac{y}{2\sqrt{\alpha t}}\right) \tag{4.11}$$

with $t_{2D} = \ell^2/4\alpha$ been the previously defined 2-D diffusion timescale, (4.3). This leads to an approximate expression for the influence function [53]

$$t \ll t_{2D}: \qquad F(x,t) \simeq F_{1D}\left(t/t_{1D}\right), \qquad F_{1D}(\tau) \equiv \frac{4}{\pi}\int_0^\infty \operatorname{Erfc}\left(\frac{\chi}{2\sqrt{\tau}}\right) G\left(\chi\right) d\chi, \tag{4.12}$$

where $t_{1D} = h^2/4\alpha$ is the previously defined 1-D diffusion timescale, (4.3). Although integral expression for $F_{1D}(\tau)$ does not appear to be treatable analytically, a useful closed-form analytical expression can be obtained for its Laplace transform ($t/t_{1D} \to s$):

$$\hat{F}_{1D}(s) = \frac{4}{\pi s^{3/2}}\left(1 + \frac{\pi}{2}\left[\mathrm{J}_1(\sqrt{s})\cos\sqrt{s} + \mathrm{Y}_1(\sqrt{s})\sin\sqrt{s}\right]\right) \tag{4.13}$$

where J_1 and Y_1 are Bessel functions of the first and second kind, respectively, and 'hat' denotes the Laplace image.

The analytical solution of the 1-D influence function to the first order ($O(1)$) is given by

$$\hat{F}_{1D}(s \gg 1) \equiv \frac{4}{\pi s^{3/2}}, \qquad F_{1D}(t \ll t_{1D}) \equiv \frac{8\sqrt{t/t_{1D}}}{\pi^{3/2}}. \tag{4.14}$$

In the general case, when the diffusion is not limited to 1-D, we substitute expression (4.7) with (4.8) for $p^{(2)}$ into expression (4.10) for the influence function $F(x,t)$, and apply Laplace transform ($t/t_{2D} \rightarrow s$) to find:

$$\hat{F}(\xi, s) = \frac{8}{\pi^2} \int_{-1}^{1} \hat{\psi}^{(2)}(\xi', s) H(\xi, \xi', s) d\xi', \tag{4.15}$$

where

$$H(\xi, \xi', s) \equiv \int_{0}^{\infty} K_0 \left(2\sqrt{s\left[(\xi - \xi')^2 + (h/2\ell)^2 \chi^2\right]} \right) G(\chi) d\chi. \tag{4.16}$$

We tabulate function $H(\xi, \xi', s)$ numerically using Mathematica software, and then use this tabulation together with the previously tabulated leak-off rate solution $\hat{\psi}^{(2)}(\xi', s)$ (shown on Figure 3.2) to evaluate the integral in $\hat{F}(x,s)$ by the Gauss-Chebyshev method, as detailed in Chapter 3. The latter is then inverted to the time domain using the Stehfest algorithm [68].

Function $F(x,t)$ depends on a single parameter, crack aspect ratio h/ℓ. Numerical solution $F(x,t)$ is shown on Figure 4.1 for the case with $h/\ell = 0.1$, where it is also contrasted to the 1-D asymptote, (4.12), shown by dashed lines. As expected, $F(x,t)$ is closely approximated by the 1-D asymptote at early times everywhere along the crack with the exception of the near fracture tip regions (where the diffusion is inherently 2-D). This bulk approximation does deteriorate somewhat with increasing time, but still remains a fairly good, "first order" representation of F even for $t \sim t_{2D}$ (note that for this example, $t_{2D}/t_{1D} = (\ell/h)^2 = 100$) when the diffusion is fully 2-D. This surprising result can be understood by the recorse to the original expression for the mode 2 opening (4.5), for which influence function $F(x,t)$ is a proxy. In the integral for the former, the pore pressure field $p^{(2)}(x,y,t)$ is weighted by the mode 1 volumetric strain field $\epsilon^{(1)}(x,y,t)$, which tends to zero at distances y from the fracture plane in excess of few crack heights h. Thus, the influence of the "2-D character" of

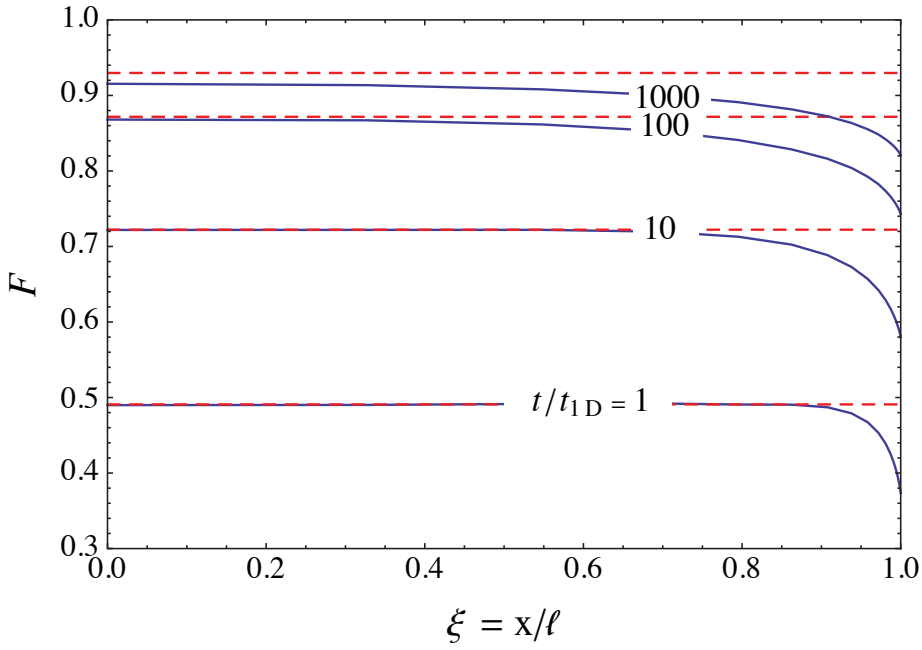

Figure 4.1: Comparison of the general numerical solution for the influence function $F(x,t)$ with its 1-D asymptote (equation (4.12)) for the case with $h/\ell = 0.1$. The time scale is $t_{1\mathrm{D}} = h^2/4\alpha$.

the pore pressure distribution at spatial scales $\sim \ell$ (i.e. much larger than h) on the crack opening is dampened by the vanishing strain at these scales, resulting in the approximate validity of the 1-D asymptote for $F(x,t)$ even when the pore pressure field is effectively 2-D.

The evolution of the crack-average of the influence function $\langle F \rangle (t) = (1/2\ell) \times \int_{-\ell}^{\ell} F(x,t)dx$ is shown on Fig. 4.2a for various values of the aspect-ratio ratio h/ℓ. (Note that the case with $h/\ell = 1$ contradicts the assumption of a fingerlike crack geometry, and, therefore, shown for reference only). The overall goodness of the crack-average $\langle F \rangle (t)$ approximation by its 1-D asymptote (4.12), shown in Fig. 4.2 by the dashed line, is evident for all but very large times ($t \gg t_{2\mathrm{D}}$).

In contrast to the above behavior of the crack-average value, and owing to the inherently two-dimensionality of the near crack tip regions (Fig. 4.1), the tip value of the influence function, $F(x = \pm\ell, t)$ is significantly different from the 1-D asymptotic solution at all times (Fig. 4.2b).

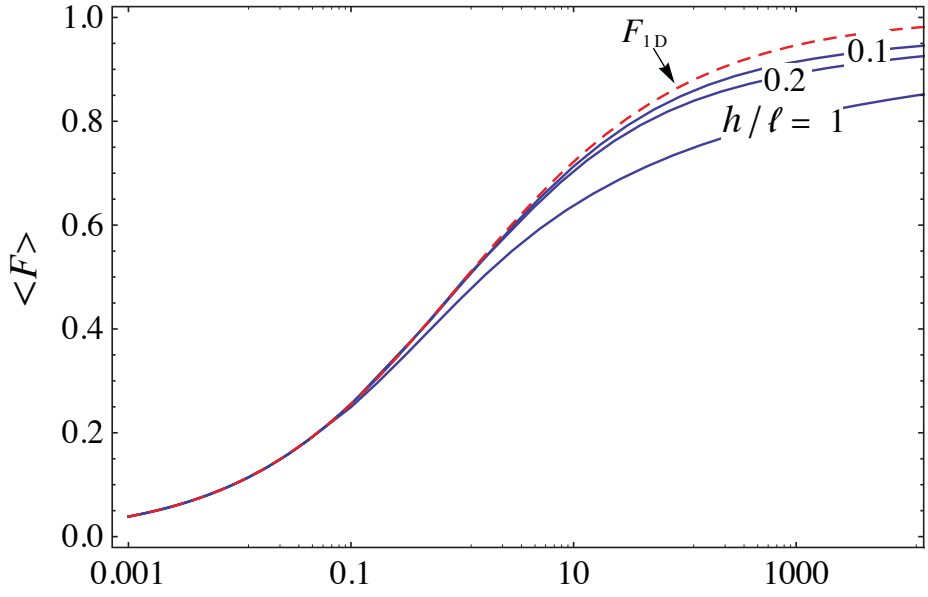

(a)

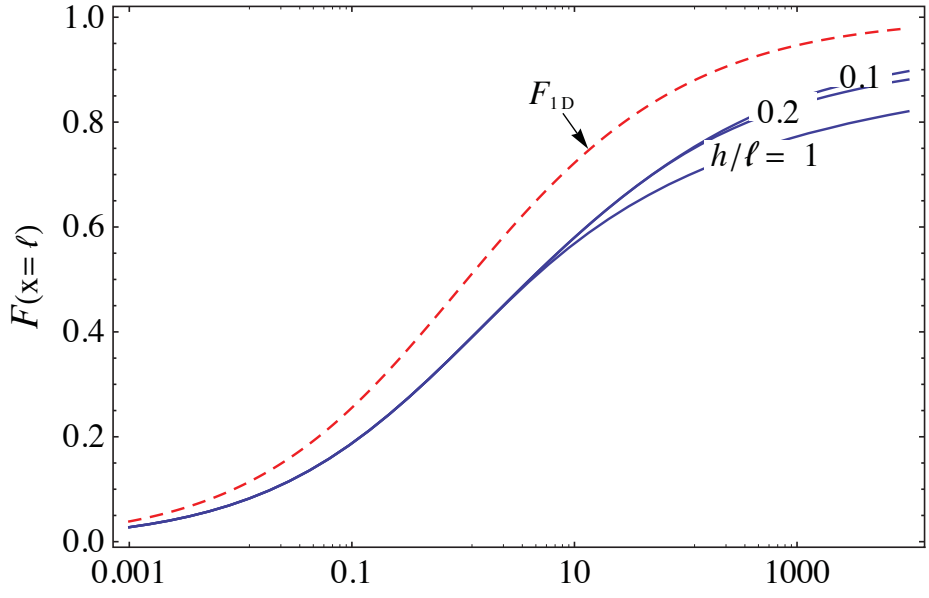

(b)

Figure 4.2: Evolution of (a) the crack-average of the influence function, $\langle F \rangle (t)$, and (b) the tip value of the influence function, $F(x = \pm\ell)$, with normalized time for various values of the crack aspect ratio h/ℓ. The timescale is $t_{1D} = h^2/4\alpha$.

As we will further show in Section 4.3, the transient pressurization problem due to the prescribed rate of fluid injection into the crack is fully defined by the fluid volume balance in the crack, and, therefore, depends only on the crack-averaged influence function $\langle F \rangle (t)$. Thus, the 1-D version of this function (which has an advantage of having an analytical expression in the Laplace domain) can be used with confidence. On the other hand, the onset of a fingerlike crack propagation is defined by the tip value of the net fluid pressure $p - \sigma_0 - \sigma_b$, and, therefore, the full solution (and not its 1-D asymptote) for $F(x = \pm\ell, t)$ will be necessary to determine the initiation of crack growth accurately.

4.2.3 Total crack opening and volume

The total crack opening in the auxiliary problem, averaged over a given x cross-section of a poroelastic fingerlike crack, is given by the superposition of the mode 1, (4.4), and mode 2, (4.9), solutions:

$$\bar{w}^{\text{aux}}(x,t) = \bar{w}^{(1)}(x,t) + \bar{w}^{(2)}(x,t) = \frac{\pi h}{2E'} \left(1 - 2\eta F(x,t)\right). \tag{4.17}$$

The poroelastic effects on the crack opening (i.e., $\bar{w}^{(2)}$) can be likened to that of the additional confining stress ("backstress") acting across the fracture plane in the purely elastic material [53],

$$\sigma_b^{\text{aux}}(x,t) = 2\eta F(x,t), \tag{4.18}$$

such that (4.17) can be written as

$$\bar{w}^{\text{aux}}(x,t) = \frac{\pi h}{2E'}(1 - \sigma_b^{\text{aux}}(x,t)). \tag{4.19}$$

The corresponding total crack volume is

$$V_{\text{crack}}^{\text{aux}}(t) = h\int_{-\ell}^{\ell} \bar{w}^{\text{aux}}(x,t)dx = \frac{\pi\ell h^2}{E'}\left(1 - 2\eta\left\langle\sigma_b^{\text{aux}}\right\rangle(t)\right), \tag{4.20}$$

where $\left\langle\sigma_b^{\text{aux}}\right\rangle(t)$ is the spatial average of $\sigma_b^{\text{aux}}(x,t)$.

4.2.4 Cumulative leak-off volume

The pore pressure diffusion is assumed to be uncoupled from the stress changes (i.e., $V_{leak}^{(1)} \simeq 0$). Hence, the cumulative leak-off volume in the auxiliary problem is given by

$$V_{\text{leak}}^{\text{aux}}(t) \backsimeq V_{\text{leak}}^{(2)}(t) = h\ell^2 S\,\Phi^{(2)}\left(\frac{t}{t_{2\text{D}}}\right), \tag{4.21}$$

where the normalized leak-off function $\Phi^{(2)}$, has been previously tabulated in Fig. 3.3.

4.3 TRANSIENT PRESSURIZATION OF THE CRACK (CONSTANT VOLUMETRIC INJECTION RATE)

The fracture response $\mathcal{F}$ to transient pressurization problem $p = p(t)$ can be obtained from the auxiliary solution $\mathcal{F}^{aux}$ by convolution [67]

$$\mathcal{F}(x,y,z,t) = \int_0^t \mathcal{F}^{aux}(x,y,z,t-t')\frac{dp}{dt'}dt', \tag{4.22}$$

where $\mathcal{F}^{aux}$ is fracture response in the auxiliary problem.

We apply (4.22) to the injected volume balance

$$V(t) = V_{crack}(t) + V_{leak}(t), \tag{4.23}$$

where $V(t) = Q_0 t$, $t \geq 0$, and Q_0 is the constant injection rate, to find

$$Q_0 t = \int_0^t V_{\text{crack}}^{\text{aux}}(t - t') \frac{dp}{dt'} dt' + \int_0^t V_{\text{leak}}^{\text{aux}}(t - t') \frac{dp}{dt'} dt'. \tag{4.24}$$

Equation (4.24) with the auxiliary crack ($V_{\text{crack}}^{\text{aux}}$) and leak-off ($V_{\text{leak}}^{\text{aux}}$) volumes given by (4.20) and (4.21), respectively, governs the evolution of fluid pressure in the crack $p = p(t)$.

$$Q_0 t = \frac{\pi h^2 \ell}{E'} \int_0^t (1 - 2\eta \langle F \rangle (t - t')) \frac{dp}{dt'} dt' + h\ell^2 S \int_0^t \Phi^{(2)} \left(\frac{4\alpha(t-t)'}{\ell^2} \right) \frac{dp}{dt'} dt'. \tag{4.25}$$

4.3.1 Transient pressurization calculation

In solving (4.24), we will make use of the following two sets of characteristic time and pressure scales (see Chapter 3)

$$t_1 = \frac{t_{1\text{D}}}{(SE')^2} = \frac{1}{(SE')^2} \frac{h^2}{4\alpha}, \qquad p_1 = \frac{Q_0 t_1}{h^2 \ell} E' \tag{4.26}$$

$$t_2 = t_{2\text{D}} = \frac{\ell^2}{4\alpha}, \qquad p_2 = \frac{Q_0 t_2}{\ell^2 h} \frac{1}{S}. \tag{4.27}$$

In view of the above scales, three different end-members, namely, the crack-storage-dominated regime ($t \ll t_1$), the 1-D leak-off dominated regime ($t_1 \ll t \ll t_2$), and the 2-D leak-off dominated regime ($t \gg t_2$) are anticipated.

Governing equation (4.24) with (4.20)-(4.21) can be written in the 1-D scaling, (4.27), using non-dimensional variables $\Pi = (p - \sigma_0)/p_1$ and $\tau = t/t_1$ as

$$\tau = \pi \int_0^\tau (1 - 2\eta \langle F \rangle (t_1(\tau - \tau'))) \frac{d\Pi(\tau')}{d\tau'} d\tau' + \frac{1}{\mathcal{A}} \int_0^\tau \Phi^{(2)}(\mathcal{A}^2(\tau - \tau')) \frac{d\Pi(\tau')}{d\tau'} d\tau'. \tag{4.28}$$

where

$$\mathcal{A} = \frac{p_1}{p_2} = \sqrt{\frac{t_1}{t_2}} = \frac{1}{SE'}\frac{h}{\ell}, \tag{4.29}$$

is s non-dimensionless number (equation (3.22)).

The solution of (4.28) in Laplace domain ($t/t_1 \rightarrow s$) is given by

$$\hat{\Pi}(s) = \frac{1}{s^2}\frac{1}{\pi\left(1 - 2\eta s(SE')^2\langle\hat{F}\rangle((SE')^2 s)\right) + s\,\hat{\Phi}^{(2)}(s/\mathcal{A}^2)/\mathcal{A}^3}. \tag{4.30}$$

For $t_1 \ll t \ll t_2$, $\hat{\Phi}^{(2)}_{1\mathrm{D}}(s/\mathcal{A}^2) \simeq 2\mathcal{A}^3 s^{-3/2}$ (see Chapter 3), and $\hat{F}_{1\mathrm{D}}$ (equation (4.13)) can be used to numerically obtain the 1-D pressure solution from (4.30) using the Stehfest algorithm [68]. We also noticed that the first-order asymptote of $\hat{F}_{1\mathrm{D}}$ (equation $(4.14)_a$) results in reasonable approximation of the 1-D pressure solution. The relative percentage error in calculation of 1-D pressure solution obtained using the first order asymptote of $\hat{F}_{1\mathrm{D}}$ (equation $(4.14)_a$) and fully defined $\hat{F}_{1\mathrm{D}}$ (equation (4.13)) is illustrated in Fig. 4.3. This approximation allows to conveniently write the closed form solution of 1-D pressure asymptote in the 1-D scaling as

$$\frac{\bar{p}}{p_1} = \frac{\pi}{4(1-4\eta')^2}\left[\mathrm{Erfc}\left(\frac{2(1-4\eta')}{\pi}\sqrt{\frac{t}{t_1}}\right)\exp\left(\frac{4(1-4\eta')^2}{\pi^2}\frac{t}{t_1}\right) - 1\right]$$

$$+\sqrt{\frac{t}{\pi(1-4\eta')^2 t_1}}, \quad (t_1 \ll t \ll t_2) \tag{4.31}$$

where $\eta' = \eta/SE'$ is the effective poroelasticity stress coefficient. Note that the 1-D non-poroelastic solution previously obtained in Chapter 3 (equation (3.23)) can be recovered from (4.31) by nullifying the poroelastic term in (4.31) by letting $\eta = 0$.

The solution in the storage ($t \ll t_1$) dominated regime is recovered as appropriate end-member of (4.31)

$$\frac{\bar{p}}{p_1} = \frac{t}{\pi t_1}, \quad (t \ll t_1)\,. \tag{4.32}$$

For $t/t_2 \gg 1$, the storage is negligible and 1-D scaling is not an appropriate scaling to

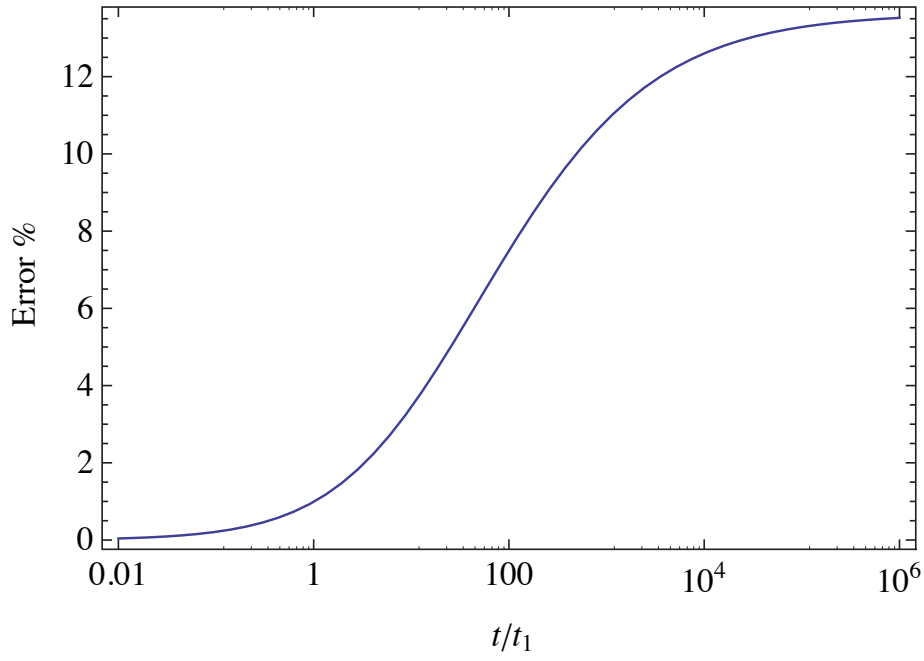

Figure 4.3: The relative percentage error in calculation of 1-D pressure solution obtained using the first order asymptote of $\hat{F}_{1D}$ (equation $(4.14)_a$) and fully defined $\hat{F}_{1D}$ (equation (4.13)). The 1-D time scale is $t_1 = (1/SE')^2(h^2/4\alpha)$.

normalize (4.28), and 2-D scaling should be used. However, we can nullify the storage term in equations (4.28) and (4.30), and use $\hat{\Phi}^{(2)}_{2D}(s/\mathcal{A}^2) \simeq \pi\mathcal{A}/(s^2\left[\ln\left(4\mathcal{A}^2/s\right) - 2\gamma\right])$ expressed in 1-D scaling (see Chapter 3) to obtain the 2-D leak-off asymptote. Resulting solution for the 2-D leak-off dominated regime follows (after inversion back to the time domain):

$$\frac{p(t) - \sigma_0}{p_2} = \frac{1}{\pi}\left[\ln\frac{4t}{t_2} - \gamma\right]. \quad (t \gg t_2) \tag{4.33}$$

In the intermediate time range, $t_1 \lesssim t \lesssim t_2$, solution is obtained by numerically evaluating the inverse Laplace transform of (4.30). Figure 4.4a shows the evolution of the normalized pressure $(p-\sigma_0)/p_1$ with normalized time t/t_1 during the transient pressurization of the crack for several values of the crack height to length ratio h/ℓ. For the numerical calculations, we choose a representative values of poroelasticity stress coefficient $\eta = 0.3$ (e.g., [10]) and $SE' = 10$. The 1-D (equation (4.31)) and

2-D leak-off (equation (4.33)) asymptotics are shown by the dashed lines. The dotted line shows the early time storage-dominated solution (equation (4.32)).

4.3.1.1 Significance of poroelastic effects on the evolution of the pressure in the crack

In Chapter 3, the evolution of the pressure in the crack assuming negligible poroelastic coupling was calculated. To underline the poroelastic effects on the transient pressurization calculations, we illustrate in Fig. 4.4b the evolution of the ratio of the poroelastic to non-poroelastic pressure (Chapter 3) solutions with normalized time for the given fracture height to length ratios. As Fig. 4.4b shows, the poroelastic and non-poroelastic pressure solutions are only different by 5% at most. In other words, the poroelastic effects in the evolution of the fluid pressure in the crack in response to injection is very weak. This surprising results allow to confidently formulate the fluid pressure evolution assuming negligible poroelastic coupling.

4.3.2 Backstress calculation

Using the convolution (4.22), we obtain expression for the backstress with the auxiliary solution (4.18)

$$\sigma_b\,(x,t) = 2\eta \int\limits_0^t F(x, t-t') \frac{dp}{dt'} dt'\,. \tag{4.34}$$

As mentioned earlier, the influence function F approaches 1 at large time when the leak-off diffusion is fully 2-D. In view of corresponding pressure asymptote (4.33), the large-time asymptote of backstress is simply

$$\sigma_b\,(x,t) \simeq 2\eta(p(t)-\sigma_0) = \frac{2\eta p_2}{\pi}\left[\ln\frac{4t}{t_2} - \gamma\right] \quad (t \gg t_2)\,, \tag{4.35}$$

Fig. 4.6 illustrates an example of the numerical calculations of the backstress at the crack tip ($x = \ell$) normalized by the net pressure in the crack for various crack height

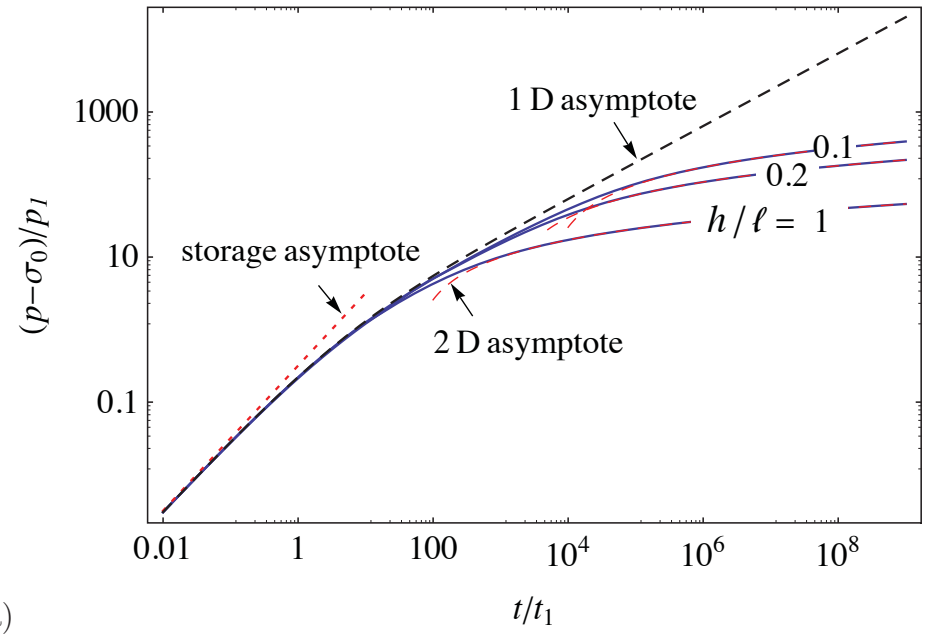

(a)

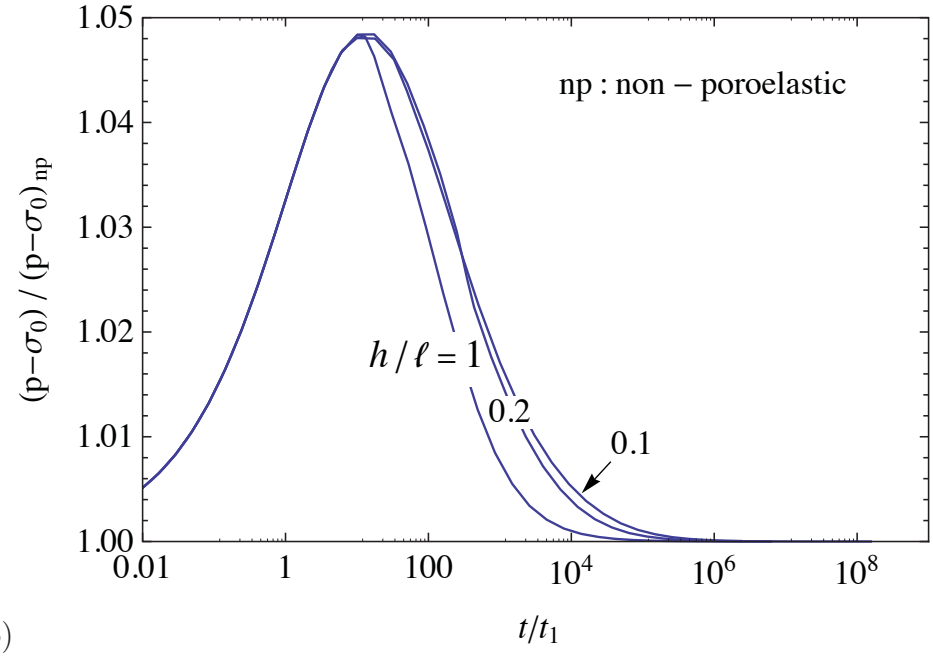

(b)

Figure 4.4: (a) Evolution of the normalized pressure $(p-\sigma_0)/p_1$ with normalized time t/t_1 during the transient pressurization of a crack for various values of the height to length ratio h/ℓ. The 1-D (equation (4.31)) and 2-D leak-off (equation (4.33)) asymptotic solutions are shown by dashed lines, respectively. The dotted line shows the early time storage-dominated solution, (equation (4.32)). (b) Evolution of the ratio of the poroelastic to non-poroelastic pressure solutions in the crack with normalized time for various values of the height to length ratio h/ℓ. The representative values $SE' = 10$ and $\eta = 0.3$ are used for numerical calculations. The 1-D pressure and time scales are $p_1 = Q_0 E' t_1/h^2\ell$ and $t_1 = (1/SE')^2(h^2/4\alpha)$, respectively.

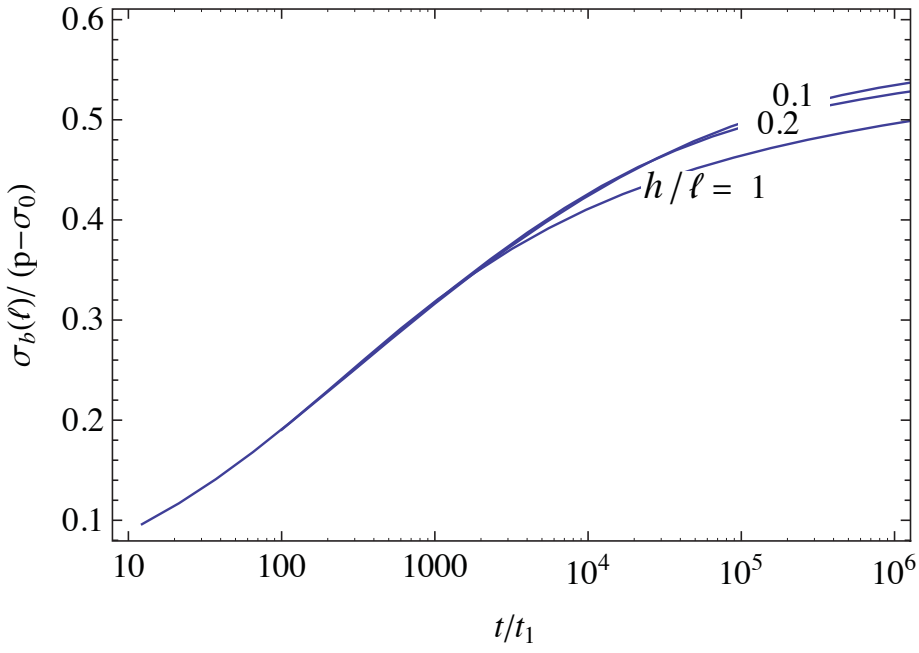

Figure 4.5: Evolution of the backstress at the crack tip ($x = \ell$) normalized by the net pressure in the crack with normalized time t/t_1 for various crack height to length ratios h/ℓ. The representative values $SE^{'} = 10$ and $\eta = 0.3$ are used for numerical calculations. The time scale is $t_1 = (1/SE^{'})^2(h^2/4\alpha)$.

to length ratios h/ℓ. As Fig. 4.6 shows, the generated backstress at early times is only a small fraction of the fluid pressure. However, the ratio of the backstress to fluid pressure will considerably increase at later injection time. From the asymptotic solution (4.35), it is evident that this ratio can not exceed 2η. As it will be further discussed in Section 4.4, the onset of fracture initiation is defined by the net fluid pressure $p - \sigma_0 - \sigma_b$ at the crack tip, and therefore the initiation of crack can be significantly affected by the poroelastic effects.

4.3.3 Fracture volume calculation

The poroelastic crack volume can be expressed as

$$V_{\text{crack}}(t) = \frac{\pi \ell h^2}{E'} \left(p - \sigma_0 - \langle \sigma_b \rangle\right), \tag{4.36}$$

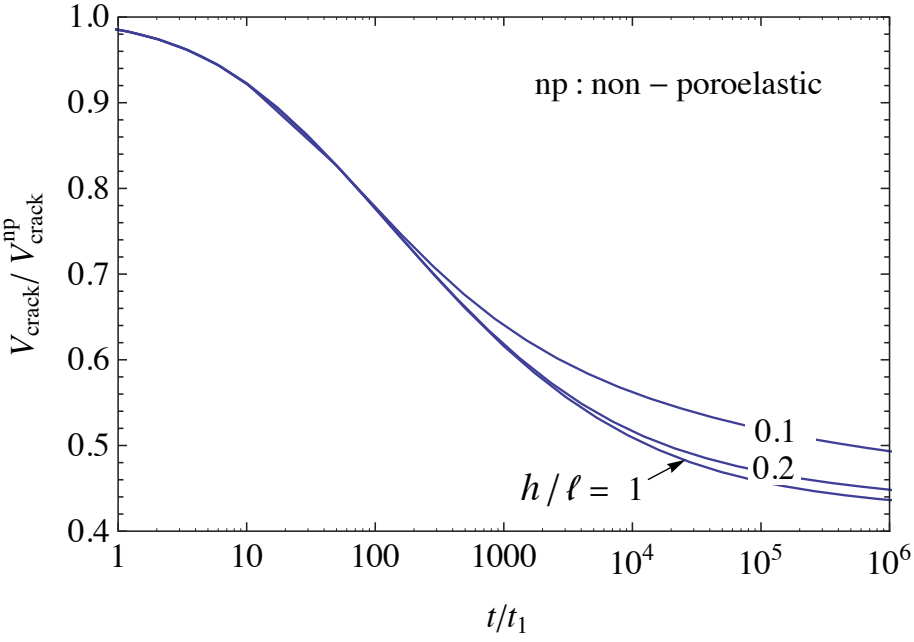

Figure 4.6: Evolution of the ratio $V_{\text{crack}}/V_{\text{crack}}^{\text{np}}$ with normalized time t/t_1 during the transient pressurization of a crack for various values of the crack height to length ratio h/ℓ. The representative values $SE^{'} = 10$ and $\eta = 0.3$ are used for numerical calculations. The time scale is $t_1 = (1/SE^{'})^2(h^2/4\alpha)$.

where $\langle\sigma_b\rangle$ is the spatial average of backstress σ_b (equation (4.34)). Due to weak poroelastic effects on the fluid pressure evolution, the fracture volume can be linked to non-poroelastic crack volume $V_{\text{crack}}^{\text{np}}$ by

$$V_{\text{crack}}(t) = V_{\text{crack}}^{\text{np}}(t)\left(1 - \frac{\langle\sigma_b\rangle}{p - \sigma_0}\right), \tag{4.37}$$

where $V_{\text{crack}}^{\text{np}} = \pi\ell h^2(p-\sigma_0)/E^{'}$. Figure 4.6 shows the evolution of the ratio $V_{\text{crack}}/V_{\text{crack}}^{\text{np}}$ with normalized time t/t_1 for various values of the crack height to length ratio h/ℓ.

4.4 BREAKDOWN CONDITION

The propagation criterion of a fingerlike crack subjected to a non-poroelastic net loading $\bar{p} = p - \sigma_0$ was introduced in Chapter 2 (equation (2.8)). The extension of the propagation criterion to the case of a poroelastic crack can be carried out by

introducing the backstress to the net loading, i.e.,

$$\bar{p}\,(x,t) = p\,(x,t) - \sigma_0 - \sigma_b\,(x,t)\,. \tag{4.38}$$

4.4.1 Example

Previously, we considered an example of the initiation of fracture propagation from a pre-existing fingerlike crack due to injection of supercritical CO_2 in a critically over pressured reservoir ($p_0 \simeq \sigma_0$). In the following, we revisit this example, now in the context of poroelastic reservoir (Chapter 3).

It was assumed that the supercritical CO_2 is injected in a sandstone formation characterized by porosity $\phi = 0.17$, permeability $k = 13$ md, minimum in-situ stress $\sigma_0 = 30.8$ MPa, ambient pore pressure $p_0 = 20$ MPa, rock toughness $K_{Ic} = 1$ MPa $\mathrm{m}^{1/2}$, Young's modulus $E = 6$ GPa, Poisson's ratio $\nu = 0.2$, and average reservoir temperature $T = 90^0$C [70, 71].

The supercritical CO_2 is assumed to be injected at the total mass flow rate $\dot{m} =$ 100 t/day into a single vertical, fingerlike fracture with half-length $\ell = 50$ m, height $h = 20$ m (assumed to span the height of the sandstone layer). The calculated values of relevant problem parameters are $Q_0 = 0.0016$ m^3/s (volumetric injection rate), $S = 2.7$ GPa^{-1} (storage), $E^{'} = 6.25$ (Young's modulus) $\alpha = 0.08$ m^2/s (diffusivity coefficient), $t_1 = 4.4$ seconds (1D time scale), $t_2 = 2.1$ mins (2D time scale), $p_1 = 2.2$ KPa (1D pressure scale), $p_2 = 91.7$ KPa (2D pressure scale), $h/\ell = 0.4$ (crack height to length ratio), and $\mathcal{A} = 0.024$ (non-dimensional aspect ratio parameter).

Figure 4.7 shows the evolution of the net loading $\bar{p} = p - \sigma_0 - \sigma_b$ on the crack calculated at the crack tip ($x = \ell$) with the normalized time for the given example. The poroelastic solution is contrasted to the reference non-poroelastic solution (Chapter 3).

Locating the point where $\bar{p}(x = \ell) = \bar{p}_B$, $\bar{p}_B/p_1 = 112$ on Fig. 4.7 (point B for

a poroelastic crack), the onset of the fracture propagation is forecasted at $t_B/t_1 = 1.5 \times 10^{11}$, or in $t_B \simeq 2099$ years from the beginning of the injection. In practical terms, obtained value for the onset of propagation is orders of magnitude larger than realistic injection times (years).

By contrast, the propagation initiation time calculated for a non-poroelastic crack for the same problem (point A) was at $t_B/t_1 = 3.6 \times 10^6$, or in $t_B \simeq 183.3$ days. This indicates that the poroelastic effects have significant effects on the onset of fracture propagation.

We also note that the poroelastic calculations based on the 1-D approximate form of the influence function, (F_{1D}) result in prediction propagation onset time (point C on Fig. 4.7) which is about one order of magnitude larger than the value obtained using the full form of the influence function F. This indicates the use of full (2-D) poroelastic influence function is necessary to correctly predict fracture propagation.

4.5 SUMMARY OF CHAPTER RESULTS

Pressurization of an underground formation during injection of a low viscosity fluid (e.g., liquid waste injection and waterflooding) may lead to reactivation of pre-existing fractures and ensuing fracture propagation. In this Chapter, the poroelastic effects on the transient pressurization and onset of fracture propagation of a stationary pre-existing fingerlike crack in a critically over-pressured reservoir were investigated. We first revisited the auxiliary problem of a crack subjected to mode 1 (traction) and mode 2 (pore pressure) poroelastic loadings [53]. We extended the auxiliary problem solution by relaxing the 1-D diffusion assumption to account for full (2-D) pore pressure. The solution to the auxiliary problem of a crack subjected to a step pressure increase is then used via the Green's function approach to formulate the solution for the transient pressurization (i.e., evolution of the pressure in the crack) due to constant volumetric rate of injection. The poroelastic crack volume and

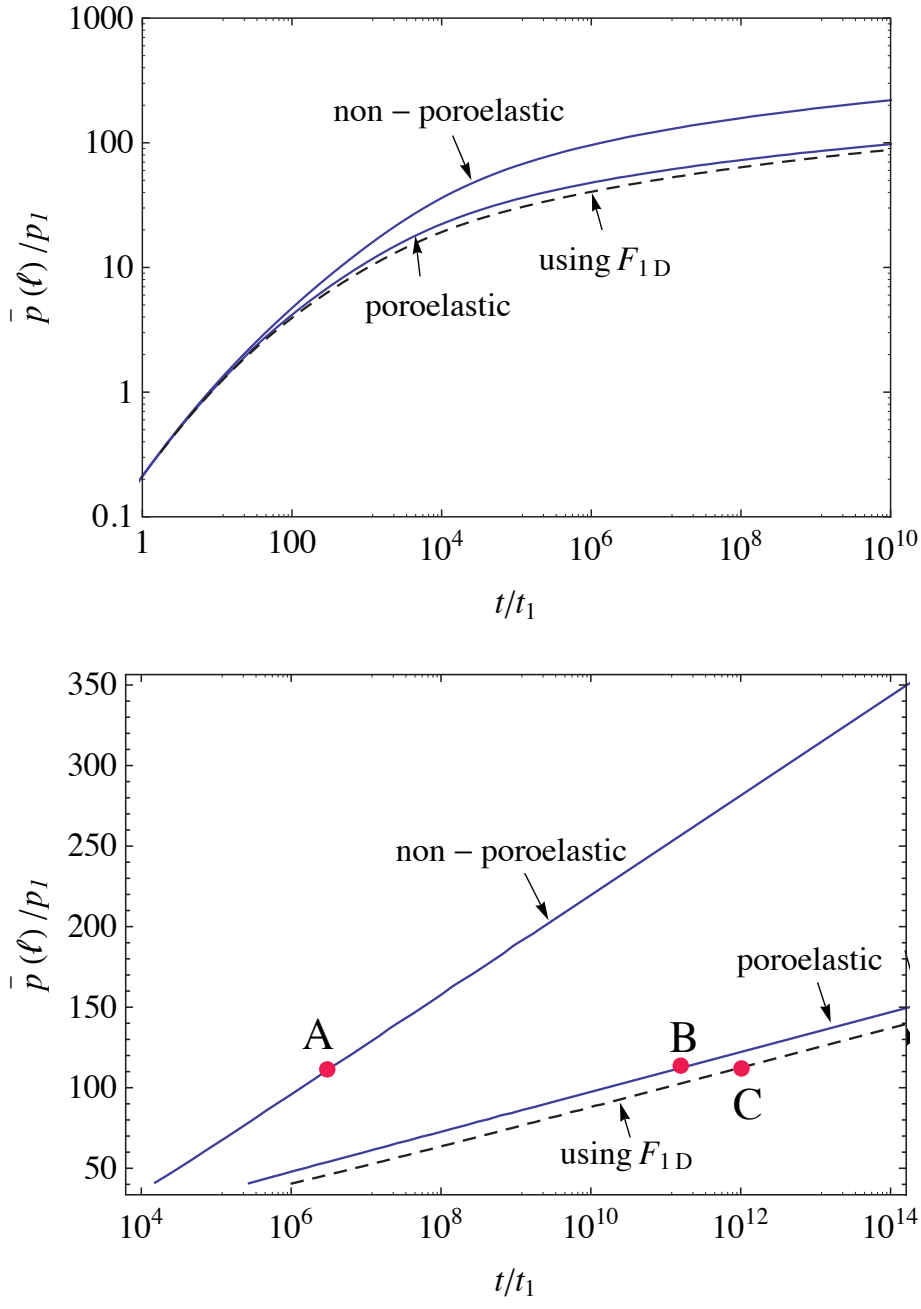

Figure 4.7: Evolution of the normalized net pressure at the crack tip $\bar{p}(\ell)/p_1 = (p(x = \ell, t) - \sigma_0 - \sigma_b(x = \ell, t))/p_1$ with normalized time t/t_1 during the transient pressurization of a crack for poroelastic and non-poroelastic cracks for the crack breakdown calculation example. The dashed line corresponds to the net loading calculation using the approximate 1-D influence function. The representative values $h/\ell = 0.4$, $\mathcal{A} = 0.024$, and $\eta = 0.3$ are used for numerical calculations. The 1-D pressure and time scales are $p_1 = Q_0 E' t_1/h^2\ell$ and $t_1 = (1/SE')^2(h^2/4\alpha)$, respectively.

generated backstress are calculated subsequently. Comparison of the behavior of a fingerlike crack due to fluid injection in non-poroelastic (Chapter 3) and poroelastic reservoirs shows that the poroelastic effects on the evolution of the fluid pressure in the crack is almost negligible. However, the poroelasticity can have significant effects on the crack opening (and, therefore volume), due to poroelastic backstress. The poroelastic effects on the onset of fracture initiation during a supercritical CO_2 injection project was also investigated. It was shown that the poroelasticity has significant impacts on the onset of fracture propagation.

CHAPTER 5: TRANSIENT PRESSURIZATION OF A CLOSED FRACTURE

5.1 OBJECTIVES

In Chapter 3, we considered the transient pressurization of a pre-existing fracture in a critically over-pressured reservoir (i.e., $p_0 \simeq \sigma_0$). In this Chapter, we relax the assumption of a critically over-pressured reservoir. We assume that the fracture is initially subjected to a negative net fluid pressure (i.e., $(p_0 - \sigma_0) < 0$) and it is initially mechanically closed. There are two classifications of initially mechanically-closed fractures, "un-propped" fractures where the opposing fracture surfaces are initially in contact preventing the complete closure of fracture, and "propped" fractures where the proppant is used to hold the fracture open.

During the transient pressurization of a pre-existing un-propped fracture, two different loading phases are expected. 1) The loading phase when the fracture surface contacts will be gradually reduced until the fracture becomes mechanically-open. The latter takes place when the pressure along the fracture becomes equal to the minimum confining stress (i.e., condition of crack re-opening). 2) The loading phase when the pressure along the crack exceeds the minimum confining stress. The pressurization of the fracture above the minimum confining stress will eventually lead to the fracture breakdown.

Although, un-propped hydraulic fracturing has been reported in reservoir stimulation (improvements of reservoir connectivity to the well) [73, 74], it is a common practice to inject proppant during hydraulic fracturing to hold the fractures open once the treatment is finished.

The mechanism of the transient pressurization of propped fractures is significantly different from that of un-propped ones. Thus, during injection and related pressur-

ization of a propped fracture, the condition of fracture re-opening is to be achieved when the pressure along the crack becomes equal or greater than the breakdown pressure.

Indeed, proppant is mixed with hydraulic fracturing fluid and it is placed inside the fracture when fracture is propagating. During the propagation of a hydraulic fracture, the pressure along the fracture is either equal (i.e., when crack propagates in toughness-dominated regime) or greater (i.e., when crack propagates in viscosity-dominated regime) than the breakdown pressure. To re-pressurize a propped fracture, now in a depleted reservoir, the pressure along the crack should be raised to the level of the pressure existed at the time of proppant placement (i.e., during fracture propagation). Hence, the condition of fracture breakdown (onset of propagation) is to be reached while the propped crack still remains mechanically-closed.

In this Chapter, the pressurization and the onset of fracture propagation is quantified for propped and un-propped closed fractures in a non-poroelastic reservoir.

5.2 CASE OF PROPPED FRACTURE

We make use of the following assumptions in this Section. 1) The deformation of the propped fracture due to fluid injection is neglected. In other words, fracture has zero compressibility. 2) The dependence of the propped fracture conductivity on pressure is negligible. 3) The proppant thickness (or, initial propped fracture aperture) is uniform along the entire fracture.

5.2.1 Conditions for a uniform pressure distribution along the crack

Consider a propped PKN fracture characterized by proppant permeability k_f. Fluid is injected in the fracture at a constant volumetric flow rate Q_0. The flow of fluid inside the fracture can be described by the lubrication equation. Due to negligible fracture compressibility, the fracture dilation due to fluid injection can be neglected.

The latter allows to nullify the storage term in the lubrication equation.

The evolution of the pore fluid pressure due to fluid leak-off along the crack is described by the diffusivity equation (2.15). The lubrication equation (2.11) with boundary conditions (2.12) and diffusivity equation (2.15) can be simultaneously solved to evaluate the transient pressurization in the crack.

We define the non-dimensional time ($\tau = t/t_*$), x coordinate ($\xi = x/\ell$), y coordinate ($\chi = y/\ell$), and pressure ($\Pi = (p - p_0)/p_*$) using the characteristic time $t_* = \ell^2/4\alpha$, length ℓ, and pressure $p_* = Q_0\ell\mu/k_f\bar{w}h$ scales, respectively to normalize the lubrication equation (2.11), initial and boundary conditions (2.12), and diffusivity equation (2.15). The resulting normalized equations, parametrized by a single non-dimensional propped fracture conductivity

$$(k_f\bar{w})_D = \frac{k_f\bar{w}}{k\ell} \tag{5.1}$$

and numerical method of their solution are discussed in Appendix E.

Figure 5.1 shows the evolution of the normalized pressure with time at selected positions ξ along the crack in the case with $(k_f\bar{w})_D = 100$. The 1-D and 2-D pressure asymptotic solutions (as obtained in Appendix E) are shown by a dashed line for comparison. As expected, for large enough time, the pressure equilibrates along the crack.

We define "uniformity" pressure (Π_{uni}) and time (τ_{uni}) thresholds corresponding to the 5% difference between the inlet and the tip values of pressure. We can show that the uniformity pressure p_{uni} is approximately given by

$$p_{uni} - p_0 \approx 5\frac{Q_0\ell\mu}{k_f\bar{w}h}, \tag{5.2}$$

if,

$$(k_f\bar{w})_D = \frac{k_f\bar{w}}{k\ell} \gtrsim 1. \tag{5.3}$$

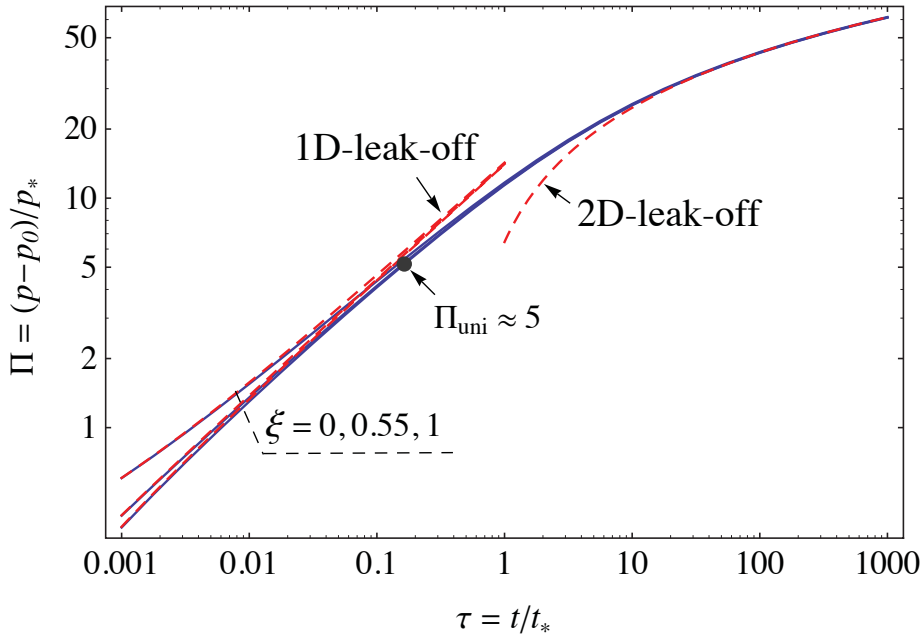

Figure 5.1: Evolution of the normalized net pressure $\Pi = (p-p_0)/p_*$ with normalized time $\tau = t/t_*$ at selected positions along the crack $\xi = x/\ell = 0$ (inlet), $0.55, 1$ (tip) in the case of a propped fracture with $(k_f\bar{w})_D = k_f\bar{w}/k\ell = 100$. The characteristic time and pressure scales are $t_* = \ell^2/4\alpha$, $p_* = Q_0\ell\mu/k_f\bar{w}h$, respectively. Marked point corresponds to the onset of approximate pressure uniformity in the crack.

As it will be later shown in the breakdown example for a propped fracture, the condition (5.3) is typically satisfied for practical reservoir applications. We also notice that the uniformity time t_{uni} does depend on $(k_f \bar{w})_D$ (see Appendix E for details).

In this Section, we showed that the condition of the pressure uniformity is approximately satisfied when $p \gtrsim p_{uni}$, with p_{uni} given by (5.2), and it can be used to predict the breakdown if $p_B \gtrsim p_{uni}$. Note that the condition of fracture propagation is achieved prior to the condition of fracture re-opening for a "propped" fracture.

5.2.2 Transient pressurization: constant rate of injection into a crack

Assuming a uniform pressure distribution along the crack, the transient pressurization of the fracture can be obtained from (3.17) by nullifying the storage term. The latter is due to the negligible compressibility of a propped fracture. Figure 5.2 illustrates the evolution of normalized pressure $(p-p_0)/p_2$ with normalized time t/t_2 due to fluid injection into propped fracture. Note that p_2 and t_2 are the 2-D pressure and time scales (equation (3.19)), respectively.

5.3 CASE OF UN-PROPPED FRACTURE

5.3.1 Conditions for a uniform pressure distribution along the crack

In this Section, we establish a criterion for the onset of pressure uniformity in the case of un-propped and mechanically-closed fracture.

5.3.1.1 Case of impermeable rock

Lubrication equation (2.11) with $\bar{g} = 0$ can be used to describe the flow of fluid inside the fracture channel. Unlike the propped fracture case where the fracture deformation can be reasonably neglected, the un-propped fracture requires an appropriate model to account for the hydraulic aperture change with pressure.

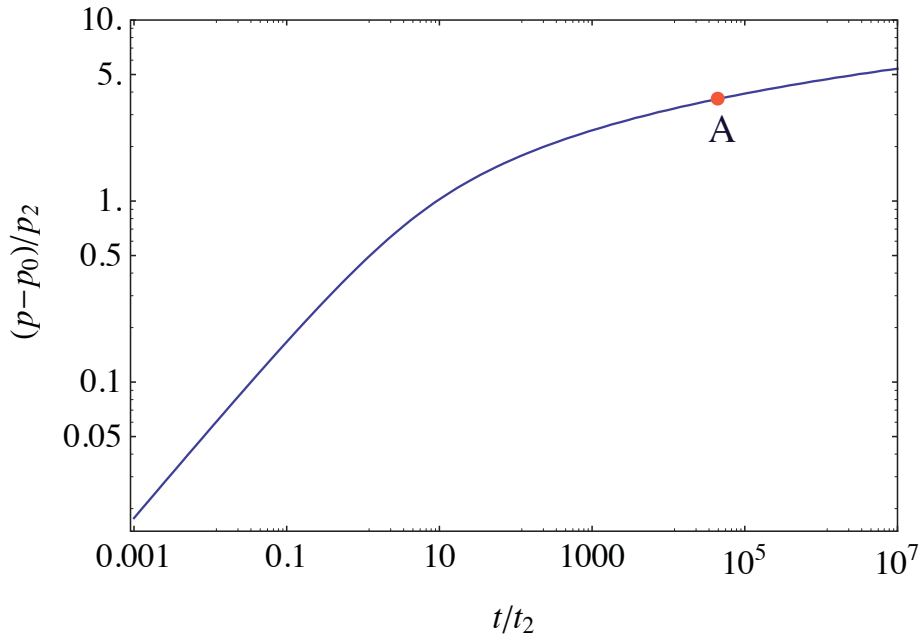

Figure 5.2: Evolution of pressure $(p - p_0)/p_2$ with time t/t_2 during the transient pressurization of a closed propped fracture: The 2-D time and pressure scales are $t_2 = \ell^2/4\alpha$, $p_2 = Q_0 t_2/\ell^2 hS$, respectively.

There are several relations in literature describing the deformation of a mechanically-closed fracture with change in the net fluid pressure $\bar{p} = p - \sigma_0$ [e.g., 75, 42, 76]. In our analysis, we use the following relation between the change of the hydraulic opening Δw and $\bar{p}$ suggested by Bandis et al. [76]

$$\Delta w = \frac{(w_0 - w_{ini})\bar{p}}{p_* - \bar{p}}, \tag{5.4}$$

where $p_* = k_{ni}(w_0 - w_{ini})$ is a characteristic value of the net pressure, expressed in terms of the initial normal crack stiffness k_{ni} and the initial hydraulic opening w_{ini}. Representative values of k_{ni}, w_{ini} and w_0 for a highly weathered fracture in sandstone and limestone formations are shown in Table 5.1, after [76]. As Table 5.1 indicates, the values of w_{ini} are small compared to w_0. In this study, in order to reduce the number of parameters, we neglect w_{ini} compared to w_0 in Bandis' equation (5.4).

We define the non-dimensional time ($\tau = t/t_*$), coordinate ($\xi = x/\ell$), and pressure

Type of formation	k_{ni}, MPa/mm	w_0, mm	w_{ini}, mm
Sandstone	2.3	0.4	0.03
Limestone	3.8	0.225	0.082

Table 5.1: Summary of values used in Bandis' equation [76].

($\Pi = (p - \sigma_0)/p_*$) using the characteristic time $t_* = h\ell w_0/Q_0$, length ℓ, and pressure $p_* = k_{ni}w_0$ scales, respectively, to normalize lubrication equation (2.11) and initial-boundary conditions (2.12), (see Appendix E for details). The resulting normalized equations depend on namely, the non-dimensional rate number

$$\mathcal{Q} = \frac{Q_0\mu\ell}{hw_0^4k_{ni}}, \tag{5.5}$$

and non-dimensional initial net pressure,

$$\Pi_0 = \frac{p_0 - \sigma_0}{k_{ni}w_0}. \tag{5.6}$$

Note that a typical range of the non-dimensional rate number for practical applications is $\mathcal{Q} \lesssim 10^{-4}$ (as it will be shown in the breakdown example for un-propped fracture).

Figure 5.3a shows an example of numerical calculations for the transient pressurization of an un-propped fracture in an impermeable reservoir carried out for representative values of the non-dimensional rate number $\mathcal{Q} = 10^{-4}$ and initial net pressure $\Pi_0 = -5$ (e.g., $p_0 - \sigma_0 \approx -5$ MPa and $k_{ni}w_0 \approx 1$ MPa). The details of the numerical calculations are described in Appendix E. The transient pressurization solution assuming a uniform pressure distribution along the crack (as later obtained in Section 5.3.2) is shown by a dashed line for comparison. As Fig. 5.3a shows, the pressure is equilibrated along the crack before the condition of the fracture re-opening (i.e., $p = \sigma_0$) is reached.

To obtain the condition of pressure uniformity, we define a threshold in which the

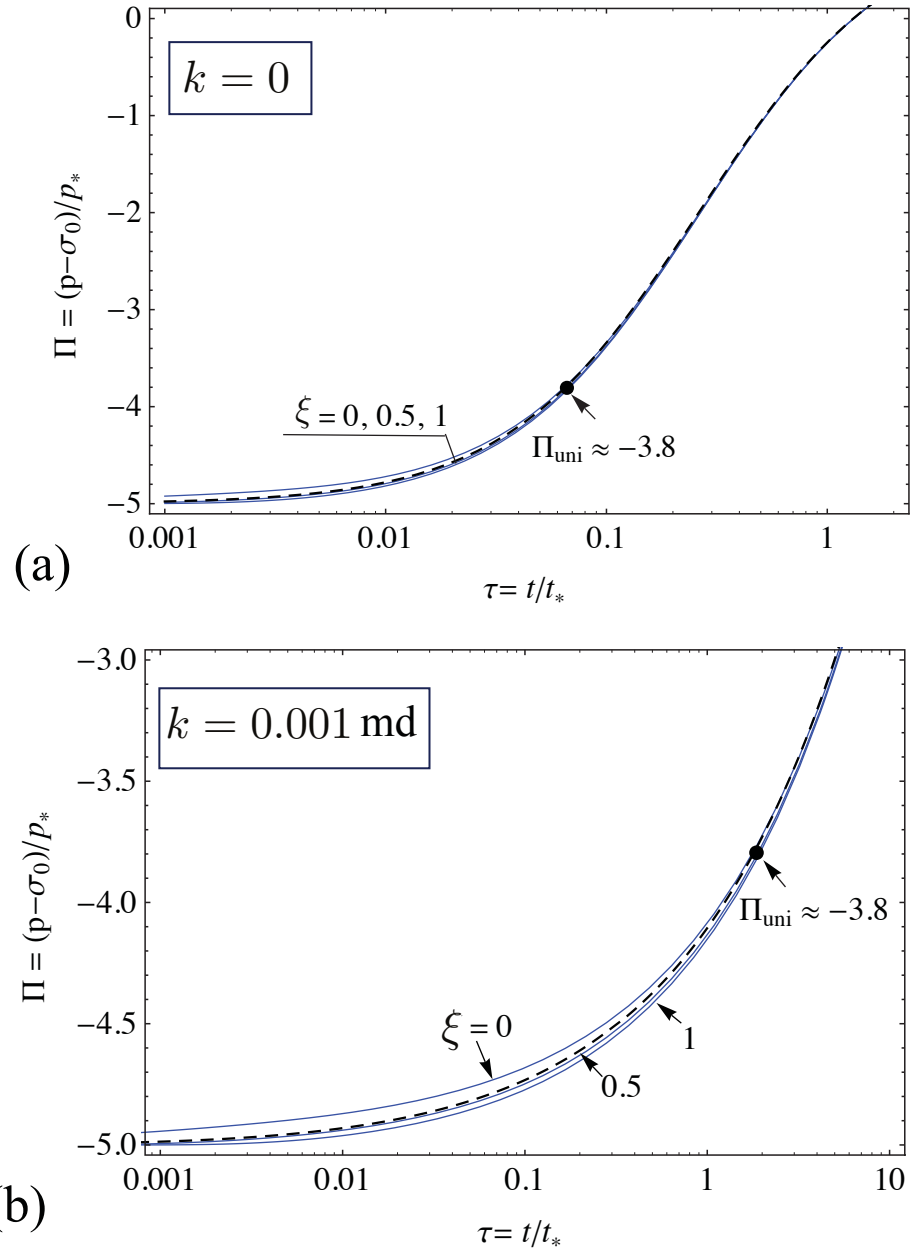

Figure 5.3: Injection at a constant rate into an un-propped crack in (a) impermeable rock ($k = 0$), and (b) permeable rock ($k = 10^{-3}$ md): evolution of the normalized net pressure $\Pi = (p - \sigma_0)/p_*$ with normalized time $\tau = t/t_*$ at selected positions along the crack $\xi = x/\ell = 0$ (inlet), $0.5, 1$ (tip). Selected non-dimensional parameters are $\mathcal{Q} = 10^{-4}$, $\Pi_0 = -5$, and $\mathcal{A}_c = 0.087$. The characteristic pressure and time scales are $p_* = k_{ni} w_0$ and $t_* = h\ell w_0/Q_0$, respectively. Marked points correspond to the onset of approximate pressure uniformity in the crack.

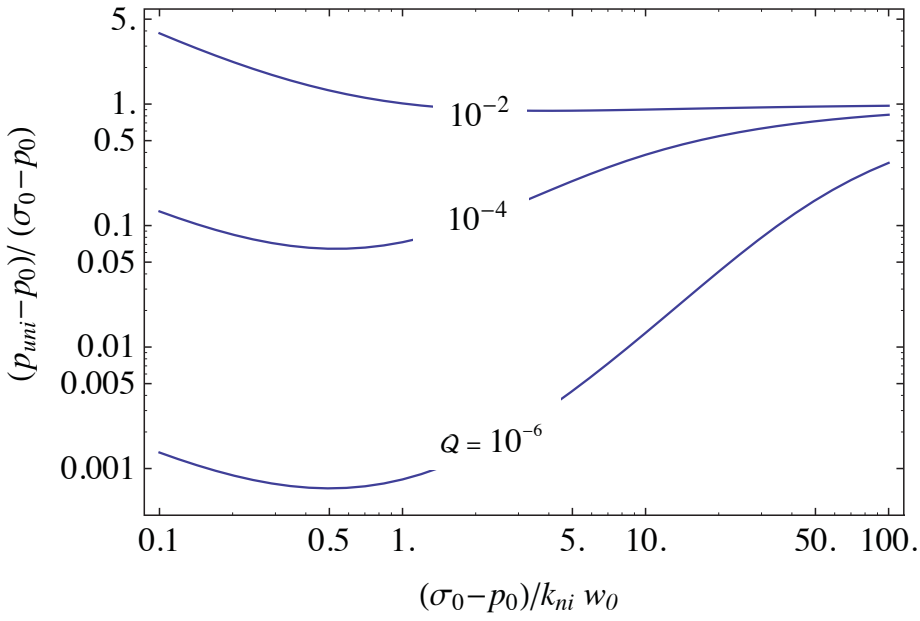

Figure 5.4: Dependence of the normalized uniformity pressure $(p_{uni} - p_0) / (\sigma_0 - p_0)$ on $(\sigma_0 - p_0) / k_{ni} w_0$ for selected values of $\mathcal{Q} = 10^{-6}, 10^{-4}, 10^{-2}$ in the case of a mechanically-closed and un-propped fracture in impermeable rock.

pressure at the inlet and tip are 5% different. Figure 5.4 illustrates the dependence of the non-dimensional uniformity pressure $(p_{uni} - p_0) / (\sigma_0 - p_0)$ on $(\sigma_0 - p_0) / k_{ni} w_0$ for various non-dimensional rate numbers $\mathcal{Q}$. As Fig. 5.4 shows, the dependence of the uniformity pressure on the non-dimensional rate number $\mathcal{Q}$ is diminished with increase of the initial effective stress (i.e., $\sigma_0 - p_0$). The asymptote of the uniformity pressure for large value of the effective stress is given by:

$$p_{uni} \approx \sigma_0, \quad \sigma_0 \gg p_0. \tag{5.7}$$

We also note that for typical reservoir applications, $\mathcal{Q} \lesssim 10^{-4}$ and $\sigma_0 - p_0 \gtrsim 0$, the uniformity pressure condition is always reached before the crack becomes mechanically-open (Fig. 5.4), i.e,

$$\frac{p_{uni} - p_0}{\sigma_0 - p_0} \leq 1, \quad \mathcal{Q} \lesssim 10^{-4}. \tag{5.8}$$

5.3.1.2 Case of permeable rock

In order to investigate the effect of formation permeability on the onset of the uniformity pressure, we include the leak-off term in lubrication equation (2.11). Problem solution depends on four group parameters, namely non-dimensional rate number $\mathcal{Q} = Q_0\mu\ell/k_{ni}w_0^4h$, non-dimensional initial net pressure $\Pi_0 = (p_0 - \sigma_0)/k_{ni}w_0$, closed-fracture aspect ratio $\mathcal{A}_c = 1/k_{ni}S\ell$, and non-dimensional un-propped fracture conductivity $(k_f\bar{w})_D = w_0^3/k\ell$.

For numerical calculations, we used the following values of the parameters: $\mathcal{Q} = 10^{-4}$, and $\Pi_0 = -5$. We also use representative values for the fracture half-length $\ell = 50$ m, fracture stiffness $k_{ni} = 2.3$ MPa/mm, neutral opening $w_0 = 0.4$ mm, and storage $S = 10^{-10}$ Pa^{-1}. Calculated corresponding value of the closed-fracture aspect ratio is, $\mathcal{A}_c = 0.087$.

Using the above selected values for the problem parameters, numerical calculations are carried out for various values of the formation permeability in order to evaluate the onset of the pressure uniformity. We showed that the uniformity pressure remains almost unchanged from its value for the impermeable case (i.e., $k = 10^{-8}$ md) (Fig. 5.5). The latter is only confirmed for the reservoirs with small formation permeability (i.e., when $k \ll 1$ md). Unfortunately, due to numerical difficulties, we could not carry out the numerical calculations for the higher values of reservoir permeabilities. As it was previously shown in Chapter 3, the uniformity pressure in impermeable/low permeable reservoirs gives the higher bound of the uniformity pressure. One may expect the uniformity pressure to decline with large enough k and approach the initial reservoir pore pressure ($p_{uni} \to p_0$) in the limit of $k \to \infty$.

An example of pressure evolution with time in the case of permeable rock ($k = 10^{-3}$ md) is shown in Fig. 5.3b.

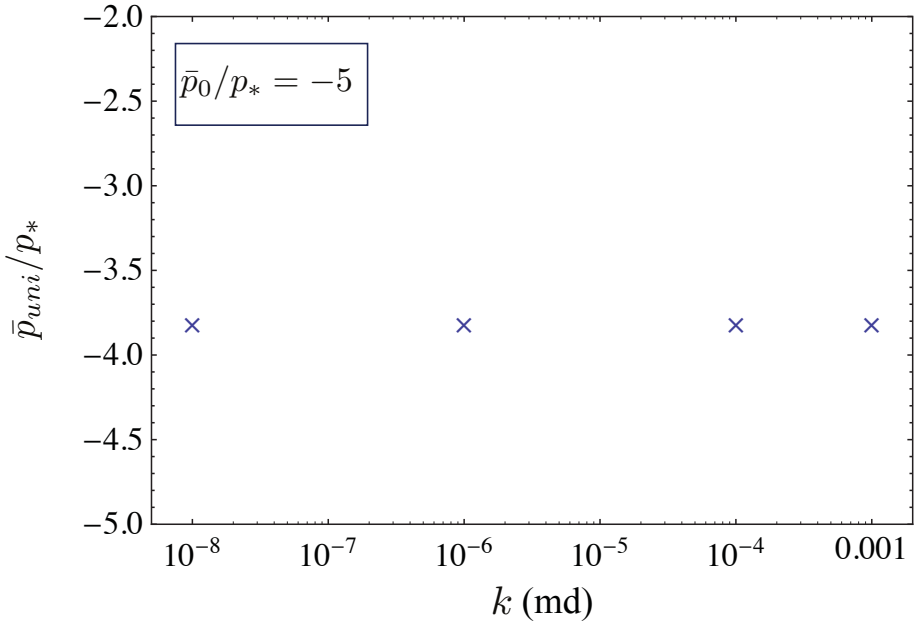

Figure 5.5: Effect of the formation permeability on the uniformity pressure $\bar{p}_{uni}/p_* = (p_{uni}-\sigma_0)/p_*$. Selected values of non-dimensional parameters are $\mathcal{Q} = 10^{-4}$, $\Pi_0 = -5$, and $\mathcal{A}_c = 1/k_{ni}S\ell = 0.087$. The characteristic pressure is $p_* = k_{ni}w_0$.

5.3.2 Transient pressurization: constant rate of injection into a crack

In this Section, the transient pressurization of an un-propped fracture before and after the crack re-opening (i.e., $p = \sigma_0$) is obtained assuming a uniform pressure distribution along the crack.

5.3.2.1 Before crack re-opening

We use the global volume balance equation (2.13) to evaluate the transient pressurization of the crack. The general expression for the fracture dilation $\triangle V_{crack}(t)$ is obtained from (2.4) as:

$$\triangle V_{crack} = \frac{\pi h \ell}{2} \left(\Delta w(\bar{p}) - \Delta w(\bar{p}_0) \right). \tag{5.9}$$

In view of (3.15) and (5.9), the global volume balance (2.13) for the particular scenario of constant injection rate (Q_0) can be expressed as

$$Q_0 t = \frac{\pi h \ell}{2} \left(\Delta w(\bar{p}) - \Delta w(\bar{p}_0)\right) +$$

$$\int_0^t V_{aux}(t - t^{'}) \frac{d\bar{p}(t^{'})}{dt^{'}} dt^{'}, \quad (\bar{p} = p - \sigma_0, \;\; t \leq t_o)\,, \tag{5.10}$$

where t_o is the onset of crack re-opening, and $V_{\text{aux}}(t) = \ell^2 h S\, \Phi_{\text{aux}}(4\alpha t/\ell^2)$ is the cumulative leak-off volume of the fracture subjected to a unit step pressure increase, with Φ_{aux} given in Fig. 3.3.

Substitution of Δw from Bandis' equation (5.4) allows to rewrite (5.10) as

$$Q_0 t = \frac{\pi h \ell w_0}{2} \left(\frac{\bar{p}}{k_{ni} w_0 - \bar{p}} - \frac{\bar{p}_0}{k_{ni} w_0 - \bar{p}_0}\right)$$

$$+ \int_0^t V_{aux}(t - t^{'}) \frac{d\bar{p}(t^{'})}{dt^{'}} dt^{'}, \quad (\bar{p} = p - \sigma_0, \quad t \leq t_o)\,. \tag{5.11}$$

Similarly to the treatment of a mechanically-open crack (Chapter 3), three length-scales can be defined for this problem: The time-dependent diffusion length $\sim \sqrt{4\alpha t}$, stiffness lengthcale $1/k_{ni}S$, and crack half-length ℓ. Similarly, the three different end-members, namely, the crack-storage-dominated regime when $\sqrt{4\alpha t} \ll 1/k_{ni}S$, the 1-D leak-off dominated regime when $1/k_{ni}S \ll \sqrt{4\alpha t} \ll \ell$, and the 2-D leak-off dominated regime when $\sqrt{4\alpha t} \gg \ell$ are anticipated.

Here, we define the corresponding closed-crack 1-D and 2-D leak-off time and net-pressure scales as

$$t_{1c} = \frac{(1/k_{ni}S)^2}{4\alpha}, \quad p_{1c} = \frac{Q_0 k_{ni} t_{1c}}{h\ell}, \tag{5.12}$$

$$t_{2c} = t_2 = \frac{\ell^2}{4\alpha}, \qquad p_{2c} = p_2 = \frac{Q_0 t_{2c}}{\ell^2 h} \frac{1}{S}. \tag{5.13}$$

Note that the corresponding 2D leak-off time and net-pressure scales for a mechanically-closed and mechanically-open fractures are identical (equation (3.19)).

Transient pressurization calculations

We formulate (5.11) in the 2-D scaling (5.13) with $\Pi = (p - \sigma_0)/p_{2c}$ and $\tau = t/t_{2c}$,

$$\tau = \frac{\pi}{2}\mathcal{A}_c \left(\frac{\Pi}{1 - \mathcal{D}\Pi} - \frac{\Pi_0}{1 - \mathcal{D}\Pi_0} \right) + \int_0^{\tau} \Phi_{aux}\left(\tau - \tau^{'}\right) \frac{d\Pi\left(\tau^{'}\right)}{d\tau^{'}} d\tau^{'}, \tag{5.14}$$

where $\mathcal{D} = Q_0/\left(4k_{ni}^2 S^2 h\ell\alpha w_0\right)$ is a non-dimensional number, which is very small for reservoir applications (i.e., $\mathcal{D} \ll 1$) (see the discussion of typical values of problem parameters in Section 5.5.2), $\Pi_0 = (p_0 - \sigma_0)/p_{2c}$, and

$$\mathcal{A}_c = \frac{p_{1c}}{p_{2c}} = \sqrt{\frac{t_{1c}}{t_{2c}}} = \frac{1}{k_{ni} S\ell} \tag{5.15}$$

is the closed-crack aspect-ratio previously defined in Section 5.3.1.2. The latter is small (i.e., $\mathcal{A}_c < 1$) for reservoir applications since $1/k_{ni}S \lesssim \ell$ for rock.

The formulation of the transient pressurization (5.14) for the special case when $\mathcal{D} \ll 1$ can be simplified to

$$\tau = \frac{\pi}{2}\mathcal{A}_c \left(\Pi - \Pi_0\right) + \int_0^{\tau} \Phi_{aux}\left(\tau - \tau^{'}\right) \frac{d\Pi\left(\tau^{'}\right)}{d\tau^{'}} d\tau^{'}, \tag{5.16}$$

with the solution in Laplace domain given by

$$\hat{\Pi}(s) = \frac{1}{s^2\left(\pi\mathcal{A}_c/2 + s\hat{\Phi}_{aux}(s)\right)} + \frac{\Pi_0}{s}. \tag{5.17}$$

Note that the solution of the transient pressurization of a mechanically-open fracture (equation (3.21)) can be recovered from (5.17) by setting $\mathcal{A}_c = 2\mathcal{A}$ and $\Pi_0 = 0$.

The transient pressurization solution in the leak-off dominated regime can be

obtained by nullifying the storage term (i.e., setting $\mathcal{A}_c = 0$) in (5.17).

Figure 5.6 illustrates the solution for pressure (5.17) in the 2-D scaling. In the numerical calculations, we use two values of initial normalized pressure $\Pi_0 = (p_0 - \sigma_0)/p_{2c} = -1$ and -2. For each assigned value of Π_0, the numerical calculations are carried out for various values of $\mathcal{A}_c$. The dashed line corresponds to the solution of the transient pressurization in the leak-off dominated regime; $\mathcal{A}_c = 0$.

As Fig. 5.6 shows, the effect of $\mathcal{A}_c$ on the transient pressurization of the crack diminishes with increase of the absolute value of the initial normalized pressure. We may observe that the storage effect (i.e., $\mathcal{A}_c = 0$) can be neglected by the time the fracture is re-opened (i.e., $p = \sigma_0$), if

$$|\bar{p}_0/p_{2c}| \gtrsim 1. \tag{5.18}$$

The above condition can be expanded in terms of the original problem parameters as:

$$\frac{hk\,(\sigma_0 - p_0)}{\mu Q_0} \gtrsim 0.25. \tag{5.19}$$

As we will further show in the breakdown example calculations for the case of unpropped, closed-fracture, condition (5.18) is valid for reservoir applications. Hence, the details of fracture deformation during the transient pressurization of the fracture can be approximately neglected by the time of fracture re-opening.

5.3.2.2 After crack re-opening

In this Section, we assume that the storage effect on the transient pressurization of the crack before the onset of crack re-opening is neglected (i.e., condition (5.19) is assumed to apply).

In view of (3.15) and (3.16), the global volume balance (2.13) after the onset of

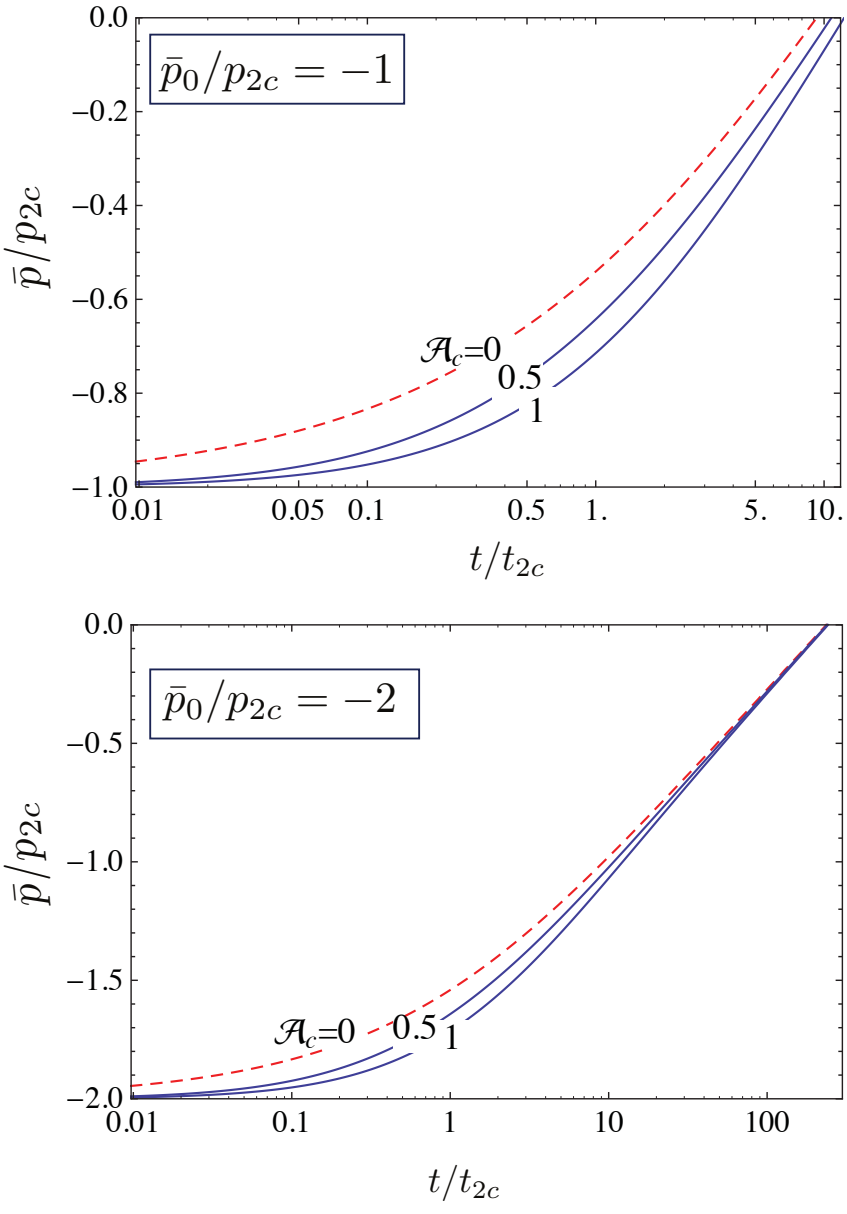

Figure 5.6: Evolution of normalized pressure $\bar{p}/p_{2c} = (p - \sigma_0)/p_{2c}$ with normalized time $\tau = t/t_{2c}$ during the transient pressurization of an un-propped and mechanically-closed fracture for various values of closed-crack aspect-ratio $\mathcal{A}_c$ and two values of the initial normalized pressure $\bar{p}_0/p_{2c} = -1$, and -2. The red dashed line corresponds to the solution of the transient pressurization in the leak-off dominated regime ($\mathcal{A}_c = 0$). The 2-D time and pressure scales are $t_{2c} = \ell^2/4\alpha$, $p_{2c} = Q_0 t_{2c}/\ell^2 hS$, respectively.

fracture re-opening can be expressed as

$$Q_0 t = \frac{\pi h^2 \ell}{E'} \bar{p}(t) + \int_0^{t_o} V_{aux}\left(t - t^{'}\right) \frac{\bar{p}(t^{'})}{dt^{'}} dt^{'} +$$

$$\int_{t_o}^{t} V_{aux}(t - t^{'}) \frac{d\bar{p}(t^{'})}{dt^{'}} dt^{'}, \qquad (\bar{p} = p - \sigma_0, \quad t \geq t_o) \tag{5.20}$$

Using the dimensionless pressure $\Pi = (p - \sigma_0)/p_{2c}$ and time $\tau = t/t_{2c}$ expressed in the 2-D scaling (equation (5.13)), allows to normalize (5.20) as

$$\tau = \pi \mathcal{A} \Pi(\tau) + \int_0^{\tau_o} \Phi_{aux}(\tau - \tau^{'}) \frac{d\Pi(\tau^{'})}{d\tau^{'}} d\tau^{'} +$$

$$\int_{\tau_o}^{\tau} \Phi_{aux}(\tau - \tau^{'}) \frac{d\Pi(\tau^{'})}{d\tau^{'}} d\tau^{'}. \tag{5.21}$$

where $\mathcal{A} = h/\ell S E^{'}$ (equation (3.22)), and $\tau_o = t_o/t_{2c}$ is the normalized re-opening time. The solution of (5.21) depends on non-dimensional parameters, Π_0 and $\mathcal{A}$.

Figure 5.7 shows the solution of the transient pressurization in the crack after the fracture re-opening. Numerical calculations are carried out for $\Pi_0 = (p_0 - \sigma_0)/p_{2c} = -1$ and various values of the crack aspect-ratio $\mathcal{A}$. The details of the numerical method are described in Appendix E.

As Fig. 5.7 shows, the storage effect on the transient pressurization of the crack is negligible for the entire range of time shown.

In summary, we established a criterion (equation (5.19)) which can be used to investigate the significance of the storage effects on the transient pressurization of the crack before and after the re-opening.

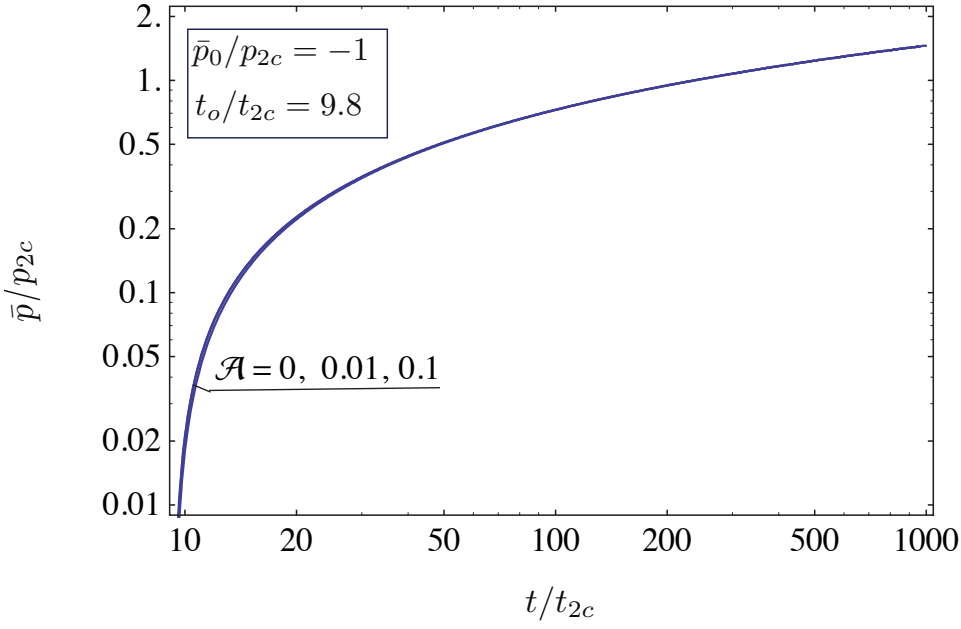

Figure 5.7: Evolution of normalized pressure $\bar{p}/p_{2c} = (p - \sigma_0)/p_{2c}$ with normalized time t/t_{2c} after the onset of crack re-opening for the initial normalized pressure $\bar{p}_0 = (p_0 - \sigma_0)/p_{2c} = -1$ and various crack aspect-ratio $\mathcal{A}$. The 2-D time and pressure scales are $t_{2c} = \ell^2/4\alpha$, $p_{2c} = Q_0 t_{2c}/\ell^2 hS$, respectively.

5.4 EXTENSION OF THE ANALYSIS TO MULTIPLE FRACTURES

In petroleum industry, the preferred method of completion during the hydraulic fracture treatment is multistage fracturing in which an array of parallel fractures is created from a borehole. In addition, in naturally fractured reservoirs, systematic sets of nearly parallel natural fractures are often observed. In this Section, we investigate the transient pressurization of multi-fractured wells.

We define a problem in which an infinite linear array of fractures is hydraulically connected to a horizontal borehole (Fig. 5.8). The pre-existing fractures characterized by the half-length ℓ and height h are uniformly distributed with spacing d. A low viscosity fluid is injected into a borehole at a constant volumetric flow rate which is assumed to be distributed equally among the fractures. Flow rate into a single fracture is denoted by Q_0^1.

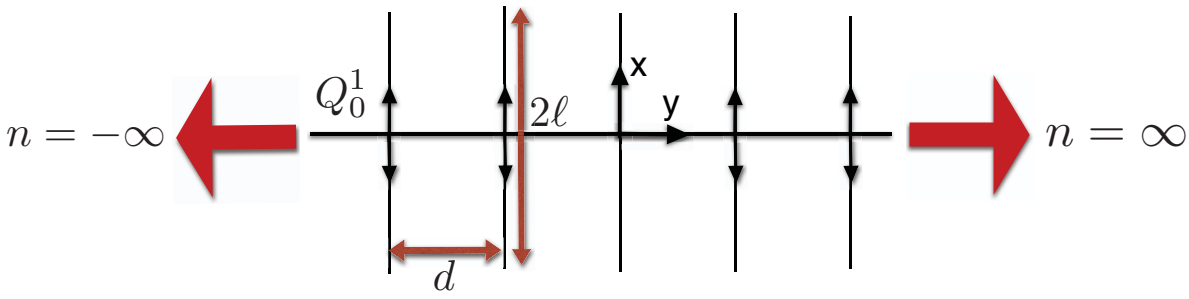

Figure 5.8: Infinite number of fractures characterized by the half-length ℓ and height h uniformly distributed at a distance d.

To aid the analysis of injection into an infinite linear array of fractures, we define an equivalent problem of fluid injection into a strip (infinite in the direction of x) of thickness d from two line sources of length 2ℓ located on the each side of the strip (Fig. 5.9). The rest of the strip boundary is impermeable (i.e., no-flow boundary). The transient pressurization solutions of the permeable strip and the infinite linear array of fractures are identical.

Figure 5.10 shows the evolution of the normalized pressure $(p - p_0)/(Q_0^1/4hS\alpha)$ with normalized time $4\alpha t/d^2$ for various values of the normalized strip thickness d/ℓ. The small time pressure asymptotic solution, marked as early linear flow on Fig. 5.9, is the 1-D asymptote of the transient pressurization solution for a single fracture given by:

$$p - p_0 = \frac{Q_0^1}{2\sqrt{\pi}hS\ell\sqrt{\alpha}}\sqrt{t}. \tag{5.22}$$

The latter corresponds to the injection times when the fractures have not yet interacted.

We also note that the numerical solution of the transient pressurization problem converges to an asymptote at the later injection time (marked as late linear flow on Fig. 5.9). This asymptote is approximately given by:

$$p - p_0 = \frac{Q_0^1}{2hSd\sqrt{\alpha}}\sqrt{t}. \tag{5.23}$$

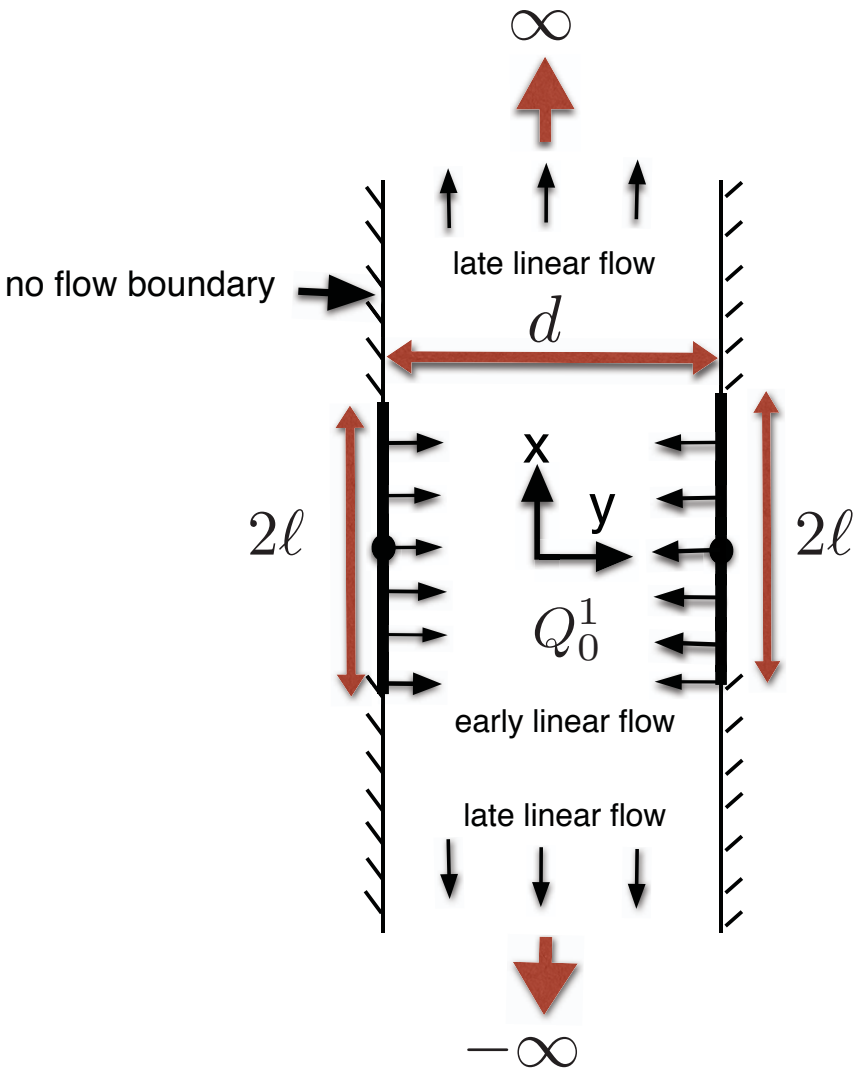

Figure 5.9: The problem of injection into a permeable strip of thickness d.

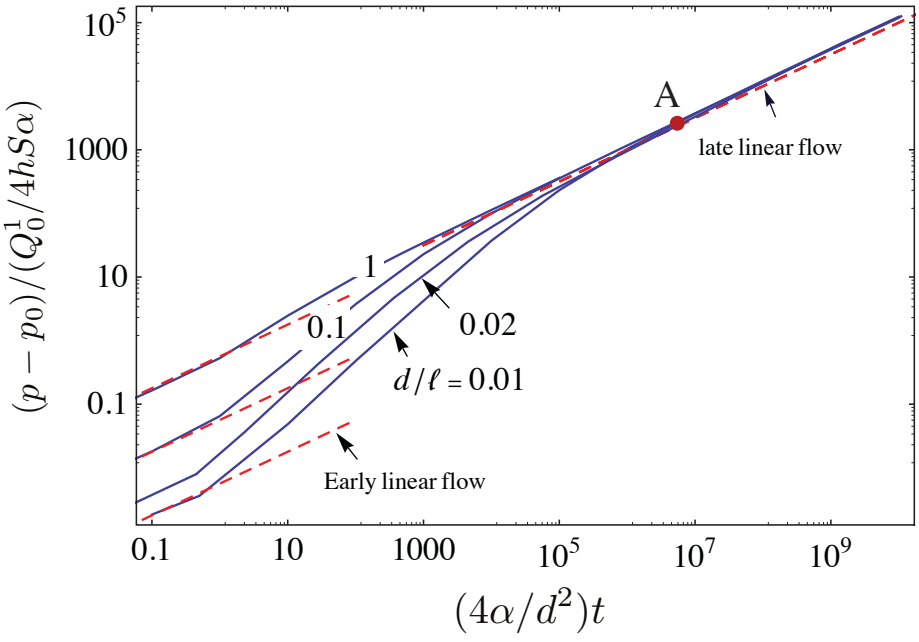

Figure 5.10: The evolution of the normalized pressure $(p - p_0)/(Q_0^1/4hS\alpha)$ with normalized time $(4\alpha/d^2)t$ for several values of the non-dimensional distance d/ℓ in the case of a permeable strip.

The details of the numerical calculations for the strip problem are described in Appendix F.

In summary, the strip solution can be used to obtain the transient pressurization of multiple fractures due to a fluid injection when the number of pre-existing fractures are sufficiently large. In case of injection into a finite number of fractures, the strip analysis is expected to be valid until times when the diffusion lengthscale becomes comparable or exceeds the fracture wellbore interval.

5.5 EXAMPLES OF THE BREAKDOWN CALCULATIONS

5.5.1 Propped fracture case (wastewater injection)

Consider a synthetic example of wastewater injection into a depleted hydraulically fractured sandstone reservoir characterized by: porosity $\phi = 0.18$, permeability $k =$ 5.1 md, minimum in-situ stress $\sigma_0 = 30$ MPa, initial reservoir pore pressure $p_0 =$

20 MPa, rock toughness $K_{Ic} = 1$ MPa $m^{1/2}$, fluid viscosity $\mu = 1$ cp, and bulk compressibility $c_t = 10^{-9}$ pa^{-1}. We assume that the wastewater is injected at a constant volumetric rate $Q_0 = 0.001$ m^3/sec into a single propped hydraulic fracture characterized by the fracture half-length $\ell = 28$ m, fracture conductivity $k_f\bar{w} = 4.4$ d-m, and fracture height $h = 18$ m [50].

The calculated values of the parameters are $S = 0.18$ GPa^{-1} (storage), $\alpha = 0.028$ m^2/s (diffusivity coefficient), $(k_f\bar{w})_D = 30.8$ (dimensionless propped fracture conductivity), $t_2 = 1.92$ hours (2D time scale), $p_2 = 2.72$ MPa (2D pressure scale), and $p_B = 30.27$ MPa (breakdown pressure). The corresponding value of the uniformity pressure is $p_{uni} = 21.77$ MPa (equation (5.2)). Since $p_B > p_{uni}$, the analysis based on the pressure uniformity assumption is valid. Locating the point with $(p_B - p_0)/p_2 = 3.8$ on Fig. 5.2 (point A), the onset of the fracture propagation is forecasted at $t_B/t_2 = 68358$, or in $t_B \simeq 15$ years.

5.5.2 Un-propped fracture case (supercritical CO_2 injection)

In Chapter 3, a synthetic example of the breakdown calculation during supercritical CO_2 injection into a single un-propped fracture in a critically over-pressured sandstone reservoir was considered (In Salah project, Algeria). In the following, we revisit this example, now in the context of naturally fractured reservoir with a normal reservoir condition (i.e., $p_0 < \sigma_0$).

The supercritical CO_2 is injected from a 1.5 km interval of a horizontal well aligned in the direction of the minimum confining stress. The horizontal well has intersected a pervasive array of pre-existing parallel natural fractures oriented perpendicular to the direction of the minimum confining stress (and, hence, well axis). The fracture density is reported to be 1/m. Hence, the total number of fractures intersected by the wellbore is $n \backsimeq 1500$. The actual rate of CO_2 injection in this project was $\dot{m} = 3500$ t/day. The sandstone formation has the with overall thickness of 20 m

(target zone for injection) consists of 5 horizontal layers of different thicknesses with some fractures span only one layer of the formation while other fractures span two layers. For the sake of simplicity, we assume that fractures have the same height, $h = 10$ m. The initial normal fracture stiffness is assumed to be $k_{ni} = 2.3$ MPa/mm (see Table 5.1 for the un-propped fracture properties in a sandstone reservoir).

Using the representative values for the supercritical CO_2 properties calculated at the breakdown pressure value (Section 3.5), the calculated values of the related parameters are: $Q_0 = 0.057$ m^3/s (total volumetric injection rate), $Q_0^1 = 3.78 \times 10^{-5}$ (volumetric injection rate per fracture), $\mathcal{Q} = 1.92 \times 10^{-4}$ (non-dimensional rate number), $(p_0 - \sigma_0)/k_{ni}w_0 = -11.74$ (non-dimensional initial net pressure), $d/\ell = 0.02$ (non-dimensional fracture spacing), $\mathcal{A}_c = 0.003$ (closed-crack aspect-ratio), $\mathcal{A} = 0.011$ (open-crack aspect-ratio), and $\mathcal{D} = 1.5 \times 10^{-5}$.

Since the calculated non-dimensional rate number is $\mathcal{Q} \lesssim 10^{-4}$ the condition of pressure uniformity is arrived at before the crack re-opening/breakdown (see Section 5.3), and, therefore, the analysis of the transient pressurization based on the pressure uniformity is valid.

We check the validity of condition (5.19) to see whether the effects of the fracture storage before and after fracture re-opening on the transient pressurization can be neglected. We have $hk(\sigma_0 - p_0)/\mu Q_0^1 = 619 \gg 0.25$ (Equation (5.19)). Hence, the effect of storage on the transient pressurization calculations can be reasonably neglected.

Since the number of fractures in this example is sufficiently large (i.e., $n = 1500$), the strip (infinite array of cracks) analysis can be used to estimate the onset of fracture breakdown. Locating the point with $(p_B - p_0)/(Q_0^1/4hS\alpha) = 2532.5$ on Fig. 5.10 (point A), the onset of the fracture propagation is forecasted at $(4\alpha/d^2)t_B = 5.9 \times 10^6$, or in $t_B \simeq 213.4$ days.

5.6 SUMMARY OF CHAPTER RESULTS

In this Chapter, we relaxed the assumption of a mechanically-open fracture to account for the possibility of an initially closed fracture. We divided the realm of closed fractures into two categories, namely, propped and un-propped closed fractures. This is due to the difference in mechanics of fracture deformation in these two cases.

Initially, we obtained the parametric range when the condition of pressure uniformity in the crack is valid. Assuming a uniform pressure distribution along the crack, the transient pressurization problems for propped and un-propped closed fractures due to a fluid injection are formulated. For the case of un-propped fracture, we obtained the parametric range when the crack storage effect on the transient pressurization calculations before and after the crack re-opening is insignificant. The latter allows for much more simpler formulation of the transient pressurization problem.

The analysis of the transient pressurization was then extended to multiple fractures. We defined the problem of fluid injection into an infinite linear array of fractures at a constant volumetric flow rate. We show that this problem is mathematically equivalent to injection into a strip from its boundaries.

The analysis of the transient pressurization of initially closed crack(s) in this Chapter was used to predict the onset of the crack propagation for the cases when these cracks are either propped or un-propped.

CHAPTER 6: CONCLUSIONS AND RECOMMENDATIONS

Extensive analytical and numerical studies were carried out to investigate the reactivation of a PKN hydraulic fracture due to the massive fluid injection in permeable rock. The objective was to quantify the transient pressurization and onset of fracture breakdown due to fluid injection.

We initially considered a pre-existing, un-propped, non-poroelastic crack in a critically over-pressured reservoir (Chapter 3). To formulate the problem, we revisited the work by Detournay and Cheng [57] in which the transient pressurization of a crack subjected to a step pressure increase was considered. The solution of this problem was then used to construct a convolution integral governing the transient pressurization of the crack due to a constant rate of injection. We derived the analytical expression for the large-time asymptotic of the fluid leak-off rate in the auxiliary problem. The transient pressurization of the fracture was formulated assuming the pressure is uniformly distributed along the fracture. We established the parametric range when the condition of the pressure uniformity is justified. Pressure uniformity allows for much simpler formulation of the transient pressurization using the Green's function approach.

In Chapter 4, we accounted for the poroelastic effects on the transient pressurization and onset of fracture propagation in a critically over-pressured reservoir. We first revisited the auxiliary problem of a crack subjected to mode 1 (traction) and mode 2 (pore pressure) poroelastic loadings [53]. In the formulation of the auxiliary problem, we accounted for full (2-D) pore pressure by relaxing the 1-D diffusion assumption of Chapter 3. We used the auxiliary problem to formulate the transient pressurization of the crack using the Green's function approach. Comparison of the transient pressurization solutions of poroelastic and non-poroelastic cracks shows that the poroelastic effect on the evolution of the fluid pressure in the crack is

negligible. However, the poroelasticity can have significant effects on the crack opening (and, therefore volume) due to the generated backstress. We also showed that the poroelastic effects will substantially delay the breakdown time compared to the non-poroelastic case when the fracture breakdown occurs at later stages of injection characterized by large-scale (2D) pore pressure perturbation in the reservoir.

In Chapter 5, we relaxed the assumption of a critically over-pressured reservoir. We considered the transient pressurization of a crack initially subjected to a compressive effective stress (i.e., $\bar{p}_0 = p_0 - \sigma_0 < 0$). The analysis is performed for the cases when the crack is either propped or not. We first established the parametric range when the condition of the pressure uniformity is reached. Assuming a uniform pressure distribution along the crack, we obtained the transient pressurization of the propped and propped fractures due to a fluid injection. For an un-propped fracture, we established the parametric range range when the storage effect on the transient pressurization can be approximately neglected. We then extended the transient pressurization analysis to multiple fractures. We defined the problem of fluid injection into an infinite linear array of fractures at a constant volumetric flow rate. We show that this problem is mathematically equivalent to injection into a strip from its boundaries. The analysis of the strip problem allows for simpler formulation of the transient pressurization in multiple fractures.

6.1 RECOMMENDATIONS FOR FUTURE RESEARCH

In Chapter 5, we neglected the poroelastic effects on the transient pressurization of propped and un-propped closed fractures. Future work should account for the poroelastic effects on the transient pressurization of a mechanically-closed crack. We may still expect that the onset of crack re-opening and breakdown to be substantially delayed compared to the non-poroelastic case when the condition of the crack re-opening and breakdown is reached at later injection time when the leak-off diffusion

is essentially 2-D.

The study of hydraulic fracture reactivation was limited to a stationary pre-existing crack in this work. As the condition of fracture breakdown is reached, the fracture will propagate. The future work should consider the fracture propagation problem. The objective will be to evaluate the crack growth rate from the onset of propagation. We should note that the history of the transient pressurization prior to breakdown can be used to provide the initial conditions for the fracture propagation problem. The analytical solution of Gordeyev and Entov (1997) [8] can be used to validate the numerical solution at large propagation time (the leak-off dominated regime). The poroelastic effects on fracture propagation should also be investigated.

In this study, the transient pressurization of multiple fractures was investigated assuming that the fluid is injected into an infinite array of fractures. The future work will consider the problem of injection into a finite number of fractures. One may use the superposition of instantaneous point sources distributed along each fracture to formulate the transient pressurization of finite number of fractures. Similar to treatment of the transient pressurization of a single fracture, we can define an auxiliary problem in which the fractures are subjected to a step pressure increase. The auxiliary problem allows one to evaluate the fluid leak-off from each fracture which then can be used to construct the convolution integral governing the transient pressurization of finite number of fractures.

Bibliography

[1] G. P. Willhite. *Waterflooding*. SPE Textbook Series. SPE, Richardson, Texas, 1986.

[2] R.G. Keck and R.J. Withers. A field demonstration of hydraulic fracturing for solids waste injection with real-time passive seismic monitoring. In *SPE Annual Technical Conference and Exhibition*. Society of Petroleum Engineers, 1994.

[3] Z.A. Moschovidis, D.C. Gardner, and R.W. Veatch. Disposal of oily cuttings by downhole periodic fracturing injections, Valhall, North Sea: case study and modeling concepts: SPEDC 9 (4): 256–262. *Trans., AIME*, 297:256–262, December 1994.

[4] G.C. Howard and C.R. Fast. Optimum fluid characteristics for fracture extension. *Drilling and Production Practices*, pages 261–270, 1957.

[5] R.P. Nordgren. Propagation of vertical hydraulic fractures. *J. Pet. Tech.*, 253:306–314, 1972. (SPE 3009).

[6] J. Hagoort, B.D. Weatherill, and A. Settari. Modeling the propagation of waterflood-induced hydraulic fractures. *Soc. Pet. Eng. J.*, 20:293–303, 1980.

[7] Y.N. Gordeyev. Growth of a crack produced by hydraulic fracture in a poroelastic medium. *Int. J. Rock Mech. Min. Sci.*, 30(3):233–238, 1993.

[8] Y. N. Gordayev and V. M. Entov. The pressure distribution around a growing crack. *J. Appl. Maths Mechs.*, 61(6):1025–1029, 1997.

[9] Y. Kovalyshen. *Fluid-Driven Fracture in Poroelastic Medium*. PhD thesis, University of Minnesota, Minneapolis, February 2010.

[10] E. Detournay and A.H-D. Cheng. *Comprehensive Rock Engineering*, volume 2, chapter 5: Fundamentals of Poroelasticity, pages 113–171. Pergamon, New York NY, 1993.

[11] A. Settari. A new general model of fluid loss in hydraulic fracturing. *Soc. Pet. Eng. J.*, 25(4):491–501, 1985. (SPE 11625).

[12] A. Settari and M.P. Cleary. Development and testing of a pseudo-three dimensional model of hydraulic fracture geometry. *SPE 10505*, pages 449 –466, 1982.

[13] S. A. Mathias and M. Reeuwijk. Hydraulic fracture propagation with 3-D leak-off. *Transport in Porous Med.*, 80:499–518, 2009.

[14] L. Murdoch and L. Germanovich. Analysis of a deformable fracture in permeable material. *Int. J. of Analytical Methods in Geomechanics*, 30:529–561, May 2006.

[15] A. Daubrée. *Etudes synthetiques de geologie experimentale.* Dunod, Éditeur, Paris, France, 1879.

[16] G. F. Becker. The structure of a portion of the Sierra Nevada of California. *Geol. Soc. Am. Bull.*, 2(1):49–74, 1891.

[17] D. D. Pollard and A. Aydin. Progress in understanding joints over the last century. *Geol. Soc. Am. Bull.*, 100:1181–1204, 1988.

[18] R. A. Hodgson. Classification of structures on joint surfaces. *AM. J. SCI.*, 259(7):493–502, September 1961.

[19] T. Engelder. Is there a genetic relationship between selected regional joints and contemporary stress within the lithosphere of north america? *Tectonics*, pages 161–177, April 1982.

[20] P. R. Pointe and J. A. Hudson. Characterization and interpretation of rock mass joint patterns. *Geol. Assoc. Am. Spec. Pap.*, 199:1–38, 1985.

[21] T. K. Perkins and L. R. Kern. Widths of hydraulic fractures. *J. Pet. Tech., Trans. AIME*, 222:937–949, 1961.

[22] Energy Information Administration. Annual energy outlook 2011 early release overview, 2011.

[23] M. J. Economides and K. G. Nolte, editors. *Reservoir Stimulation*. John Wiley & Sons, Chichester UK, 3rd edition, 2000.

[24] M. Deutsch. Ground water contamination and legal controls in Michigan. Technical Report 1691, US Geological Survey Water Supply, Printing Office, Washington DC, 1963.

[25] C. Nicholson and R.L. Wesson. Earthquake hazard associated with deep well injection. Report to the US Environmental Protection Agency, US Geological Survey Bulletin, 1951.

[26] H.L Dearing and S.A. Ali. Drill-in fluid selection crucial to well productivity. *Petroleum Engineer International*, 69, 1996.

[27] D.B. Bennion. Low permeability gas reservoirs: Problems, opportunities and solutions for drilling, completion, stimulation and production. *SPE 35577*, 1996.

[28] S.A. Khristianovic and Y.P. Zheltov. Formation of vertical fractures by means of highly viscous fluids. In *Proc. 4th World Petroleum Congress, Rome*, volume II, pages 579–586, 1955.

[29] D. A. Spence and P. W. Sharp. Self-similar solution for elastohydrodynamic cavity flow. *Proc. Roy. Soc. London*, Ser. A(400):289–313, 1985.

[30] J. Geertsma and F. de Klerk. A rapid method of predicting width and extent of hydraulic induced fractures. *J. Pet. Tech.*, 246:1571–1581, 1969. (SPE 2458).

[31] J. I. Adachi. *Fluid-Driven Fracture in Permeable Rock*. PhD thesis, University of Minnesota, Minneapolis, 2001.

[32] E. Detournay. Propagation regimes of fluid-driven fractures in impermeable rocks. *Int. J. Geomechanics*, 4(1):1–11, 2004.

[33] D. I. Garagash. Propagation of a plane-strain hydraulic fracture with a fluid lag: Early-time solution. *Int. J. Solids Structures*, 43:5811–5835, 2006.

[34] Pennsylvania Department of Environmental Protection. Marcellus shale permits issued and wells drilled, December 2011.

[35] S. Bachu. Screening and ranking of sedimentary basins for sequestration of CO2 in geological media in response to climate change. *Environmental Geology*, 44:277–289, 2003.

[36] J. Bradshaw, S. Bachu, D. Bonijoly, R. Burruss, S. Holloway, N. P. Christensen, and O. M. Mathiassen. CO2 storage capacity estimation: Issues and development of standards. *Int. J. of Greenhouse Gas Control*, 1:62–68, 2007.

[37] N.R. Warpinski, Z.A. Moschovidis, C.D. Parker, and I.S. Abou-Sayed. Comparison study of hydraulic fracturing models: Test case GRI-staged field experiment No. 3. 9(1):7–16, 1994. (SPE 25890).

[38] C.B. Raleigh, J.H. Healy, and J.D. Bredehoeft. An experiment in earthquake control at Rangely, Colorado. *Science*, 191(4233):1230–1237, 1976.

[39] P. Talwani and S. Acree. Pore pressure diffusion and the mechanism of reservoir-induced seismicity. *Pure Appl. Geophys.*, 122:947–965, 1985.

[40] P. A. Hsieh and J.D. Bredehoeft. A reservoir analysis of the Denver earthquakes: A case of induced seismicity. *J. Geophys. Res.: Solid Earth*, 86:903–920, 1981.

[41] C. R. Van Hise. Principles of North American Pre-Cambrian geology. Technical report, U.S. Geological Survey, 1896.

[42] J.B. Walsh. Effect of pore pressure and confining pressure on fracture permeability. *Int. J. Rock Mech. Min. Sci.*, 18:429–435, 1981.

[43] C. Louis. *A study of groundwater flow in jointed rock and its influence on the stability of rock masses*. Imperial College of Science and Technology, 1969.

[44] D.T. Snow. *A parallel plate model of fractured permeable media*. PhD thesis, Univ. of Calif., Berkeley, USA, 1965.

[45] L. Smith, C. W. Mase, and F. W. Schwartz. Estimation of fracture aperture using hydraulic and tracer tests. In *Proc 28th U.S. Symp. On Rock Mechanics*, Tucson, 1987.

[46] S. R. Brown. Simple mathematical model of a rough fracture. *J. Geophys. Res.*, 100(B4):5941–5952, 1995.

[47] R. W. Zimmerman and G. S. Bodvarsson. Hydraulic conductivity of rock fractures. *Transport in Porous Media*, 23:1–30, 1996.

[48] E. Hakami and E. Larsson. Aperture measurement and flow experiments on a single natural fracture. *Int. J. Rock Mech. Min. Sci.*, 33(4):395–404, 1996.

[49] A. C. Gringarten, H. J. Ramey Jr., and R. Raghavan. Applied pressure analysis for fractured wells. *J. of Petroleum Technology*, pages 887–892, July 1975.

[50] L.H. Cinco-Ley, V.F. Samaniego, and A.N. Dominguez. Transient pressure behavior for a well with a finite-conductivity vertical fracture. *Soc. Pet. eng. J.*, 18(4):253–264, 1978.

[51] A. Settari and R.C. Bachman. Numerical simulation of hydraulic fracturing treatments with low-viscosity fluids. *J. of Canadian Petroleum Technology*, 26, 1987.

[52] Y. N. Gordayev and A. F. Zazovsky. Self-similar solution for deep-penetrating hydraulic fracture propagation. *Transport Porous Med.*, 7(3):283–304, 1992.

[53] E. Detournay and A.H-D. Cheng. *Fundamentals of Poroelasticity*, volume II of *Comprehensive Rock Engineering: Principles, Practice and Projects*. Pergamon Press, Elmsford, NY, 1993.

[54] A. P. Bunger, E. Detournay, and D. I. Garagash. Toughness-dominated hydraulic fracture with leak-off. *Int. J. Fracture*, 134:175–190, 2005.

[55] D. I. Garagash. Plane-strain propagation of a fluid-driven fracture in a permeable medium: leak-off dominated regime. *Int. J. Solids Structures*, in preparation, 2009.

[56] T. W. Patzek and D. B. Silin. Water injection into a low-permeability rock-1:hydrofracture growth. *Transport in Porous Media*, pages 537–555, 2001.

[57] E. Detournay and A.H-D. Cheng. Plane strain analysis of a stationary hydraulic fracture in a poroelastic medium. *Int. J. Solids Structures*, 27(13):1645–1662, 1991.

[58] I. Berchenko, E. Detournay, and N. Chandler. Propagation of natural hydraulic fractures. *Int. J. Rock Mech*, 1997.

[59] M.A. Biot. General theory of three-dimensional consolidation. *J. Appl. Phys.*, 12:155–164, 1941.

[60] E. Detournay, A.H-D. Cheng, and J.D. McLennan. A poroelastic PKN hydraulic

fracture model based on an explicit moving mesh algorithm. *ASME J. Energy Res. Tech.*, 112:224–230, 1990.

[61] T.J. Boone, A.R. Ingraffea, and J.C. Roegiers. Simulation of hydraulic fracture propagation in poroelastic rock with application to stress measurement techniques. *Int. J. Rock Mech. Min. Sci. & Geomech. Abstr.*, 28(1):1–14, 1991.

[62] Y. Abousleiman, Y.G. Yuan, and J. C. Roegiers. Propagation/recession of a penny-shaped fracture in a permeable diffusive formation. *SPE-28086*, 1994.

[63] J. W. Hutchinson and Z. Suo. Mixed mode cracking in layered materials. *Adv. Appl. Mech.*, 29:63–191, 1992. pdf.

[64] K. G. Nolte. Fracturing-pressure analysis for nonideal behavior. *J. Pet. Tech.*, pages 210–218, February 1991.

[65] Y. Kovalyshen and E. Detournay. A reexamination of the classical PKN model of hydraulic fracture. *Transport Porous Med.*, 2009.

[66] J. Bear. *Dynamics of Fluids in Porous Media*. Dover Publications, 1988.

[67] H. Carslaw and J. C. Jaeger. *Conduction of Heat in Solids*. Oxford University Press, 2nd edition, 1959.

[68] H. Stehfest. Numerical inversion of laplace transform. *Commun. ACM*, 13(1):47–49, 1970.

[69] H. Tada, P.C. Paris, and G.R. Irwin. The stress analysis of cracks handbook ASME. *New York*, pages 55–56, 2000.

[70] K. Michael, A. Golab, V. Shulakova, J. Ennis-King, G. Allinson, S. Sharma, and T. Aiken. Geological storage of CO2 in saline aquifers-a review of the experience from existing storage operations. *Int. J. Greenhouse Gas Control*, 4(4):659–667, 2010.

[71] J. Rutqvist, W.V. Donald, and M. Larry. Coupled reservoir-geomechanical analysis of CO2 injection and ground deformations at in Salah, Algeria. *Int. J. Greenhouse Gas Control*, 4(2):225–230, 2010.

[72] S. C. Bandis, A. C. Lumsden, and N. R. Barton. Fundamentals of rock joint deformation. *Int. J. Rock Mech. Min. Sci. and Geomech. Abstr.*, 20(6):249–268, 1983.

[73] R.L. Mazza. Liquid-free CO2/sand stimulations: An overlooked technology production update. *SPE*, pages 1–12, 2001.

[74] M. Pagels, D. Willberg, and E. Edelman. Chemo-mechanical effects of fluid invasion into low permeability rocks. In *EOS Trans. AGU (Fall Meeting Suppl.)*, 2011.

[75] A.F. Gangi. Variation of whole and fractured porous rock permeability with confining pressure. *Int. J. Rock Mechanics and Mining Sciences*, 15:249–257, 1978.

[76] S. C. Bandis, A. C. Lumsden, and N. R. Barton. Fundamentals of rock joint deformation. *Int. J. Rock Mech. Min. Sci.*, 20(6):249–268, 1983.

[77] L.I. Sedov. *A Course in Continuum Mechanics*. Walters-Noordhoff Publishing, 1971–1972.

[78] A. T. Zehnder. *Fracture Mechanics*. Lecture Notes in Applied and Computational Mechanics. Springer, Ithaca, New York, 2012.

[79] S.V. Patankar. *Numerical Heat Transfer and Fluid Flow*. Hemisphere Publ. Corp., Washington DC, 1980.

[80] M. Abramowitz and I.A. Stegun, editors. *Handbook of Mathematical Functions*

with Formulas, Graphs, and Mathematical Tables. Dover Publications Inc., New York NY, 1972.

[81] G. N. Watson. *A treatise on the theory of Bessel functions*. Cambridge university press, London, England, 1995.

[82] F. Erdogan, G. D. Gupta, and T. S. Cook. *Numerical solution of singular integral equations*, volume 1 of *Mechanics of Fracture*, chapter 7, pages 368–425. Noordhoff International Publ., Leyden, 1973.

APPENDIX A: ENERGY RELEASE RATE OF AN INTERNALLY LOADED CRACK

The first law of thermodynamics in application to fracture states that the internal energy (U) of the body $\mathscr{V}$ changes due to (i) the work of tractions $\mathbf{p}^n = \sigma_{ji} n_j \mathbf{e}_i$ on the displacement increments $d\mathbf{w}$ at the body's boundary S (inclusive of crack surfaces) characterized by external normal $\mathbf{n}$ ($dA^{(e)}$) and (ii) the energy released in extending the surface of the crack(s) by $d\Sigma$ ($dA^{(e)}_{d\Sigma} \leq 0$) [77]:

$$dU = dA^{(e)} + dA^{(e)}_{d\Sigma}, \tag{A.1}$$

$$U = \int_{\mathscr{V}} \left(\int \sigma_{ij} d\varepsilon_{ij} \right) dV, \qquad dA^{(e)} = \int_S \mathbf{p}^n d\mathbf{w}\, dS \tag{A.2}$$

Defining the energy release rate as

$$G \equiv -\frac{dA^{(e)}_{d\Sigma}}{d\Sigma}, \tag{A.3}$$

(A.1) can be rewritten as

$$\frac{dU}{d\Sigma} = \int_S \mathbf{p}^n \frac{d\mathbf{w}}{d\Sigma}\, dS - G \tag{A.4}$$

Consider U and G to be functions of the crack surface area Σ and boundary tractions, the latter - a function of a loading parameter(s) p. Variation of the internal energy when the crack is not propagating (fixed Σ condition) is equal to the work of tractions on the corresponding change of displacements, i.e. $(\partial U/\partial p)_\Sigma = \int_S \mathbf{p}^n \left(\partial \mathbf{w}/\partial p\right)_\Sigma\, dS$. Expanding the derivative $d/d\Sigma = (\partial/\partial\Sigma)_p + (dp/d\Sigma)(\partial/\partial p)_\Sigma$ in (A.4) and using the latter (fixed Σ) result allow to reduce Eq. (A.4) to

$$\left(\frac{\partial U}{\partial \Sigma}\right)_p = \int_S \mathbf{p}^n \left(\frac{\partial \mathbf{w}}{\partial \Sigma}\right)_p dS - G \tag{A.5}$$

Further, using the well-known result of linear elasticity, stating that variation of the internal energy under conditions of fixed boundary tractions is equal to a half of the work of these tractions, i.e., $\left(\partial U/\partial\Sigma\right)_p = \frac{1}{2}\int_S \mathbf{p}^n \left(\partial\mathbf{w}/\partial\Sigma\right)_p \, dS$, in (A.5), we arrive to the result

$$G = \left(\frac{\partial U}{\partial \Sigma}\right)_p \tag{A.6}$$

which is usually exposed in the literature in the framework of traction-free cracks [e.g. 78]. Essentially, (A.6) implies that the energy release rate associated with fracture growth is a function of the instantaneous loading, and is, therefore, independent of the loading history.

APPENDIX B: NON-UNIFORM PRESSURE SOLUTION (VISCOUS PRESSURE DROP IN THE CRACK)

B.1 NORMALIZED EQUATIONS

Using the non-dimensional time (τ), coordinate (ξ), and pressure (Π) defined in Section 3.2, and introducing the non-dimensional y coordinate ($\chi = y/\ell$) , the lubrication equation (2.11) and initial-boundary conditions (2.12) are normalized as

$$\frac{\partial \Pi}{\partial \tau} - \frac{4\mathbb{K}}{\pi} \left.\frac{\partial \Pi}{\partial \chi}\right|_{\chi=0} = \frac{1}{16} \frac{\partial^2 (\mathcal{W}_0/2+\Pi)^4}{\partial \xi^2}, \tag{B.1}$$

$$\Pi|_{\tau=0} = 0, \quad \left.\frac{\partial (\mathcal{W}_0/2+\Pi)^4}{\partial \xi}\right|_{\xi=0^+} = -\frac{16}{\pi}, \quad \left.\frac{\partial (\mathcal{W}_0/2+\Pi)^4}{\partial \xi}\right|_{\xi=1} = 0, \tag{B.2}$$

respectively, where $\mathcal{W}_0$ is the non-dimensional neutral hydraulic opening parameter (equation (3.1)), and $\mathbb{K}$ is the non-dimensional permeability parameter (equation (3.3)). Note that the induced crack width for a mechanically-open fracture (equation (2.2)) is used to obtain the height average crack opening (equation (2.3)).

The normalized form of the diffusivity equation (2.15),

$$\frac{\partial \Pi}{\partial \tau} = \mathcal{A}\,\mathbb{K} \left(\frac{\partial^2 \Pi}{\partial \xi^2} + \frac{\partial^2 \Pi}{\partial \chi^2} \right), \tag{B.3}$$

completes the set of normalized governing equations (B.1)-(B.3). (Here $\mathcal{A} = h/(\ell S E')$ is the scaled crack aspect ratio parameter). The transient pressurization of fracture in impermeable formation can be extracted as a special case from above formulation by letting $\mathbb{K} = 0$.

B.2 NUMERICAL SCHEME

The adopted numerical method to solve (B.1)-(B.3) is based on the method-of-lines approach in which the unknown field function Π is discretized in space but not in time. This allows to reduce the system of PDEs, (B.1) and (B.3), to a system of ordinary differential equations in time at the space discretization nodes. We use the central finite-difference representation [e.g., 79] for a set of non-uniformly spaced grid points $\{0 \leq \xi_i < \infty, 0 \leq \chi_j < \infty\}$, $i = 1, ..., M$ and $j = 1, ..., N$, spanning the quarter space (owing to the problem symmetry). In view of (i) the initially high pressure gradient near the fluid injection point (located at the crack inlet $\xi = 0$), and (ii) singular leak-off rates at the crack tip ($\xi = 1$), as observed from the solutions neglecting pressure drop in the crack (Sections 3.3-3.4), we use the ξ-mesh with logarithmically-concentrated nodes near the inlet and near the tip of the crack, connected by the intermediate region with uniform mesh. Outside of the crack ($\xi > 1$), we also make use of logarithmic ξ-node spacing in order to span a computational domain which is sufficiently large to model diffusion in the infinite space. For the same reason, we use logarithmic grid spacing in the direction normal to the crack plane (χ-mesh). The numerical results reported in this Appendix and Section 3.2 are based on the computational domain with $\xi_M = \chi_N = 10^7$ (as proved to be necessary for cases when $\mathbb{K}$ is not small, and large injection time is required to achieve approximate pressure uniformity), and the mesh with total $M = 200$ and $N = 100$ nodes in the ξ and χ directions, respectively. We have verified robustness of the numerical solution by carrying tests for a refined (doubled) discretization.

B.3 PARAMETRIC DEPENDENCE OF THE "UNIFORMITY" PRESSURE AND TIME

Figure B.1 illustrates the effect of the non-dimensional neutral hydraulic opening $\mathcal{W}_0$ on the "uniformity values" of the pressure ($\bar{p}_{uni}/p_*$) and time (t_{uni}/t_*) for the case

of impermeable rock (i.e., $\mathbb{K} = 0$). (As per the main text, the "uniformity" values correspond to the 5% maximum pressure variation along the crack, see, e.g., Fig. 3.1). Evidently, the case with zero neutral opening gives the upper bound of the uniformity pressure and time.

The effect of non-zero rock permeability (quantified by the non-dimensional parameter $\mathbb{K}$) on the uniformity pressure and time is illustrated in Fig. B.2 for a reference case with zero neutral opening, $\mathcal{W}_0 = 0$, and the crack-aspect ratio parameter $\mathcal{A} = 0.01$. The numerical results show that the uniformity pressure remains almost unchanged from its value in the impermeable case, if $\mathbb{K} \lesssim 1$. However, the uniformity time t_{uni} does change (increase) with $\mathbb{K}$ (Fig. B.2b).

For large values of $\mathbb{K}$, computational time required to reach pressure uniformity becomes prohibitively large, but one may expect the uniformity pressure to decline with large enough $\mathbb{K}$ (e.g., $\mathbb{K} > 10$), and approach the initial reservoir pore pressure ($p_{uni} \to p_0$ or $\overline{p}_{uni} \to 0$) in the limit of $\mathbb{K} \to \infty$, as the uniformity time diverges in the same limit.

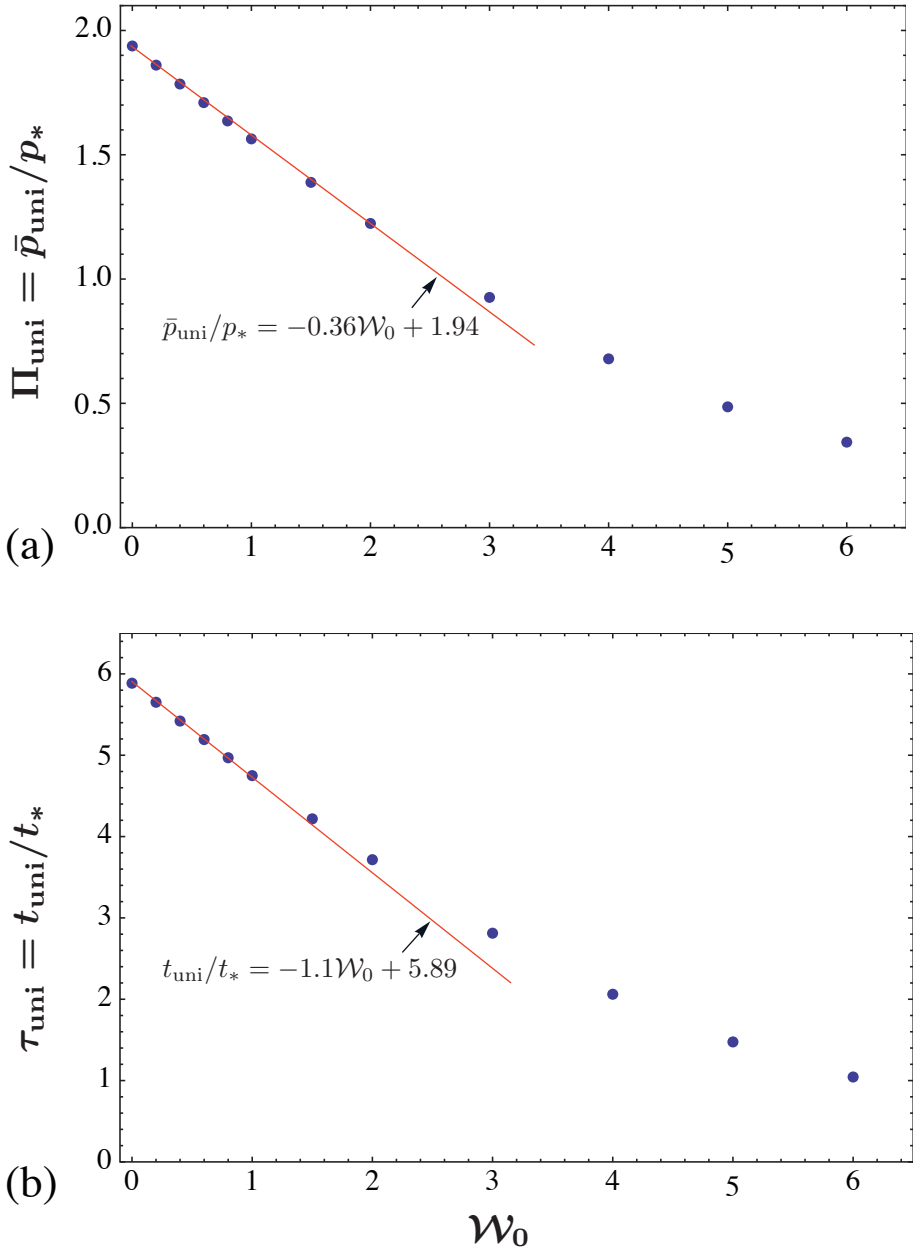

Figure B.1: Dependence of (a) uniformity net pressure $\bar{p}_{uni}/p_*$ and (b) uniformity time t_{uni}/t_* on the non-dimensional neutral hydraulic opening $\mathcal{W}_0 = w_0(E'/\mu Q_0 \ell)^{1/4}$ during the transient pressurization of a mechanically-open fracture in impermeable rock. The characteristic pressure and time scales are $p_* = \left(\mu Q_0 E'^3 \ell/h^4\right)^{1/4}$ and $t_* = \left(\mu \ell^5 h^4/E' Q_0^3\right)^{1/4}$, respectively.

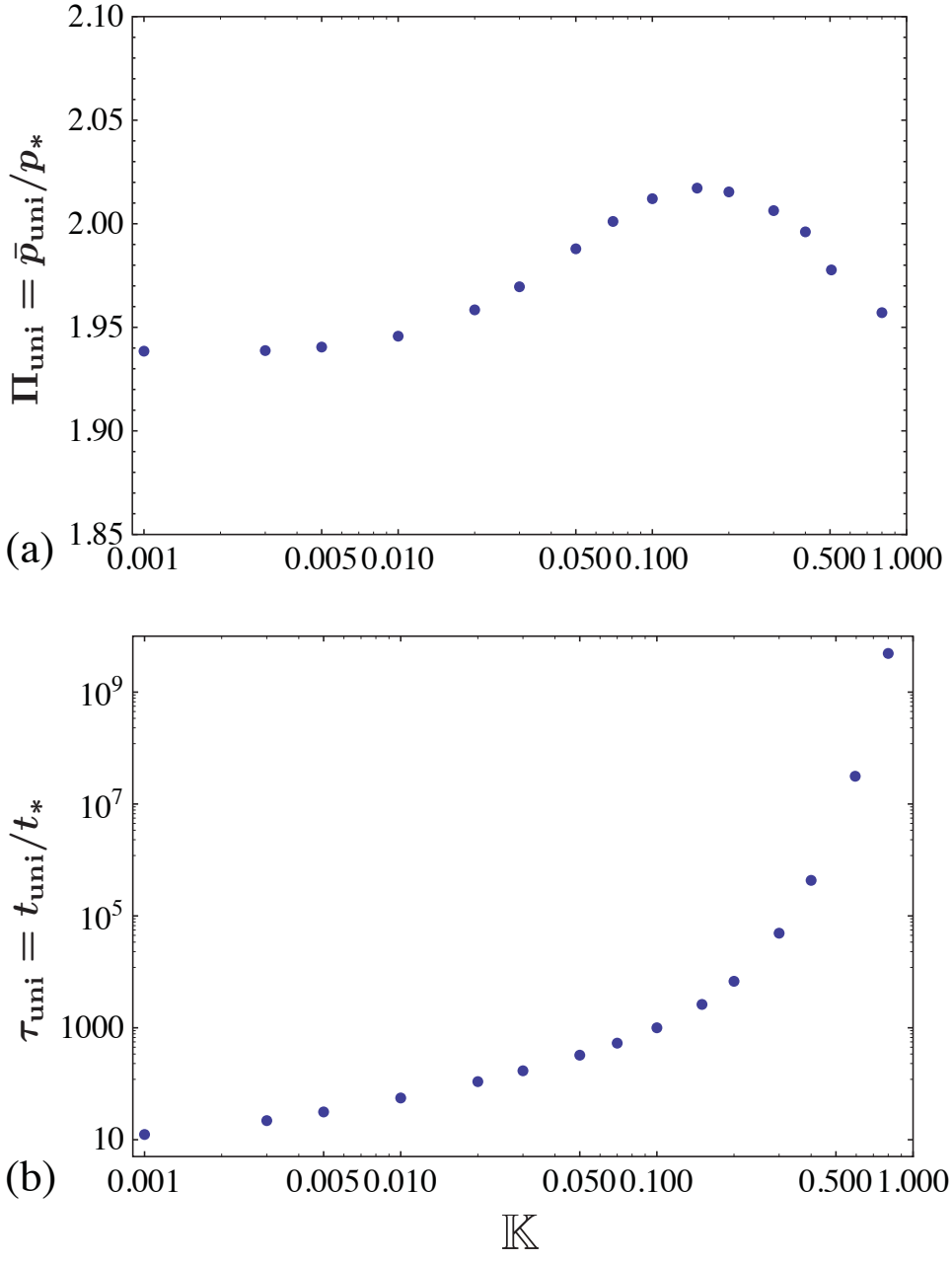

Figure B.2: Dependence of (a) uniformity net pressure $\bar{p}_{uni}/p_*$ and (b) uniformity time t_{uni}/t_* on the non-dimensional permeability parameter $\mathbb{K} = k\left(\ell^{1/3}E'/Q_0\mu\right)^{3/4}$ during the transient pressurization of a mechanically-open fracture with the aspect-ratio parameter $\mathcal{A} = 0.01$ and negligible neutral hydraulic opening $\mathcal{W}_0 = 0$.

APPENDIX C: LARGE-TIME ASYMPTOTE OF THE LEAK-OFF RATE IN THE AUXILIARY PROBLEM

C.1 LAPLACE DOMAIN

Using asymptotic expression $K_0(z) = -\ln(z/2) - \gamma$, $z \ll 1$ [80], to approximate the Bessel kernel in (3.8) leads to:

$$\frac{1}{s} = -\frac{2}{\pi}\int_{-1}^{1} \hat{\psi}(\xi', s)\left(\ln(\sqrt{s}|\xi - \xi'|) + \gamma\right) d\xi', \qquad s \ll 1. \tag{C.1}$$

where γ is the Euler constant. Differentiating (C.1) in ξ, and inverting the resulting Cauchy integral equation, $0 = \int_{-1}^{1} \hat{\psi}(\xi', s)\, d\xi'/(\xi - \xi')$, yields

$$\hat{\psi}(\xi, s) = \frac{C(s)}{\sqrt{1-\xi^2}} \tag{C.2}$$

To constrain yet unknown function $C(s)$, we substitute (C.2) back into (C.1) and evaluate it at, e.g., $\xi = 0$,

$$\frac{1}{s} = -\frac{2C(s)}{\pi}\int_{-1}^{1} \frac{\ln|\sqrt{s}\xi| + \gamma}{\sqrt{1-\xi^2}} d\xi \tag{C.3}$$

Carrying out the integral in the above leads to the expression

$$C(s) = -\frac{1}{s}\frac{1}{\ln(s/4) + 2\gamma} \tag{C.4}$$

which together with (C.2) provides the asymptotic large-time solution to the auxiliary problem in the Laplace domain, as recorded in (3.10).

C.2 INVERSION TO THE TIME-DOMAIN

Let us formally define the Laplace inverse of (C.4):

$$c(\tau) = \mathscr{L}^{-1}[C](\tau). \tag{C.5}$$

We suggest the following asymptotic expansion for $c(\tau)$:

$$\tau \gg 1: \qquad c(\tau) = \sum_{n=1}^{\infty} \frac{c_n}{(\ln 4\tau - 2\gamma)^n}, \quad c_1 = 1 \tag{C.6}$$

where in practice we will be interested in the first few terms of the series. (The impetus for suggesting the form (C.6) stems from the well-known leading order asymptotics, $c(\tau) = 1/\ln\tau + O(1)$, $\tau \gg 1$, which can be extracted by analogy from, e.g., the solution of the heat conduction problem from a circular hole due to imposed temperature step [67]).

To furnish a proof of series expansion (C.6) and find the expansion coefficients, consider the Laplace image of (C.6),

$$\mathscr{L}[c](s) = \frac{1}{s}\sum_{n=1}^{\infty} c_n \int_0^{\infty} \frac{e^{-z}dz}{(\ln z + 1/\epsilon(s))^n}, \qquad \epsilon(s) \equiv sC(s) = -\frac{1}{\ln(s/4) + 2\gamma} \ll 1 \tag{C.7}$$

where the integration variable has been changed from s to $z = s\tau$. Expanding the integrands in the small parameter $\epsilon(s)$ and integrating leads to the expansion, which first three terms are shown as follows

$$\mathscr{L}[c](s) = \frac{1}{s}\left(c_1\,\epsilon(s) + (c_2 + \gamma c_1)\,\epsilon^2(s) + (c_3 + 2\gamma c_2 + (\gamma^2 + \pi^2/6)c_1)\,\epsilon^3(s) + ...\right) \tag{C.8}$$

In view of $c_1 = 1$ and of the definition of $\epsilon(s)$, the first term in the above series gives the sought Laplace image $C(s)$, while the values of coefficients c_n with $n > 1$ are selected such as to nullify the $\epsilon^n(s)/s$ terms in the expansion. Namely,

$$c_2 = -\gamma, \quad c_3 = \gamma^2 - \frac{\pi^2}{6}, \quad c_4 = -\gamma^3 + \frac{\gamma\pi^2}{2} - 2\zeta(3), \tag{C.9}$$

and so on. Here ζ denotes the Riemann zeta function, $\zeta(3) \approx 1.2021$ [80].

C.2.1 Simplified form of the asymptotic expansion

The form (C.6) with (C.9) of the large-time expansion can be considerably simplified by re-expanding it in a modified parameter $(\ln 4\tau - \gamma)$ (compare to $(\ln 4\tau - 2\gamma)$ in (C.6)):

$$\tau \gg 1 : \qquad c(\tau) = \sum_{n=1}^{\infty} \frac{c'_n}{(\ln 4\tau - \gamma)^n}, \quad c'_1 = 1 \tag{C.10}$$

where the corresponding coefficients given by

$$c'_2 = 0, \quad c'_3 = -\frac{\pi^2}{6}, \quad c'_4 = -2\zeta(3), \tag{C.11}$$

and so on. Corresponding large-time expansion of $\psi(\xi, \tau) = c(\tau)/\sqrt{1 - \xi^2}$ with $c(\tau)$ given by (C.10) and (C.11), truncated to the first three terms, is recorded in (3.11).

APPENDIX D: NUMERICAL SOLUTION OF THE AUXILIARY PROBLEM

This Appendix deals with the solution of integral equation (3.8) for the Laplace image of the normalized leak-off rate ($\hat{\psi}(\xi, s)$) in the auxiliary problem. This equation is characterized by a logarithmically-singular kernel. Differentiation of (3.8) in ξ reduces it to the following equation,

$$\int_{-1}^{1} G\left(2\sqrt{s}(\xi - \xi')\right) \hat{\psi}(\xi', s)\, d\xi' = 0, \tag{D.1}$$

with a Cauchy-singular kernel G, which can be defined in terms of the modified Bessel function of second kind as $G(\zeta) = \text{sign}(\zeta)\, \text{K}_1(|\zeta|)$. Furthermore, this kernel can be explicitly decomposed in the sum of the Cauchy-singular and regular parts as,

$$G(\zeta) = \frac{1}{\zeta} + \text{sign}(\zeta)\, \tilde{K}_1(|\zeta|) \tag{D.2}$$

where

$$\tilde{K}_1(\zeta) = \ln\left(\frac{\zeta}{2}\right) I_1(\zeta) - \frac{\zeta}{4} \sum_{k=0}^{\infty} \left[\Psi(k+1) + \Psi(k+2)\right] \frac{\zeta^{2k}}{4^k k!\,(k+1)!}, \tag{D.3}$$

I_1 is the Bessel function of the first kind, and Ψ is the digamma function [81].

Singular integral equation (D.1)-(D.2) lands itself to the solution by the Gauss-Chebyshev quadrature method [82]. Namely, we seek the solution in the form

$$\hat{\psi}(\xi, s) = \frac{1}{\sqrt{1-\xi^2}} f(\xi, s), \tag{D.4}$$

where f is a bounded, continuous function of ξ, and the inverse-square-root-singular prefactor is the fundamental function of the Cauchy integral. Substituting (D.4) into

(D.1) with (D.2), we find that the singular integral takes a form approximable by a Gauss-Chebyshev quadratures

$$\sum_{i=1}^{n} \frac{1}{n} f(\xi_i', s) \left(\frac{1}{2\sqrt{s}(\xi - \xi_i')} + \text{sign}(\xi - \xi_i') \tilde{K}_1 \left(2\sqrt{s}|\xi - \xi_i'| \right) \right) = 0, \tag{D.5}$$

with n collocation points, $\xi_i' = \cos\left(\pi\left(2i-1\right)/2n\right)$, $i = 1, ..., n$, provided that ξ is evaluated at points $\xi_k = \cos\left(\pi k/n\right)$, $k = 1, ..., n-1$. This yields a system of $n-1$ algebraic equations in n unknowns (values of f at ξ_i''s).

An additional constraint is extracted from the original integral equation (3.8) (which derivative (D.1) has been addressed in so far) by, first, integrating it in ξ in order to eliminate the logarithmic singularity, and then writing the result in the Gauss-Chebyshev quadratures:

$$\sum_{i=1}^{n} \frac{1}{n} f(\xi_i', s) A\left(\xi_i', s\right) = \frac{1}{s}, \tag{D.6}$$

where $A\left(\xi', s\right) \equiv \int_{-1}^{1} \mathrm{K}_0\left(2\sqrt{s}|\xi - \xi'|\right) d\xi$ can be evaluated in the form

$$A\left(\xi', s\right) = \frac{1}{2\sqrt{s}} \left[F\left(2\sqrt{s}(1-\xi')\right) - F(-2\sqrt{s}(1+\xi')) \right]$$

with

$$F(\zeta) \equiv \int_0^{\zeta} \mathrm{K}_0\left(|\zeta|\right) d\zeta = \frac{\pi}{2} \left(\zeta\, \mathrm{K}_0\left(|\zeta|\right) \mathrm{L}_{-1}\left(\zeta\right) + |\zeta|\, \mathrm{K}_1\left(|\zeta|\right) \mathrm{L}_0\left(\zeta\right) \right) \tag{D.7}$$

defined in terms of the modified Bessel (K's) and Struve (L's) functions.

The set of equations (D.5) with $\xi = \xi_k$ $(k = 1, ..., n-1)$ and (D.6) is solved using the Newton-Raphson method for $n = 100$ and value of s varying from 10^{-5} to 10^{4}. Once the discrete solution of $f(\xi, s)$ (and $\hat{\psi}(\xi, s)$ via (D.4)) is obtained, it is inverted to the time domain using the Stehfest algorithm [68].

APPENDIX E: NON-UNIFORM PRESSURE SOLUTION (VISCOUS PRESSURE DROP IN THE CRACK) FOR THE TRANSIENT PRESSURIZATION OF A CLOSED FRACTURE

E.1 CASE OF PROPPED FRACTURE

E.1.1 Normalized equations

Using the non-dimensional time (τ), x coordinate (ξ), y coordinate (χ), and pressure (Π) defined in Section 5.2.1, the lubrication equation (2.11) and initial-boundary conditions (2.12) are normalized as

$$-\left.\frac{\partial \Pi}{\partial \chi}\right|_{\chi=0} = \frac{(k_f \bar{w})_D}{2} \frac{\partial^2 \Pi}{\partial \xi^2}, \tag{E.1}$$

with initial-boundary conditions:

$$\Pi|_{\tau=0} = 0, \quad \left.\frac{\partial \Pi}{\partial \xi}\right|_{\xi=0^+} = -\frac{1}{2}, \quad \left.\frac{\partial \Pi}{\partial \xi}\right|_{\xi=1} = 0. \tag{E.2}$$

Note that $k_f = \bar{w}^2/\pi^2$ is used to reformulate the lubrication equation (2.11) for a propped fracture.

The normalized form of the diffusivity equation (2.16),

$$\Pi(\xi, \tau) = \frac{-1}{2\pi} \int_0^{\tau} \int_{-1}^{1} \left.\frac{\partial \Pi}{\partial \chi}\right|_{\chi=0} \exp\left(-\frac{\left|\xi - \xi'\right|^2}{(\tau - \tau')}\right) \frac{d\xi' d\tau'}{(\tau - \tau')}, \tag{E.3}$$

completes the set of normalized governing equations (E.1)-(E.2).

Applying Laplace transform to the set of equations (E.1)-(E.2) results:

- Lubrication equation

$$-\left.\frac{\partial \hat{\Pi}}{\partial \chi}\right|_{\chi=0} = \frac{(k_f \bar{w})_D}{2} \frac{\partial^2 \hat{\Pi}}{\partial \xi^2}, \tag{E.4}$$

with boundary conditions:

$$\left.\frac{\partial \hat{\Pi}}{\partial \xi}\right|_{\xi=0^+} = -\frac{1}{2s}, \quad \left.\frac{d\hat{\Pi}}{d\xi}\right|_{\xi=1} = 0. \tag{E.5}$$

- 2-D Diffusivity equation

$$\hat{\Pi} = \frac{-1}{\pi} \int_{-1}^{1} \left.\frac{\partial \hat{\Pi}}{\partial \chi}\right|_{\chi=0} K_0\left(2\sqrt{s}\left|\xi - \xi'\right|\right) d\xi'. \tag{E.6}$$

E.1.2 Asymptotic solutions

E.1.2.1 Small-time asymptote

The special form of (E.6) when the leak-off diffusion is 1-D is given by [67]

$$\left.\frac{\partial \hat{\Pi}}{\partial \chi}\right|_{\chi=0} = -2\sqrt{s}\hat{\Pi}. \tag{E.7}$$

Substitution of (E.7) in (E.4) gives an ordinary differential equation which can be analytically solved along with boundary conditions (E.5). The closed-form analytical expression for $\hat{\Pi}$ in Laplace domain is given by:

$$\hat{\Pi}(\xi, s) = \frac{(k_f \bar{w})_D^{1/2}}{4} \frac{\cosh\left(2(k_f \bar{w})_D^{-1/2} s^{1/4}(1-\xi)\right)}{s^{5/4} \sinh\left(2(k_f \bar{w})_D^{-1/2} s^{1/4}\right)}. \tag{E.8}$$

The expression (E.8) can be inverted in time domain using Stehfest algorithm [68].

E.1.2.2 Large-time asymptote

At long injection times, the pressure along the fracture will be equilibrated. The large-time asymptote of uniformly pressurized fracture was previously obtained (Section 3.4). This expression in terms of non-dimensional parameters defined in Section 5.2.1 is given by:

$$\Pi(\tau) = \frac{(k_f \bar{w})_D}{4\pi} \ln\left(4 \exp(-\gamma)\, \tau\right). \tag{E.9}$$

E.1.3 Numerical solution

In order to accurately describe the behavior of fluid leak-off rate at the vicinity of crack tips where the singularity behavior is observed, we introduce the following expression for the leak-off rate:

$$\left.\frac{\partial\hat{\Pi}}{\partial\chi}\right|_{\chi=0} = \frac{a(s)}{\sqrt{1-\xi^2}} + \left.\frac{\partial\hat{\Pi}^{reg.}}{\partial\chi}\right|_{\chi=0}, \tag{E.10}$$

where $a(s)$ is the strength of singularity at the crack tips and $\partial\Pi^{reg.}/\partial\chi|_{\chi=0}$ is the regular (non-singular) part of the fluid leak-off rate. Substitution of the expression (E.10) in (E.6) yields:

$$\hat{\Pi}\left(\xi,s\right) = -\frac{2}{\pi}\int_{-1}^{1}\frac{a(s)K_0\left(2\sqrt{s}\left|\xi-\xi^{'}\right|\right)d\xi^{'}}{\sqrt{1-\xi^{'2}}} -$$

$$\frac{2}{\pi}\int_{-1}^{1}\left.\frac{\partial\hat{\Pi}^{reg.}}{\partial\chi}\right|_{\chi=0}K_0\left(2\sqrt{s}\left|\xi-\xi^{'}\right|\right)d\xi^{'} \tag{E.11}$$

The corresponding approximation of (E.11) is

$$\frac{\pi\hat{\Pi}_{j+1/2}}{2} = -a(s)B\left(\xi_{j+1/2},s\right) - \sum_{i=1}^{N}\left.\frac{\partial\hat{\Pi}^{reg.}_{i+1/2}}{\partial\chi}\right|_{\chi=0}C_{i+1/2}(\xi_{j+1/2},s)\ \ ,(j=1,...,N), \tag{E.12}$$

where $B\left(\xi,s\right) = \int_{-1}^{1}K_0\left(2\sqrt{s}\left|\xi-\xi^{'}\right|\right)/\sqrt{1-\xi^{'2}}d\xi^{'}$ is tabulated numerically, and $C_{i+1/2}(\xi,s) = F(\xi,\xi_{i+1},s) - F(\xi,\xi_i,s)$ where $F(\left|\xi-\xi^{'}\right|) = \int_0^{\xi^{'}}K_0(2\sqrt{s}\left|\xi-\xi^{'}\right|)d\xi^{'}$ is previously obtained (equation (D.7)).

The adopted numerical scheme has been carried out for $\xi\in[-1,1]$ using $N=50$ discretization nodes along the crack. This numerical scheme relies on the piecewise constant approximation of normalized pressure $\hat{\Pi}$ and leak-off $\partial\hat{\Pi}^{reg.}/\partial\chi\Big|_{\chi=0}$ in the

Laplace domain within the crack over the grid element $\xi_j, (j = 1, ..., N)$. Note that $\xi_1 = -1$ and $\xi_{N+1} = 1$. A uniformly equal space grids are used from $\xi \in [-0.9, 0.9]$ and a finer mesh scheme is used for the region near the crack tip.

For a pre-assigned value of s (E.12) can be written for $\hat{\Pi}$ and $\partial\hat{\Pi}^{reg.}/\partial\chi\Big|_{\chi=0}$ at the grid elements midpoints $\xi_{i+1/2} = (\xi_i + \xi_{i+1})/2$, $(i = 1, .., N)$. Due to the symmetry with respect to the crack inlet, the pressure and fluid leak-off rate are only solved along the half-crack length. This leads to a system of algebraic equations with $N/2$ equations. The $(N/2 + 1)$th equation can be obtained by letting $\xi = 1$.

To complete the system of equations, we use the discretized form of lubrication equation (E.1). The second-order central difference for the space derivative is used discretize the lubrication equation. In order to properly use the discretized form of lubrication equation, a new system of grid points is defined. We include $\xi = 0$ and $\xi = 1$ to the set of grid mid points $\xi_{i+1/2} = (\xi_i + \xi_{i+1})/2$, $(i = N/2 + 1, .., N)$ perviously defined to discretize the general 2-D integral. The new grid points are called $\xi_i^*(1, ..., m)$ where $m = N/2 + 2$, $\xi_1^* = 0$, and $\xi_m^* = 1$.

The discretized form of lubrication equation is

$$-\left.\frac{\partial\hat{\Pi}_{i+1}^{reg.}}{\partial\chi}\right|_{\chi=0} - \frac{a(s)}{\sqrt{1-\xi_{i+1}^{*2}}} =$$

$$(k_f\bar{w})_D \frac{\Delta\xi_2\left(\hat{\Pi}\left(\xi_{i+2}^*, s\right) - \hat{\Pi}\left(\xi_{i+1}^*, s\right)\right) - \Delta\xi_1\left(\hat{\Pi}\left(\xi_{i+1}^*, s\right) - \hat{\Pi}\left(\xi_i^*, s\right)\right)}{\Delta\xi_1\Delta\xi_2(\Delta\xi_1 + \Delta\xi_2)}, (i = 1, .., m-2). \tag{E.13}$$

where $\Delta\xi_2 = \xi_{i+2}^* - \xi_{i+1}^*$, $\Delta\xi_2 = \xi_{i+1}^* - \xi_i^*$.

The first-order forward difference scheme is used to discretize the boundary conditions

$$\frac{\hat{\Pi}\left(\xi_2^*, s\right) - \hat{\Pi}\left(\xi_1^*, s\right)}{\xi_2^* - \xi_1^*} = -\frac{1}{2s}, \tag{E.14}$$

and

$$\hat{\Pi}\left(\xi_m^* = 1, s\right) = \hat{\Pi}\left(\xi_{m-1}^*, s\right). \tag{E.15}$$

For a pre-assigned value of s, the recurrence equation (E.13) and boundary conditions (E.14) and (E.15) give another $m = N/2 + 2$ equations which together with previous $N/2 + 1$ equations give $N + 3$ equations. The number of unknowns are $N + 3$. Thus, $(N + 3)$ equations with $N + 3$ unknowns can be numerically solved using the Newton-Raphson method.

This procedure is repeated for several values of s. The numerical results for $\hat{\Pi}$ and $\partial\hat{\Pi}^{reg.}/\partial\chi\Big|_{\chi=0}$ at at each grid point $\xi_i^*(1, ..., m)$ are inverted in actual time domain using the Stehfest algorithm [68].

E.1.3.1 Parametric dependence of the "uniformity" pressure and time

Figure E.1 shows the dependence of the uniformity pressure $(\bar{p}_{uni}/p_*)$ and time (t_{uni}/t_*) on the non-dimensional fracture conductivity parameter $(k_f\bar{w})_D$ (equation (5.3)).

The approximate analytical expression for the uniformity pressure (Π_{uni}) when $(k_f\bar{w})_D \gg 1$ is given by (Fig. E.1a):

$$\Pi_{uni} = \frac{p_{uni} - p_0}{p_*} \approx 5 \tag{E.16}$$

which can be expressed in the problem parameters as:

$$p_{uni} - p_0 \approx 5\frac{Q_0\ell\mu}{k_f\bar{w}h}. \tag{E.17}$$

For the practical range of reservoir applications (i.e., $(k_f\bar{w})_D \gtrsim 1$), the relative deviation of the uniformity pressure from its value (E.16) is approximately $\pm 20\%$. Hence, the expression (E.16) can be approximately used to estimate the uniformity pressure for the reservoir problems. However, the uniformity time t_{uni} does change (increase)

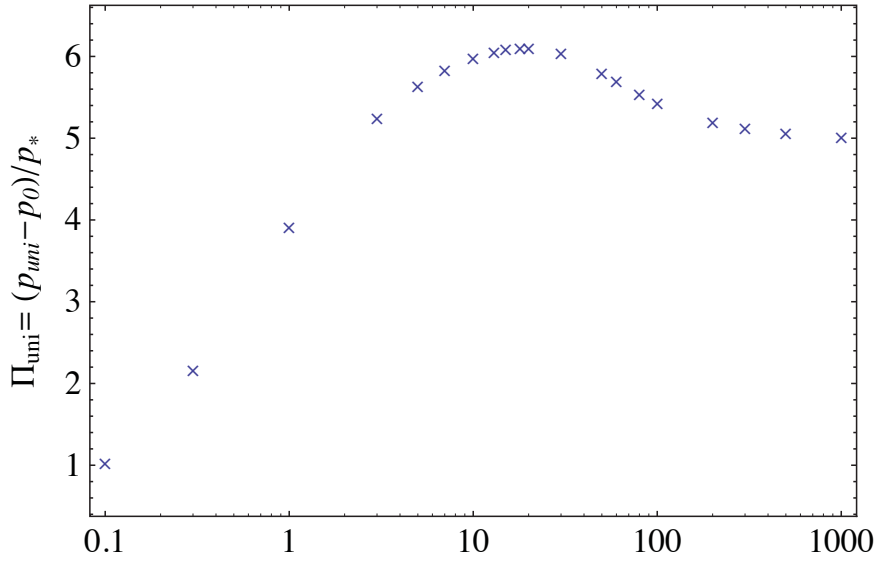

(a)

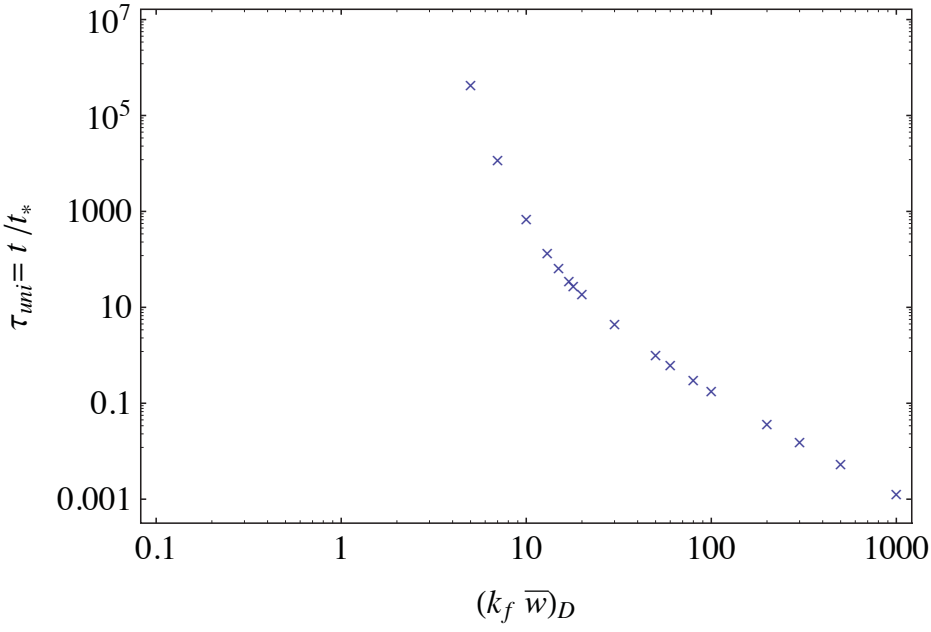

(b)

Figure E.1: Dependence of uniformity pressure $\Pi_{uni} = (p_{uni} - p_0)/p_*$ and time $\tau_{uni} = t_{uni}/t_*$ on the fracture conductivity $(k_f\bar{w})_D = k_f\bar{w}/k\ell$ during the transient pressurization of a propped fracture. The pressure and time scales are $p_* = Q_0\ell\mu/k_f\bar{w}h$ and time $t_* = \ell^2/4\alpha$, respectively.

with $(k_f\bar{w})_D$ (Fig. E.1b).

E.2 CASE OF UN-PROPPED FRACTURE

E.2.1 Normalized equations

Using the non-dimensional time (τ), x coordinate (ξ), and pressure (Π) defined in Section 5.3.1.1, and introducing the non-dimensional y coordinate ($\chi = y/\ell$) the lubrication equation (2.11) and initial-boundary conditions (2.12) are normalized as

$$\frac{\partial}{\partial\tau}\left(\frac{1}{1-\Pi}\right) - \frac{8}{\pi}\frac{1}{(k_f\bar{w})_D\mathcal{Q}}\left.\frac{\partial\Pi}{\partial\chi}\right|_{\chi=0} = \frac{1}{16}\frac{1}{\mathcal{Q}}\frac{\partial}{\partial\xi}\left(\frac{1}{(1-\Pi)^3}\frac{\partial\Pi}{\partial\xi}\right), \tag{E.18}$$

$$\Pi|_{\tau=0} = \Pi_0, \quad \frac{1}{(1-\Pi)^3}\left.\frac{\partial\Pi}{\partial\xi}\right|_{\xi=0^+} = -\frac{32}{\pi}\mathcal{Q}, \quad \frac{1}{(1-\Pi)^3}\left.\frac{\partial\Pi}{\partial\xi}\right|_{\xi=1} = 0, \tag{E.19}$$

where $\mathcal{Q} = Q_0\,(\mu\ell/hw_0^4k_{ni})$, $(k_f\bar{w})_D = w_0^3/k\ell$, and $\Pi_0 = (p-\sigma_0)/k_{ni}w_0$. Note that the height-averaged crack opening (i.e., $\bar{w}$) (equation (2.3)) is formulated using the Bandis' equation (5.4) to be used in the lubrication equation (2.11) and initial-boundary conditions (2.12).

The normalized form of the diffusivity equation (2.15),

$$\frac{\partial\Pi}{\partial\tau} = \frac{\mathcal{A}_c}{(k_f\bar{w})_D\mathcal{Q}}\left(\frac{\partial^2\Pi}{\partial\xi^2} + \frac{\partial^2\Pi}{\partial\chi^2}\right), \tag{E.20}$$

where $\mathcal{A}_c = 1/k_{ni}S\ell$ (equation (5.15)), completes the set of normalized governing equations (B.1)-(B.3).

The details of numerical solutions of the governing equations (E.18)-(E.20) such as, method of solution, space discretization, and number of grids, are similar to the numerical treatment presented in Section B.2.

The transient pressurization of fracture in impermeable formation can be extracted as a special case from above formulation by letting $(k_f\bar{w})_D = \infty$.

E.3 NUMERICAL SCHEME FOR THE TRANSIENT PRESSURIZATION OF A UNIFORMLY PRESSURIZED CRACK (BEFORE CRACK RE-OPENING)

We use the piecewise constant approximation method to solve (5.14). The latter can be linearly discretized in time as

$$\tau_{k'} = \frac{\pi}{2}\mathcal{A}_c \left(\frac{\Pi_{k'}}{1-\mathcal{D}\Pi_{k'}} - \frac{\Pi_0}{1-\mathcal{D}\Pi_0} \right) + \sum_{j=0}^{k'-1} \Phi_{aux} \left(\tau_{k'} - \tau_{j+1/2} \right) \left(\Pi_{j+1} - \Pi_j \right), \quad \text{(E.21)}$$

where k' is the number of discretized time steps required to obtain the transient pressurization until the crack becomes mechanically-open (i.e., $\Pi = 0$) .

The algorithm to solve the above discretized equation is :

1. The representative values for $\mathcal{D}$, $\mathcal{A}_c$, and Π_0 are selected.

2. We choose sufficient number of discretized time steps k'.

3. Using the initial normalized pressure Π_0 at $\tau = 0$ and a given small time increment $\Delta\tau$, we obtain a linear equation with one unknown corresponding to the normalized pressure at $\Delta\tau$.

4. We select another time increment from previous time step to obtain a linear equation which can be solved for a new pressure. We continue the procedure until the condition of crack opening is reached.

E.4 NUMERICAL SCHEME FOR THE TRANSIENT PRESSURIZATION OF A UNIFORMLY PRESSURIZED CRACK (AFTER CRACK RE-OPENING)

Equation (5.21) can be linearly discretized as

$$\tau_n = \pi\mathcal{A}\Pi_n + \sum_{j=0}^{k'-1} \Phi_{aux}(\tau_n - \tau_{j+1/2}) \left(\Pi_{j+1} - \Pi_j \right)$$

$$\sum_{i=0}^{n-1} \Phi_{aux} \left(\tau_n - \tau_{i+1/2}\right) \left(\Pi_{i+1} - \Pi_i\right). \tag{E.22}$$

The algorithm to solve the above discretized equation is:

1. The representative values for $\mathcal{A}$ and Π_0 are selected.

2. We choose n number of time steps with $\tau_{n=0} = \tau_o$. The normalized pressure at the onset of crack opening is zero, i.e., $\Pi(\tau_{n=0}) = 0$. The choice of the number of the time steps n depends on how far in time the numerical calculation are carried out.

3. Using a small time increment after the onset of crack opening and previously developed normalized pressure before the crack becomes mechanically open (Section E.3), we obtain a linear equation which can be solved for the normalized pressure at the given time step. We continue the procedure for the new time increments and solve for the new pressure.

APPENDIX F: TRANSIENT PRESSURIZATION OF MULTI FRACTURED WELLS

F.1 PERMEABLE STRIP PROBLEM

In this Section, the transient pressurization of the permeable strip (Fig. 5.9) due to a fluid injection is obtained. We make use of the following assumptions. 1) The pressure distribution along the fracture is uniform. 2) The storage effects on the transient pressurization can be neglected.

F.1.1 Governing equations

The diffusivity equation (2.15) is used to describe the pore pressure change in the problem of the permeable strip. The corresponding initial and boundary conditions to solve the diffusivity equation are

- Initial condition

$$p = p_0, |x| < \infty,\ |y| \leq \frac{d}{2},\ t = 0. \tag{F.1}$$

- Boundary condition

$$\frac{\partial p}{\partial y} = 0,\ |x| > \ell,\ y = \pm\frac{d}{2} \tag{F.2}$$

$$p = p(t),\ |x| \leq \ell,\ y = \pm\frac{d}{2}, \tag{F.3}$$

Note that the boundary condition (F.2) signifies the no-flow boundary assumption.

The global volume balance equation (2.13) with V_{leak} substituted from (2.14) is used to complete the system of equations. This equation for the problem of the permeable strip injected by a fluid at the constant volumetric flow rate Q_0^1 is given by

$$Q_0^1 t = h \int_0^t \int_{-\ell}^{\ell} \bar{g}(x,t) dx dt, \;\; \bar{g}\,(x,t) = -\frac{2k}{\mu} \left. \frac{\partial p}{\partial y} \right|_{y=\pm d/2}. \tag{F.4}$$

Note that the storage term in (F.4) is nullified due to the negligible fracture volume change.

F.1.2 Normalized equations

We define the non-dimensional time ($\tau = t/t_*$), pressure ($\Pi = (p - p_0)/p_*$), x coordinate ($\xi = x/\ell$), y coordinate ($\chi = y/\ell$) using the characteristic time $t_* = d^2/4\alpha$, length ℓ, and pressure $p_* = Q_0^1/4hS\alpha$ scales, respectively. Introducing the non-dimensional parameters in the diffusivity equation (2.15), initial-boundary conditions (F.1)-(F.3), and the global volume balance equation (F.4) yield:

- Diffusivity equation

$$\frac{\partial \Pi}{\partial \tau} = \left(\frac{d}{\ell}\right)^2 \left(\frac{\partial^2 \Pi}{\partial \xi^2} + \frac{\partial^2 \Pi}{\partial \chi^2}\right). \tag{F.5}$$

- Initial condition

$$\Pi = 0, |\xi| < \infty, \; |\chi| \leq \frac{d}{2\ell}, \; t = 0. \tag{F.6}$$

- Boundary conditions

$$\frac{\partial \Pi}{\partial \chi} = 0, \; |\xi| > 1, \chi = \pm \frac{d}{2\ell}, \tag{F.7}$$

$$\Pi = \Pi(\tau), \; |\xi| \leq 1, \chi = \pm \frac{d}{2\ell}. \tag{F.8}$$

- Global volume balance equation

$$\tau = \frac{1}{2} \int_0^{\tau} \int_{-1}^{1} \left. \frac{\partial \Pi}{\partial \chi} \right|_{\chi = \pm d/2\ell} d\chi d\tau. \tag{F.9}$$

It is more convenient to work in Laplace transform domain. Applying the Laplace transform to (F.5)-(F.9) results

$$s\hat{\Pi} = \left(\frac{d}{\ell}\right)^2 \left(\frac{\partial^2 \hat{\Pi}}{\partial \xi^2} + \frac{\partial^2 \hat{\Pi}}{\partial \chi^2}\right), \tag{F.10}$$

$$\frac{\partial \hat{\Pi}}{\partial \chi} = 0,\ |\xi| > 1, \chi = \pm\frac{d}{2\ell}, \tag{F.11}$$

$$\hat{\Pi} = \hat{\Pi}(s),\ |\xi| \leq 1, \chi = \pm\frac{d}{2\ell}, \tag{F.12}$$

$$\frac{1}{s} = \frac{1}{2}\int_{-1}^{1} \left.\frac{\partial \hat{\Pi}}{\partial \chi}\right|_{\chi=\pm d/2\ell} d\xi. \tag{F.13}$$

The system of equations (F.10)-(F.13) can be simultaneously solved to find the pressure evolution with time for the problem of the permeable strip.

F.1.3 Numerical calculations

The central finite-difference representation is used to discretize the diffusivity equation (F.10) into a set of non-uniformly spaced grid points $\{0 \leq \xi_i < \infty,\ d/2\ell \leq \chi_j < -d/2\ell\}$, $i = 1, ..., M$ and $j = 1, ..., N$. Note that due to the symmetry with respect to ξ, the numerical calculations are carried out in the half space (i.e., $\xi > 0$).

For fracture discretization in the region $0 < \xi < 1$, a logarithmic grid spacing with the concentrated nodes near the crack tip is used. The latter is necessary to capture the singular leak-off rates at the crack tip ($\xi = 1$). Outside of the fracture ($\xi > 1$), a logarithmic grid spacing is used to span a computational domain to model diffusion in the infinite space. We also make use of a uniform grid spacing in the χ direction (i.e., $d/2\ell \leq \chi < -d/2\ell$). The numerical results reported in Section 5.4 are based on the computational domain with $\xi_M = 10^7$ and $d/2\ell < \chi_N < -d/2\ell$, and the mesh with total $M = 200$ and $N = 50$ nodes in the ξ and χ directions, respectively. The discretization of the integral (F.13) is based on the simple piecewise constant

approximation method in ξ direction.

For a pre-assigned value of s, the Newton-Raphson method is used to numerically solve for $\hat{\Pi}_{i,j}$ at each grid point in Laplace domain. The numerical results are inverted in actual time domain using the Stehfest algorithm [68].

APPENDIX G:COPYRIGHT PERMISSIONS

G.1 COPYRIGHT PERMISSION FOR CHAPTER 3

August 10th 2015,

International Journal of Applied Mechanics:

I am preparing my Ph.D. thesis for submission to the Faculty of Graduate Studies at Dalhousie University , Halifax, Nova Scotia, Canada. I am seeking your permission to include some part of the following paper in a chapter in my PhD thesis: [Sarvaramini, Erfan, and Dmitry I. Garagash. "*Breakdown of a Pressurized Fingerlike Crack in a Permeable Solid.*" Journal of Applied Mechanics 82.6 (2015): 061006.]

Full publication details and a copy of this permission letter will be included in the thesis.

Sincerely yours,

Erfan Sarvaramini

August 18th 2015,

From International Journal of Applied Mechanics:

It is our pleasure to also grant you permission to use all or any part of the ASME paper "Breakdown of a Pressurized Fingerlike Crack in a Permeable Solid," by Erfan Sarvaramini; Dmitry I. Garagash, J. Appl. Mech. 2015; 82(6), cited in your letter for inclusion in Ph.D. thesis for submission to the Faculty of Graduate Studies at Dalhousie University, Halifax, Nova Scotia, Canada.

Permission is granted for the specific use as stated herein and does not permit further use of the materials without proper authorization. Proper attribution must be made to the author(s) of the materials. Please note: if any or all of the figures and/or

Tables are of another source, permission should be granted from that outside source or include the reference of the original source. ASME does not grant permission for outside source material that may be referenced in the ASME works.

As is customary, we request that you ensure full acknowledgment of this material, the author(s), source and ASME as original publisher. Acknowledgment must be retained on all pages printed and distributed.

Many thanks for your interest in ASME publications.

Sincerely,
Beth Darchi
Publishing Administrator
ASME 2 Park Avenue
6th Floor New York, NY 10016-5990
Tel 1.212.591.7700
darchib@asme.org